EFFECTS OF BOTTOM CHORD EXTENSIONS ON THE STATIC AND DYNAMIC PERFORMANCE OF STEEL JOIST SUPPORTED FLOORS

Onur AVCI

Dissertation submitted to the faculty of the Virginia Polytechnic Institute and State University in partial fulfillment for the requirements for the degree of

Doctor of Philosophy

in

Civil Engineering

Thomas M. Murray, Co-Chair

Mehdi Setareh, Co-Chair

Finley A. Charney

Raymond H. Plaut

Alfred L. Wicks

September 8, 2005

Blacksburg, Virginia

Keywords: Floor vibrations, joist, truss, bottom chord extension, stiffness testing, vibration testing, natural frequency, mode shape, damping, effective mass, acceleration response, resonance, experimental modal analysis, finite element modeling, dynamic analysis, digital signal processing

EFFECTS OF BOTTOM CHORD EXTENSIONS ON THE STATIC AND DYNAMIC PERFORMANCE OF STEEL JOIST SUPPORTED FLOORS

Onur Avci

ABSTRACT

The purpose of this study was to examine the effect of bottom chord extensions on deflections and vibration characteristics of joist supported floor systems when joist bottom chord extensions are installed. To understand the effect of bottom chord extensions on deflections, natural frequency, damping, mode shape and effective mass, extensive analytical and experimental studies were conducted on single span and three span joist supported laboratory footbridges with different bottom chord extension configurations. Finite element computer models were created to simulate and compare the results of stiffness and vibration tests. Testing was done with a) the bottom chord extensions in-place before the concrete was placed, b) with all or part of the bottom chord extensions removed, and c) after the bottom chord extensions had been reinstalled with jacking for the single span footbridge and without jacking for the three-span footbridge.

Results from the stiffness tests indicate that re-installing the bottom chord extensions to the joists of the single span footbridge with cured concrete with the center of the span raised helps to reduce the uniform load deflections to some extent, but not as much as placing the bottom chord extensions before the concrete placement. Likewise, for the three span footbridge, placing the bottom chord extensions before the concrete placement is observed to be a better solution.

Results from the dynamic tests indicate that the effect of bottom chord extensions on the single span footbridge is consistent for natural frequency, 20 psf live load deflections, sinusoidal excitations with high amplitudes, quarter point heel drop excitations, walking excitations, and effective mass values. The effect of bottom chord extensions on the three span footbridge is consistent for the natural frequency and 20 psf deflections.

However, the FRF (Frequency Response Function) peaks of chirp, heel drop, sinusoidal excitations, accelerations from walking data, and the MEScope and Finite Element model effective mass results do not follow a common trend.

It can be concluded that even though the footbridge was stiffened by the bottom chord extensions, that does not necessarily mean that the acceleration levels, and hence the frequency response function peaks, decrease. However, bottom chord extensions do increase the natural frequencies for all the three governing bending modes.

ACKNOWLEDGEMENTS

I would like to extend my gratitude to Dr. Thomas M. Murray for his guidance, depth of knowledge, motivation, encouragement and patience during the research and in general. Giving me the opportunity to perform this research at Virginia Tech is greatly appreciated. I would like to express my sincere appreciation to Dr. Mehdi Setareh for his mentorship throughout the research. I learned a lot from him. His advice, motivation and patience during modal testing and research are tremendously appreciated. I would like to thank Dr. Finley Charney for his advice, providing the finite element software and for serving on my committee. I am extremely grateful to Dr. Plaut for his input, serving on my committee and for his constant support throughout my graduate studies at Virginia Tech. I would like to extend thanks to Dr. Alfred Wicks for providing the vibration software, serving on my committee, and for his support and enthusiasm. I would also like to thank Dr. Sam Easterling, Dr. Carin Roberts-Wollmann and Dr. Tommy Cousins for their advice and constant support during my studies at Virginia Tech.

I am grateful to NUCOR Research and Development for funding this project.

I would like to thank fellow classmates at Virginia Tech: Anthony “Major” Barrett, David “My Favorite” Martin, Kyle Dominisse, Steve “Skinny” Blumenbaum, Ben “MC” Mohr, Mike “Digity” Seek, Chuck Newhouse, Devin Harris, John Ryan, Don Scholz, Greg Williamson, Brad Davis and anybody I missed who deserves a mention, for their help in testing and for their friendship. Special appreciation goes to lab technicians Brett “Uncle” Farmer, Dennis “Uncle” Huffman and Clark “Uncle” Brown; they became my family during the five years I spent at the Virginia Tech Structures Lab.

I would like to thank all the friends in Blacksburg, my classmates from Middle East Technical University and friends in Turkey; I drew from your memories everyday. Thank you: Fenerbahce, Erinc, Olgun, Rahmi, Umur, Ahmet, Umut, Yaman, Harun, Murat Dilek, Murat Cinar, Edib, Omer, Adnan, Alperen, Bahadir, Mehmet, Cemil, Serkan, Ufuk, Aziz, Aysegul, Emre, Aysen, Guney, Raci, Ozan, Murat, Sinan, Alp, Berna, Demirtas, Mustafa, Serdar, Sonja, Aylin, Burcu, Sinem.

I would especially like to express my gratitude to my family for their love, unending support, motivation, encouragement, devotion and dedication without which none of this would have been possible.

Finally, I thank ALLAH who has already given me more than I deserve.

TABLE OF CONTENTS

LIST OF FIGURES

LIST OF TABLES

CHAPTER 1
INTRODUCTION AND LITERATURE REVIEW

1.1 Introduction

Advances in construction technology have led to use of lightweight and high strength materials in floor systems. Larger bays, longer spans and lighter materials result in floor systems with less mass and stiffness. At the same time, the trend towards a "paperless" office decreases damping and the amount of live load on the floors. As a result, office floors have become more vulnerable to annoying vibrations induced by human occupancy (Figure 1.1). The number of complaints by occupants has increased in recent years and floor vibrations have become an area of serviceability concern.

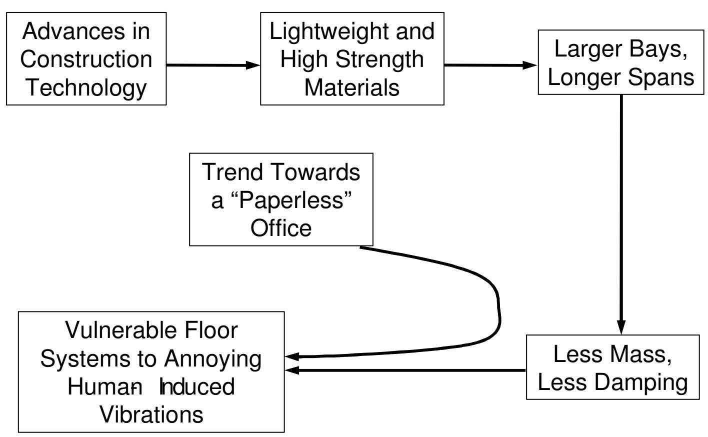

Figure 1.1 Floor Vibrations as a Serviceability Concern

Activities like walking, dancing, running, jumping, aerobics, etc. generate floor vibrations and humans have different tolerance levels for these vibrations. Because humans are both the source and the sensor, human-induced vibration can not be isolated from the structure; vibration must be controlled by the floor system. Extensive research has been conducted on human perceptibility of floor vibrations and dynamic behavior of floor systems. The procedures in the AISC/CISC Design Guide 11- *Floor Vibrations Due to Human Activity* (Murray et al. 1997) are available for designers to determine acceptable acceleration levels and minimize excessive floor vibrations.

The best approach is to design floors that do not allow annoying vibrations, as remedies for floors susceptible to excessive floor vibrations are very expensive. Possible modifications of existing problem floors include adding mass, increasing damping (using partitions, damping posts, tuned mass dampers) and increasing structural stiffness of the floor systems.

The use of joists and joist girders began with the development of steel trusses which dates from the 1850's (Fisher et al. 1991). Open web steel joists are still very popular in steel framed buildings (Figure 1.2). The open web allows the duct work to be run through the web and maintenance can be done easily after the construction is completed as shown in Figures 1.3 and 1.4. This makes open web steel joists very feasible and economical for the designers; however, vibrations of joist supported floor systems, and in particular, the effect of extended bottom chords, are still not very well understood. Further research on joist supported floor systems and their modifications can provide valuable information and confidence to design joist supported floor systems that do not have annoying vibrations.

Figure 1.2 Joist Supported Floor System

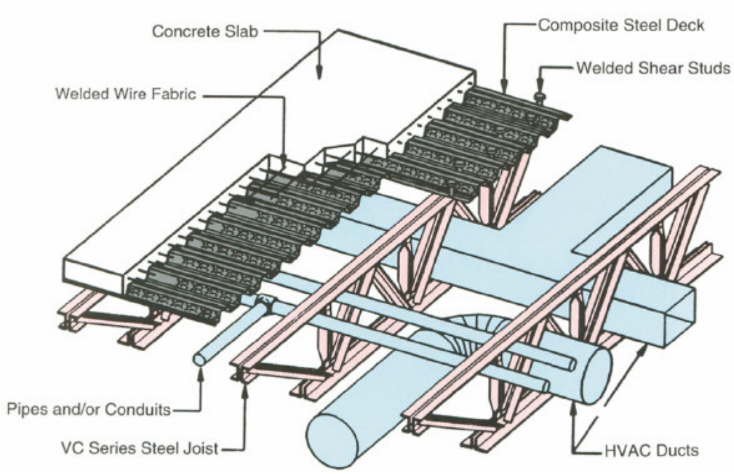

Figure 1.3 Open Web Steel Joist Floor System

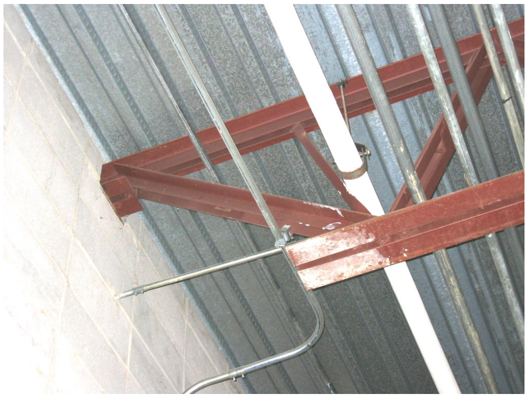

Figure 1.4 Open Web Allows the Duct Work to be Run Through the Web

1.2 Scope of Research

Joists are fabricated with or without bottom chord extensions. When they are manufactured with extensions on bottom chords (bottom chord length is approximately equal to the top chord length), most of the time the bottom chords are installed (bolted or welded) to the support location (Figure 1.5). Joists manufactured without bottom chord extensions can be modified by welding steel struts to connect/extend the end of the bottom chords to the support member (Figures 1.6 and 1.7). This can be done before or after the concrete is poured. The effect of bottom chord extensions on the vibration response of joist supported floors is largely unknown. Extending joist bottom chords in an attempt to improve problem floors has been reported but without success. However, these retrofits were done after fit-out of the buildings and without introducing a preload into the extensions.

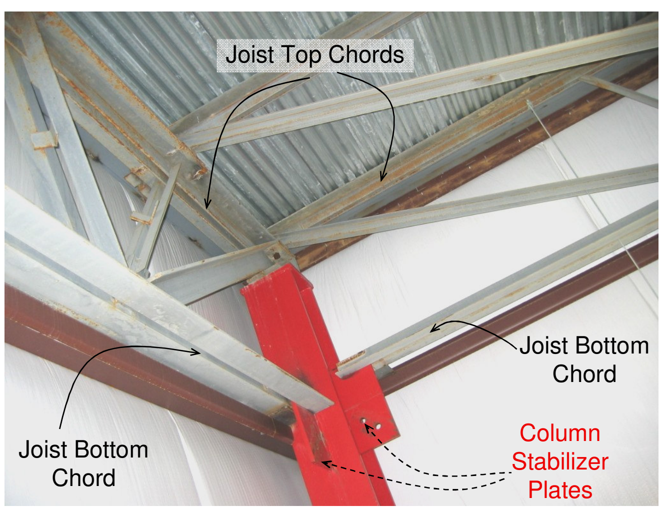

Figure 1.5 Bottom Chord Length is Equal to the Top Chord Length

 

a) Not Extended **b) Extended to Support**

Figure 1.6 Joist Bottom Chords

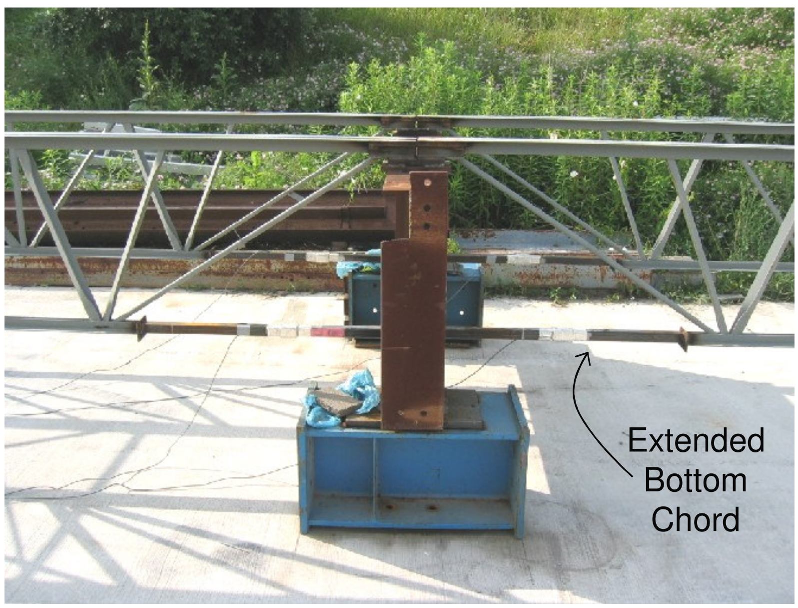

Figure 1.7 Extended Bottom Chords on an Interior Support

The purpose of this study is to examine the effect of bottom chord extensions on deflections and vibration characteristics of joist supported floor systems when joist bottom chord extensions are installed (a) before the concrete was placed, (b) after the fit-out with jacking for the single span footbridge, and (c) after the fit-out without jacking for the three span footbridge. Analytical and experimental studies are performed to understand the effect of extended bottom chords on deflection, natural frequency, damping, mode shape and effective mass. The desired goals are:

- Determine the load vs. deflection behavior of joists with and without bottom chord extensions in single span and three span laboratory footbridges.

- Measure the reduction in 20 psf live load deflection with and without bottom chord joist extensions in place.

- Monitor the load on the bottom chord extensions under different loadings and different bottom chord extension configurations.

- Determine the natural frequency, damping, mode shapes, and effective mass properties of the laboratory footbridges by experimental modal analysis.

- Investigate the effect of bottom chord extensions on the static and dynamic characteristics of the footbridges by three dimensional finite element models.

- Measure the acceleration response of the floors under different dynamic loads and compare with AISC/CISC Design Guide 11 predictions. Identify the effect of interior bottom chord extensions, exterior bottom chord extensions, and combinations.

- Investigate the potential advantages of continuous joists with bottom chord extensions.

An extensive experimental study is conducted on single span and three span joist supported laboratory footbridges with different bottom chord extension configurations. Finite element computer models are created to simulate and compare the results of stiffness and vibration tests.

1.3 AISC/CISC Steel Design Guide Series- 11

AISC/CISC Design Guide 11- *Floor Vibrations Due to Human Activity* (Murray et al. 1997) is extensively used by the designers to determine acceptable acceleration levels and provide structural framing which minimizes floor vibrations (Figure 1.8). Based on the research conducted by Allen and Murray (1993), the peak acceleration limits are proposed as shown in Figure 1.9. The acceleration limits are based on a scale published by the International Standards Organization (ISO 2631-2: 1989). The procedure presented in Design Guide 11 is divided into two sets of calculations considering the floor as a single degree of freedom system (Figure 1.10): fundamental natural frequency predictions and estimation of peak accelerations due to human activity.

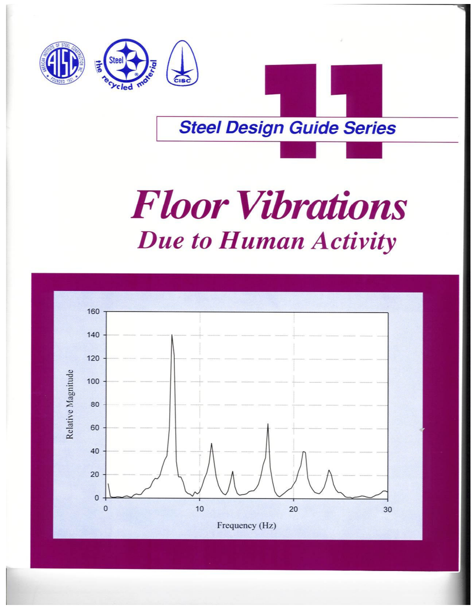

Figure 1.8 AISC/CISC Design Guide 11

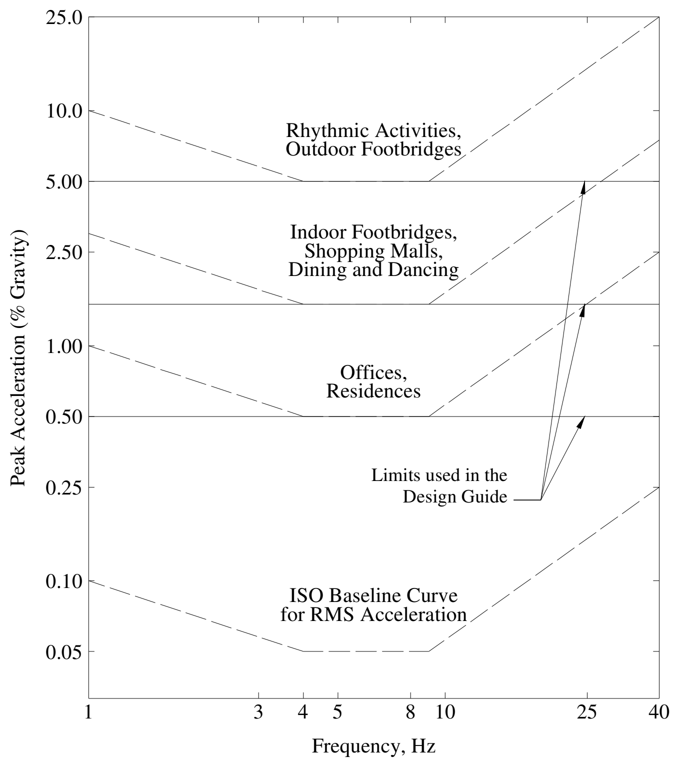

Figure 1.9 Recommended Peak Accelerations (Allen and Murray 1993; ISO 2631-2: 1989)

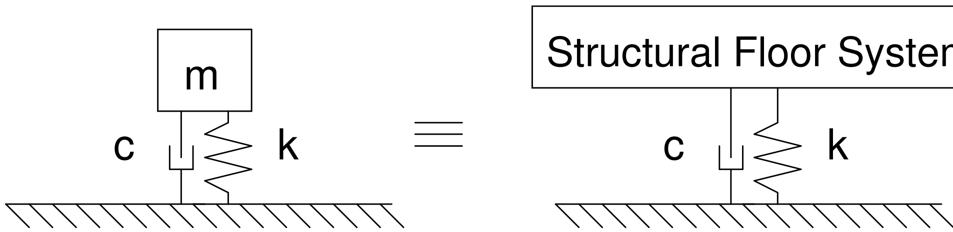

Figure 1.10 Single Degree of Freedom (SDOF) System

According to Design Guide 11 criteria, if the peak acceleration due to human walking excitation as a fraction of the acceleration of gravity does not exceed the limit for the appropriate occupancy, then the floor system is deemed satisfactory:

$$\frac{a_p}{g} = \frac{P_0 e^{-0.35 f_n}}{\beta W} \leq \frac{a_o}{g} \qquad (1.1)$$

where

a_p/g = estimated peak acceleration from walking excitation.

P_0 = constant force (65 lb for offices, residences, church structures and shopping malls; 92 lb for footbridges).

f_n = system natural frequency

β = modal damping ratio

W = effective weight of the floor

a_o/g = acceleration limit for walking excitation from Figure 1.9; 0.5 % of gravity

A harmonic forcing function is used for the peak acceleration prediction due to a person walking across the floor. In this model a person is repeatedly stepping at the midpoint of the floor with a frequency that is a harmonic of the fundamental frequency of the floor system. The harmonic forcing function is defined as:

$$F_i = P\alpha_i \cos(2\pi i f_{step} t) \qquad (1.2)$$

where

P = weight of the person; 157 lb is used for this weight

i = harmonic multiple of the step frequency

f_{step} = step frequency

α_i = dynamic coeeficient from Table 1.1

Table 1.1 – Common Forcing Frequencies, *f*, and Dynamic Coefficients, α_i

(from AISC/ CISC Design Guide 11)

Harmonic, *i*	Person Walking	
	f (Hz)	α_i
1	1.6 – 2.2	0.5
2	3.2 – 4.4	0.2
3	4.8 – 6.6	0.1
4	6.4 – 8.8	0.05
α=dynamic coefficient =[the peak sinusoidal force] / [weight of person(s)]		

A resonance response function that predicts the peak acceleration is defined as:

$$\frac{a}{g} = \frac{R\alpha_i P}{\beta W}\cos(2\pi i f_{step} t) \tag{1.3}$$

where

a/g = ratio of the floor acceleration to the acceleration due to gravity

R = reduction factor which takes into account that full steady-state resonant motion is not reached for walking and the walking person and the person annoyed are not at the location of maximum modal displacement at the same time. (R is recommended as 0.7 for footbridges and 0.5 for floor structures with two-way mode shape configurations).

β = modal damping ratio

W= effective weight of the floor

For the natural frequency predictions of the beams, girders, and floor systems, the members are assumed to be simply supported with the exception of cantilever sections. The first bending frequency of a joist or beam panel mode is given as:

$$f_j = 0.18\sqrt{\frac{g}{\Delta_j}} \tag{1.4}$$

The first bending frequency of a girder panel mode is given as:

$$f_g = 0.18\sqrt{\frac{g}{\Delta_g}} \tag{1.5}$$

where Δ_j and Δ_g are the deflections of the members under uniformly distributed loading. Δ_j is the mid-span deflection of the beam or joist, Δ_g is the mid-span deflection of the girder, and g is the acceleration due to gravity. Since the members are assumed to be simply supported with uniform loading, the maximum deflections are:

$$\Delta_j = \frac{5w_j L_j^4}{384E_s I_j} \tag{1.6}$$

$$\Delta_g = \frac{5w_g L_g^4}{384E_s I_g} \tag{1.7}$$

where Δ_j is weight per linear length per joist or beam and, Δ_g is weight per linear length per girder.

The fundamental frequency of the floor system is predicted using Equation 1.8.

$$f_n = 0.18\sqrt{\frac{g}{\Delta_j + \Delta_g}} \tag{1.8}$$

Equation 1.8 can also be written as

$$\frac{1}{f_n^{\ 2}} = \frac{1}{f_j^{\ 2}} + \frac{1}{f_g^{\ 2}} \tag{1.9}$$

which is known as Dunkerly's relationship.

The effective weight of a floor system is a combination of the effective weights of the beam and girder panels. The effective weight of a panel is:

$$\mathrm{W} = w\mathrm{BL} \tag{1.10}$$

where

W= effective panel weight

w = supported weight per unit area

L = length of the panel

B = effective width of the panel

The effective width of a joist panel is:

$$B_j = C_j \left(D_s / D_j\right)^{1/4} L_j \leq \frac{2}{3} \text{ (Building Floor Width)} \qquad (1.11)$$

where B_j is the effective width of the joist panel, C_j is 2.0 for most joist panels and 1.0 for panels with joists or beams parallel to an interior edge (mezzanine condition), D_s is slab transformed moment of inertia per unit width, D_j is the effective moment of inertia of the joist per unit of width, and L_j is the length of the joist.

The effective width of a girder panel is:

$$B_g = C_g \left(D_j / D_g\right)^{1/4} L_g \leq \frac{2}{3} \text{ (Building Floor Length)} \qquad (1.12)$$

where B_g is the effective width of the girder panel, C_g is 1.6 for girders supporting joists connected to the girder flange and 1.8 for girders supporting beams connected to the girder web, D_j is the same as previous, D_g is the effective moment of inertia of the girder per unit width, and L_g is the length of the girder.

When $B_j > L_g$, the mid-span girder deflection is reduced by $L_g / B_j \geq 0.5$, that is

$$\Delta_g{}' = \frac{L_g}{B_j} \Delta_g \qquad (1.13)$$

The effective weight for the combined mode is:

$$\mathrm{W} = \frac{\Delta_\mathrm{j}}{\Delta_\mathrm{j} + \Delta_\mathrm{g}} \mathrm{W}_\mathrm{j} + \frac{\Delta_\mathrm{g}}{\Delta_\mathrm{j} + \Delta_\mathrm{g}} \mathrm{W}_\mathrm{g} \qquad (1.14)$$

The effective weight for the combined mode of vibration is a function of the relative stiffness of the beam or joist to the girder and the effective weight of the beam or joist panel and the girder panel, where

$$W_j = w_j B_j L_j \text{ , the weight of the joist panel} \qquad (1.15)$$

and

$$W_g = w_g B_g L_g \text{ , the weight of the girder panel} \qquad (1.16)$$

If beams, joists, or girders are continuous over their supports and an adjacent span is greater than 70 % of the center span length, then the effective weight of that panel (W_j or W_g) can be increased 50% to account for continuity. While hot-rolled sections shear-connected to girder webs are acceptable for this, the joists connected only at their top chords are not. The shear connections for hot-rolled members provide enough stiffness to make the continuity adjustment, on the other hand, joists that are only connected by the top chord and girders that frame into columns are excluded from the continuity increase. The rule and value for the 50 % increase in effective weight seem to be based on engineering judgement as no reference is given. Thus, the basic reason for this study is to investigate the effect of the bottom chord extensions on continuity.

1.4 Previous Research

There have been many floor vibration research projects involving the acceleration response prediction, human perception and finite element analysis. Experimental and analytical studies related to this study are summarized in this section.

Gibbings (1990) investigated long span joists. He tested full scale single span composite joists to failure to evaluate their performances in elastic and inelastic ranges. He found that the finite element joist model was overly stiff if the members of a web-chord connection shared a common node, and introduced the joint eccentricities to more accurately model the load path from the chord member to the web member. He recommended that a more complete finite element model should be developed especially for nonlinear behavior. Traditionally, the effective moment of inertia of steel joists has been assumed to be 85% of the theoretical moment of inertia of the chords; however, Gibbings suggested that a more accurate prediction was needed to expand the research to predict vibration characteristics of these members.

Kitterman (1994) investigated the behavior of steel joists, joist-girders and the vibration characteristics of floors supported by them. He found that the effective moment of inertia of joist members is strongly dependent on the span-to-depth ratio of the member and in the range of 65-87% of I_{chords}. He developed an equation to calculate the effective moment of inertia of joist members based on test results and finite element modeling:

$$I_{eff} = \left(62.45 + 0.84\left(\frac{L}{D}\right)\right)\left(\frac{I_{chords}}{100}\right) \qquad (1.17)$$

where

L= length of the joist

D= depth of the joist

I_{chords}= moment of the inertia of the chords neglecting the web elements, in^4.

It is noted that Equation 1.17 was only valid for span-to-depth ratios between 10 and 24.

Kitterman also studied the effects of extending and restraining the bottom chords of joist members. Stiffness tests were performed to determine the load-deflection relationship of the vibration test floor. For one of the stiffness tests a small beam was welded to the columns of the support stands at the level of the girder bottom chords. The legs of the girder bottom chords were then welded to the beam section to provide stiffness and prevent displacement. It was found that the beams did not have sufficient stiffness to prevent the bottom chords from moving. To further restrain the bottom chords, ratchet binders were attached to the end of the bottom chords and the reaction floor and tensioned, which caused the frequency to increase slightly. Another test was performed to ascertain if the support stands were deflecting out of plane due to the thrust imparted by the girder seats. A dial gauge was placed at the web of the support beam and a heel drop executed. The deflection due to a heel drop was significant. To prevent out of plane movement of the support stands, braces were installed from the girder top chord at the seat to the reaction floor. Finally, the girder seats were welded to the top flange of the supporting member. The floor frequency increased slightly from these modifications on the joist bottom chords.

The task of restraining the bottom chords was found to be very difficult. The extended chord angles were very flexible and simply welding the chord ends to a column, wall, or the joist chords from an adjacent bay did not provide much restraint. The measured natural frequency also stayed the same even with the bottom chord ends restrained; that is, the floor stiffness did not increase. Therefore, extending the bottom chords of joist members was not recommended as a solution for a floor exhibiting annoying vibration or as a method of designing to prevent floor vibration (Kitterman 1994).

Hanagan (1994) studied the use of an active tuned mass damper to control annoying floor vibrations. She conducted experimental and analytical research implementing active control techniques to improve the vibration characteristics of problem floors. She introduced linear springs for the supports in her finite element computer model to match the measured natural frequencies.

Rottmann (1996) also studied the use of a tuned mass damper to control floor vibrations. In her computer model the beams and girders were all modeled as frame elements located in the same plane as the slab which was modeled with plate elements. She also used linear and rotational springs on the edges of the slabs to match the measured natural frequencies.

Band (1996) researched the vibration characteristics of joist and joist girder supported floors and helped develop the reduction factor used in calculating the effective moment of inertia for a joist. He updated the effective joist moment of inertia equation separating the round bar web and angle web joist designs considering Kitterman's conclusion that round bar web joist test data did not correlate well with the angle web joist test data:

$$I_{eff} = 0.8455\left(1 - e^{-0.28(L/D)}\right)^{2.8} I_{chords} \qquad \text{for angle web joists} \tag{1.18}$$

$$I_{eff} = \left[0.721 + 0.00725(L/D)\right] I_{chords} \qquad \text{for round bar web joists} \tag{1.19}$$

Band's results are incorporated into the Design Guide 11 with slight modifications. The effective moment of inertia of joists or joist girders is given as:

$$I_{\text{mod}} = C_r I_{chords} \tag{1.20}$$

In Equation 1.20, C_r is the modification factor that accounts for the reduction in the moment of inertia due to shear deformations and joint eccentricity in the web members of joists and joist girders:

$$C_r = 0.9\left(1 - e^{-0.28(L/D)}\right)^{2.8} \quad \text{for angle web joists } (6 \le L/D \le 24) \tag{1.21}$$

$$C_r = 0.721 + 0.00725(L/D) \quad \text{for round rod web joists } (10 \le L/D \le 24) \tag{1.22}$$

Also, the effective composite moment of inertia for joist supported tee-beams is going to be less than the fully composite moment of inertia of the entire cross section due to shear deformations and joint eccentricity (Band and Murray 1996). The effective composite moment of inertia of joist supported tee-beams is given as:

$$I_{eff} = \frac{1}{\dfrac{\gamma}{I_{chords}} + \dfrac{1}{I_{comp}}} \tag{1.23}$$

where

$$\gamma = \frac{1}{C_r} - 1 \tag{1.24}$$

I_{chords} = moment of inertia of the joist chords, in.^4

For the girders supporting joist seats, the moment of inertia is reduced because the joist seats are not stiff enough to allow the use of the full composite moment of inertia. The effective moment of inertia of joist girders supporting joist seats was recommended by Allen and Murray (1993) as:

$$I_g = I_{nc} + \left(I_c - I_{nc}\right)/4 \tag{1.25}$$

where

I_{nc} = non-composite moment of inertia

$$I_{nc} = I_{\text{mod}} = C_r I_{chords} \quad \text{for joist girder} \tag{1.26}$$

I_c = fully composite moment of inertia

$$I_c = I_{eff} \quad \text{for joist girder} \tag{1.27}$$

Band (1996) also investigated adding steel to the bottom chord of the joists and/or joist girders to increase the stiffness of the floor system. He added steel to the bottom chords (without any chord extensions) with two different methods. He used steel post-tensioned rods suspended from the bottom chords along the whole length of the chord. The tension load on the rod was increased at one-kip increments from one to ten kips. The results showed that the case where there was only one kip of post-tension force on the rod was the most efficient case as far as the increase in the natural frequency of the floor is concerned. He also increased the diameter of the rods and realized that as the weight and stiffness increase with the rods, there may be a point where the frequency comes to a maximum and then begins to decrease as larger rods are used. He concluded that the amount of increase in the frequency of the floor is very limited and will be of little benefit to correct floor vibrations. In another test series, the floor was jacked up and the rods were stitch welded to the bottom chords to provide the same amount of stress on the bottom chord and the added rods. There was better improvement on the natural frequency and the moment of inertia of the floor with the welded steel rods on the bottom chords. His finite element models matched his experimental results.

Beavers (1998) studied the use of a finite element program to model single-bay joist-supported floors with the intent of predicting the fundamental frequency of the floors. He researched finite element modeling techniques to model the joist supported floor systems. In his finite element model he used frame elements to model the entire truss of the joist. Rigid link elements were used to connect the top chord of the joists to the slab. This was the same type of model used by Kitterman (1994) and Band (1996) to determine the effective moment of inertia of steel joists (Figures 1.11 and 1.12). Beavers also used the joint eccentricities (introduced by Gibbings (1990)) on web member-chord member nodes (Figure 1.13). With this computer model, he was able to match the first bending natural frequency of the floors.

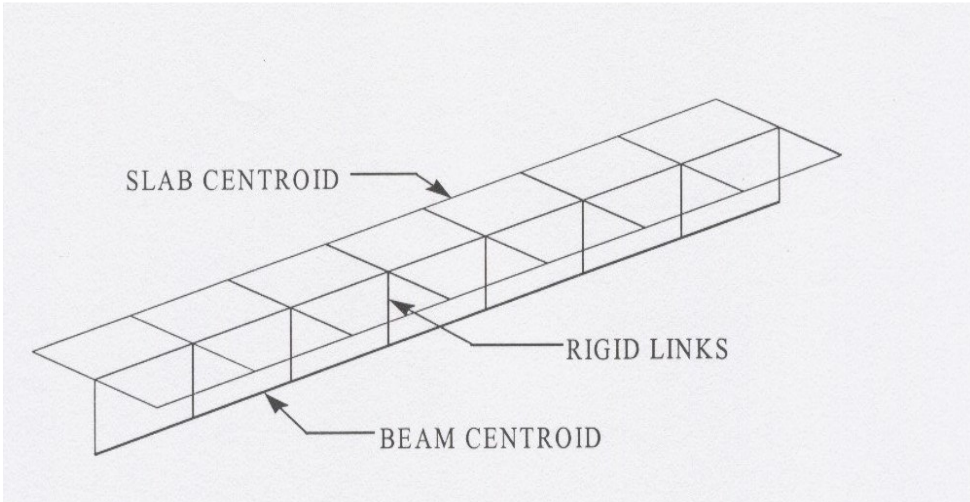

Figure 1.11 Hot-Rolled Beam- Slab Model (Beavers 1998)

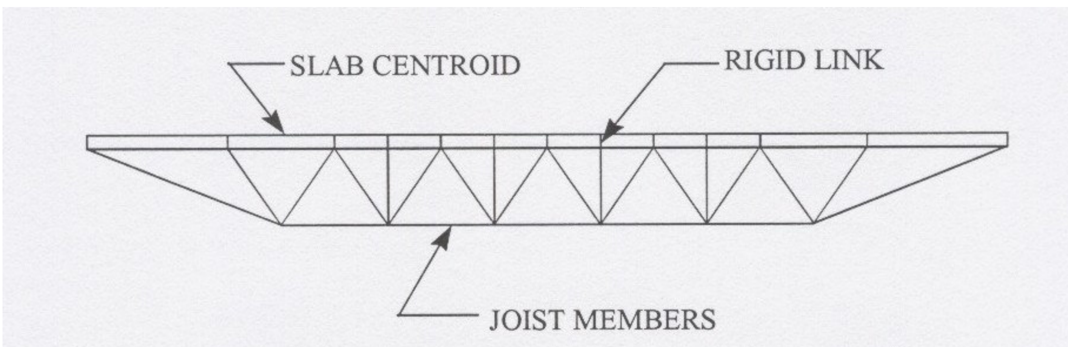

Figure 1.12 Full Joist- Slab Model (Beavers 1998)

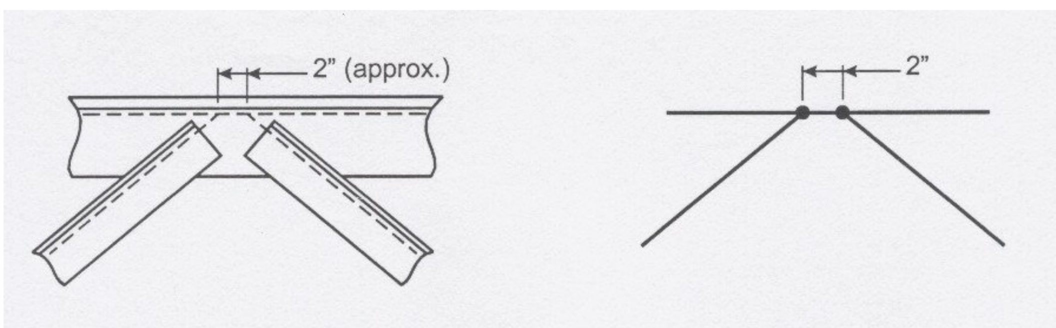

a) Web member- Chord member Node **b) Finite Element Model**

Figure 1.13 Joint Eccentricity (Beavers 1998)

Falati (1999) studied the effect of non-structural components to the overall dynamic behavior of pre-stressed concrete floors using a slender one-way, 50 % scaled post-tensioned concrete slab (3ft by 17 ft). He found that the increase in the pre-stressing force increases the natural frequency and decreases damping of the system. From his human-structure interaction tests, he observed that humans contribute to the damping of the floor systems. However, as far as the non-structural elements are concerned he concluded that contrary to popular belief, the presence of non-structural elements does not necessarily improve the dynamic behavior of floors; the nature of their installation is the key issue.

Sladki (1999) investigated the use of a finite element software to predict the natural frequency of a floor system as well as its predicted peak acceleration. He introduced joist seat elements in his finite element model (Figure 1.14). He concluded that using a finite element program to model a floor system is an efficient tool for prediction of the natural frequency of a floor system, but insufficient for the prediction of the peak acceleration.

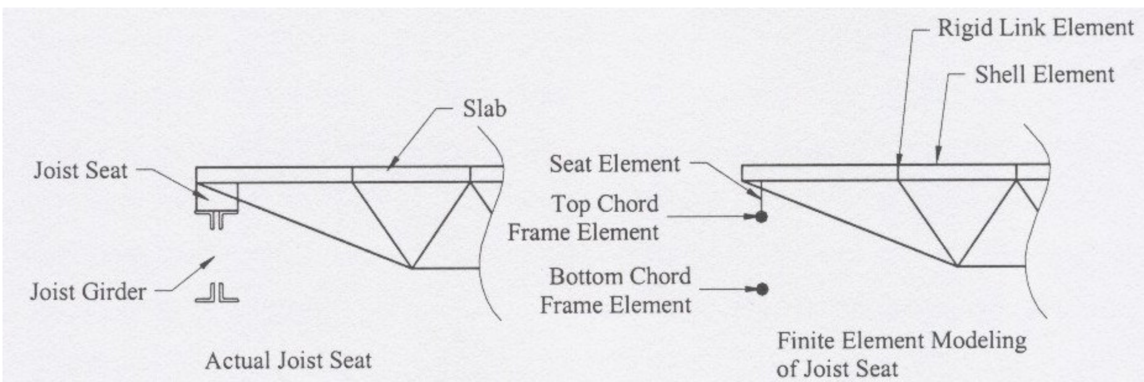

Figure 1.14 Joist Seat Model (Sladki 1999)

Alvis (2001) concentrated on the prediction of the peak accelerations in his study. He investigated finite element modeling techniques and conducted modal analyses. The damping values and the peak accelerations did not match very well. He suggested that the error is due to the fact that the finite element software did not directly account for frictional damping in systems and it can not account for energy dispersion.

Warmoth (2002) studied the effect of joist seats on the effective girder moment of inertia and girder frequency. He found that Equation 1.25 depended largely on the joist type and seat connection type used. He proposed a new calculation for the girder moment of inertia based on the joist type and seat connection type. He also did a cost efficiency analysis comparing composite and non-composite floor systems.

Jackson (2002) researched the properties of castellated beams with respect to vibrations. His research confirmed the accuracy of the Design Guide-11 prismatic beam procedures when applied to castellated beams.

Boice (2003) studied different methods of predicting the first bending natural frequency and the response of floor systems in comparison to measured data. He also compared acceptability criteria used in the United States and the United Kingdom. He concluded that the procedure outlined in the AISC/CISC Design Guide 11 is an effective method for the prediction of the fundamental frequency and peak acceleration of a floor system.

Ritchey (2003) studied the effectiveness of tuned mass dampers that incorporate semi-active magneto-rheological fluids as an effective means to reduce floor vibrations. He conducted experimental modal analysis to verify the effectiveness of a commercial Pendulum Tuned Mass Damper (PTMD) in reducing floor vibrations.

Perry (2003) conducted a study on computer modeling techniques to predict the response of floor systems due to walking. He used five different methods in an attempt to determine the source of discrepancies between the finite element program and the Design Guide 11 method. He concluded that the effective mass difference between the two methods is the source of discrepancy in peak acceleration prediction.

1.5 Need For Research

The effect of bottom chord extensions on the vibrations of joist supported floor systems is largely unknown. Further research on joist bottom chord extensions can provide valuable information to design joist supported floor systems without annoying vibrations.

This dissertation is a result of an extensive experimental and analytical study conducted on single span and three span joist supported laboratory footbridges with different bottom chord extension configurations. The purpose is to study the effect of bottom chord extensions on deflections, natural frequency, damping, mode shape and effective mass characteristics of the joist supported footbridges.

The experimental setup and finite element modeling are presented in Chapter 2. In Chapter 3, the stiffness test results (midspan point loading and 20 psf distributed loading) are discussed. Vibration test results and experimental modal analysis are presented in Chapter 4. In Chapter 5, conclusions are drawn. Appendix A contains the joist dimensions of the single span and three span footbridges, while Appendix B contains sample Design Guide 11 calculations. The detailed stiffness test results of the three span footbridge are presented in Appendix C. Appendices D and E include data from modal testing conducted on the single span and three span footbridges, respectively.

.

CHAPTER 2

EXPERIMENTAL SETUP AND FINITE ELEMENT MODELING

2.1 Introduction

The primary objective of this research is to investigate the effect of bottom chord extensions on load-deflection behavior, natural frequency, damping, mode shape and effective mass characteristics of non-composite joist supported floors. To determine the effects of bottom chord extensions, stiffness and vibration tests are performed on two laboratory footbridges.

2.2 Steel Joist Basics

A steel joist is made up of a top chord, a bottom chord and web members between the chords (Figure 2.1). The web members are welded to chords unlike an ideal truss where members are connected by frictionless pins. For non-composite joists, the composite effect of the steel and concrete acting together is neglected. For composite joists, the top chords are designed for non-composite action before the concrete has cured and for composite action after the concrete has cured. The top chord resists the construction loads and weight of the wet concrete, forming the compressive force component of the moment developed in the truss. After the concrete has hardened, the horizontal shear force is transferred through the shear screws or shear studs into the concrete.

For either joist type, the bottom chord provides the tensile force component of the moment developed in the truss. The entire vertical shear is carried by the web members of a truss since neither chords nor the concrete slab resists any vertical shear. For floor vibration computations, a non-composite section is treated as composite since the levels of stresses and strains due to human induced floor vibrations are very low.

Figure 2.1 Steel Joist Member

2.3 Experimental Setup

A single span footbridge (Figure 2.2) and a three span footbridge (Figure 2.3) were constructed at the Structures and Materials Research Laboratory, Virginia Tech, Blacksburg, Virginia. The single span footbridge (7 ft by 30 ft) was built inside the laboratory, while the three span footbridge (7 ft by 90 ft) was built outside. Both of the footbridges were constructed using 1.5VL Vulcraft deck (depth=1.5 in.) and a 4.5 in. normal weight concrete slab (total slab depth= 6.0 in., Figure 2.4) supported on two parallel lines of 30K7 x 30 ft span, non-composite, Vulcraft joists at 4 ft on center.

Stand-off screws were used to connect the cold-formed steel decks to joist top chords before the concrete was placed (Figure 2.5). The 28-day concrete compressive strengths are 4320 psi for the single span footbridge and 5000 psi for the three span footbridge. For floor vibration computations the modulus of elasticity of concrete is taken as $1.35E_c$ (dynamic concrete modulus of elasticity), as recommended in Design Guide-11. Thus,

For Single Span Footbridge:

$w_{concrete}$= 142 lb/ ft^3

f_c'= 4317 psi = 4.317 ksi

$$E_c = w^{1.5}\sqrt{f'_c} = (142.32)^{1.5}\sqrt{4.317} = 3528 ksi$$

$$Dynamic E_c = 1.35 w^{1.5}\sqrt{f'_c} = 4762 ksi$$

Total Weight= 13986 lbs

For Three Span Footbridge:

$w_{concrete}$= 138 lb/ ft^3

f_c'= 4954 psi = 4.954 ksi

$$E_c = w^{1.5}\sqrt{f'_c} = (138.00)^{1.5}\sqrt{4.954} = 3608ksi$$

$$Dynamic E_c = 1.35w^{1.5}\sqrt{f'_c} = 4871ksi$$

Total Weight= 40824 lbs

Figure 2.2 Single Span Floor (7 ft x 30 ft)

Figure 2.3 Three Span Floor (7 ft x 90 ft)

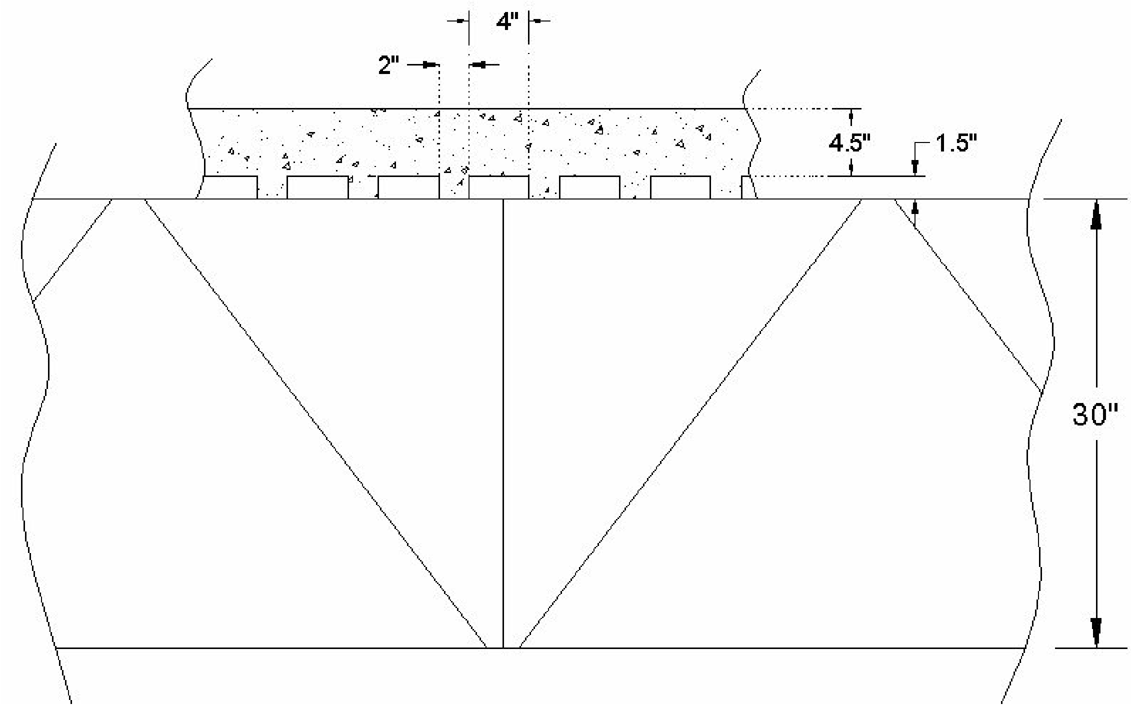

Figure 2.4 Steel Joist Member

Figure 2.5 Stand-off Screws Connect Steel Decks to Joist Top Chords

Two concrete walls were used as supports for the single span bridge as shown in Figure 2.2. The joists were welded to the bearing plates located on the concrete walls (Figure 2.6). The same bearing walls were used for the exterior supports of the three span footbridge, with built-up cross sections used for interior supports (Figure 2.7). At the interior supports, the two top chords were welded to each other using a steel bar to provide top chord continuity. The top chords were also welded to the continuity plates located on the interior supports (Figure 2.8). Bottom chord continuity was provided by the bottom chord extensions which are HSS 1.5 x 1.5 x 3/16 cross sections. The bottom chord extensions were constructed as load cells through which the amount of axial load on the member was monitored and recorded (Figures 2.9 and 2.10). Two of the four bottom chord extensions of the single span footbridge (S1 and S2 in Figure 2.11) and all of the twelve bottom chord extensions of the three span footbridge (Figure 2.12) were instrumented as load cells. During the stiffness tests, a Measurements Group System 6000 data acquisition system was used to monitor and record the load data. To determine the effect of bottom chord extensions on stiffness and vibration characteristics, both the single span and three span footbridges were tested with different bottom chord extension configurations (Figures 2.13 and 2.14). Stiffness and vibration tests were repeated for each stage after the modifications of the joist bottom chords. Joist cross section properties are shown in Appendix A.

The tested bottom chord configurations for the single span footbridge are:

Stage 1) Bottom chord extensions in place

Stage 2) Bottom chord extensions removed

Stage 3) Bottom chord extensions re-installed

The tested bottom chord configurations for the three span footbridge are:

Stage 1) All bottom chord extensions in place

Stage 2) Exterior bottom chord extensions removed

Stage 3) All bottom chord extensions removed

Stage 4) Interior bottom chord extensions re-installed

Stage 5) All bottom chord extensions re-installed

Exterior bottom chord extensions are the ones that are connected to the concrete walls on the two exterior supports (Extensions N1, S1, N6 and S6 in Figure 2.12). Interior bottom chord extensions are the ones connected to the interior supports (Extensions N2, S2, N3, S3, N4, S4, N5 and S5 in Figure 2.12). The three stages of the single span footbridge and the five stages of the three span footbridge include all the bottom chord extension configurations needed to compare the two cases: removing the bottom chord extension elements from the structure and re-installing them to an existing structure when the concrete slab is already in place and cured.

Figure 2.6 Joist Seat Welded to Bearing Plate on Concrete Wall

Figure 2.7 Three Span Floor Supports

Figure 2.8 Top Chord Continuity at Interior Supports

Figure 2.9 Exterior Bottom Chord Extensions

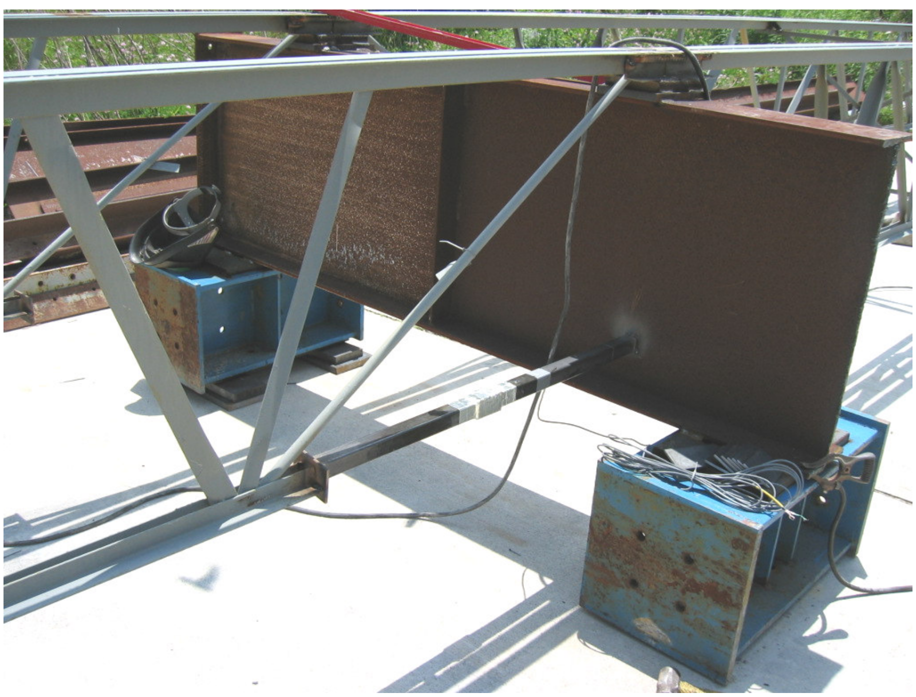

Figure 2.10 Interior Bottom Chord Extension

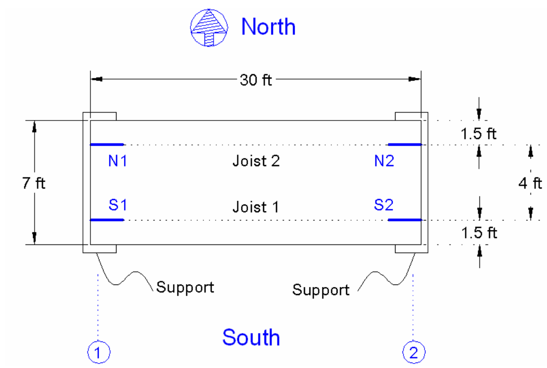

Figure 2.11 Load Cell Configurations- Single Span Footbridge

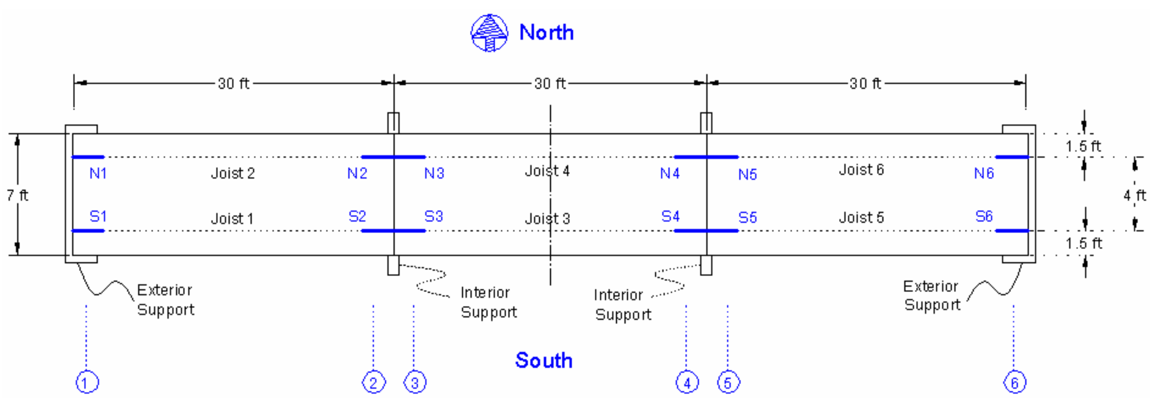

Figure 2.12 Load Cell Configurations- Three Span Footbridge

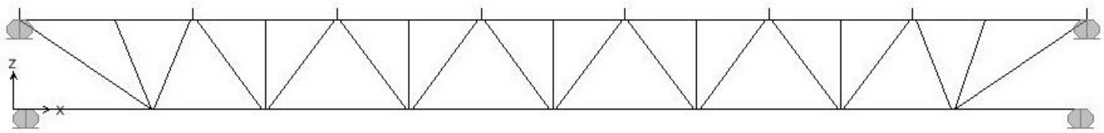

a) Stage 1: Bottom Chord Extensions In Place

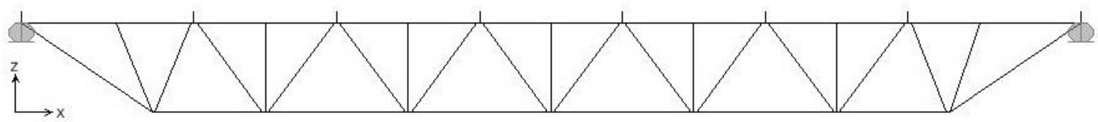

b) Stage 2: Bottom Chord Extensions Removed

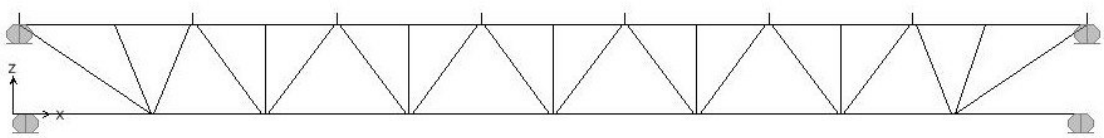

c) Stage 3: Bottom Chord Extensions Re-installed

Figure 2.13 Bottom Chord Extension Configurations for Single Span Footbridge

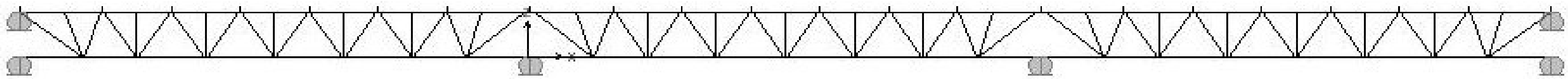

a) Stage 1: All Bottom Chord Extensions In Place

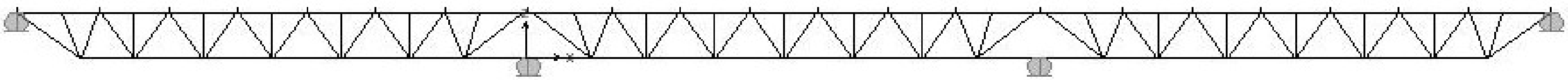

b) Stage 2: Exterior Bottom Chord Extensions Removed

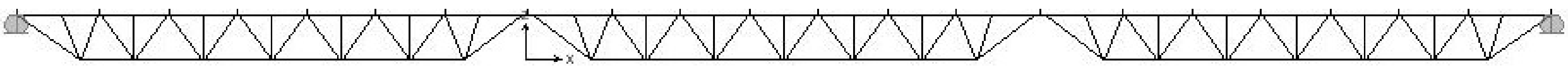

c) Stage 3: All Bottom Chord Extensions Removed

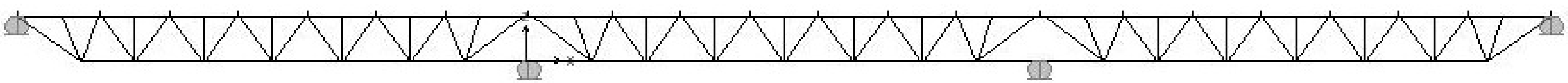

d) Stage 4: Interior Bottom Chord Extensions Re-installed

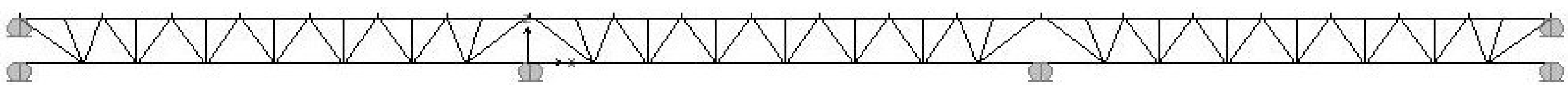

e) Stage 5: All Bottom Chord Extensions Re-installed

Figure 2.14 Bottom Chord Extension Configurations for Three Span Footbridge

2.4 Finite Element Modeling

2.4.1 Steel Beam and Joist- Concrete Slab Systems

Three finite element modeling techniques have been used to simulate the steel beam and joist- concrete slab floor systems and they have been successful to some extent. The first type of finite element model is the in-plane model where the slab and supporting beams lie in the same plane. In that case, the moment of inertia of the beam is input as the total transformed moment of inertia of the single-tee beam, minus the moment of inertia of the slab. All the girders and beams are modeled as frame elements and placed in the same plane as the concrete slab which is modeled with shell elements (Figure 2.15). Hanagan (1994), Rottmann (1996) and Perry (2003) used this technique in their studies.

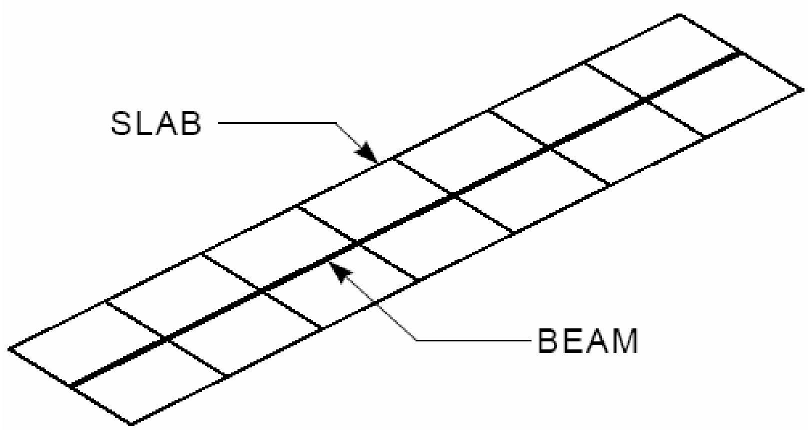

Figure 2.15 The In-Plane Model

The next type of finite element model is to place the beams and slabs at the elevation of their centroidal axes and link them together with rigid link members (Figure 1.11). This model has more degrees of freedom, elements and nodes than the previous model, however it is more realistic since the distance between the slab and beam centroids varies from design to design. This technique was used by Shamblin (1989) in her analyses.

The full joist-slab model is another type of finite element model where the entire truss of the joist is input by frame elements. Rigid links are used to connect the top chord of the joists to the concrete slab (Figure 1.12). This technique was used by Kitterman (1994), Band (1996), Beavers (1998) and Sladki (1999). It is the most useful method of the above three models since it is allows the user to investigate the separate behavior of a joist or a specific joist member in composite action with the concrete slab. The model can be modified easily for addition or removal of any members and the effect of any joist member can be analyzed under static and dynamic loading.

The full joist-slab model is used in this study, as it is the only method to accurately investigate the effect of bottom chord extensions analytically.

2.4.2 Finite Element Modeling of the Laboratory Footbridges

Three dimensional finite element models of the footbridges were created using a commercial software program. SAP2000 Nonlinear Version 8.3.3 was used for this study for the simulation of all stiffness and vibration tests. The program has a user friendly graphical interface and it can perform both static and dynamic analyses of structures.

In this study, frame elements are used to model the chords and the truss elements of the joists. Joint eccentricities are taken into consideration for the web member-chord nodes. The concrete slab is modeled with shell elements and connected to top joist chords with rigid links as described by Beavers (1998) and Sladki (1999). However, the use of fixed-fixed rigid links on every node of the joist top chords resulted in discrepancies between the measured deflections from stiffness tests and natural frequency values from vibration tests. Thus, the moment is released on the slab end of the links while the top chord ends of the links remain fixed. Also, rigid links are introduced on every other node of the joist top chord (Figure 2.16). All the chords and the web members of the trusses are pin-connected to each other.

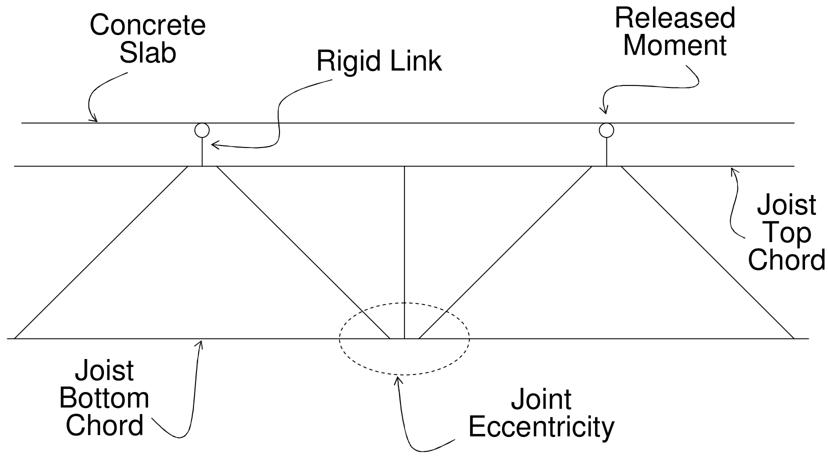

Figure 2.16 Rigid Link Model

Using the data obtained from stiffness and vibrations tests, the finite element models were adjusted. After every stiffness test series, the models were updated to match the latest and also all the previous measured deflections and bottom chord extension force records. In the same way, after every vibration test series, the models were adjusted to match the measured natural frequencies. Matching measured deflections, bottom chord extension forces and natural frequencies at the same time for a specific bottom chord extension configuration was a very complex process. The addition or removal of bottom chord extensions theoretically results in “different” structures with different stiffness and vibration properties. The finite element model has to account for all these changes (all stages shown in Figures 2.13 and 2.14). Using common support conditions like rollers and pins in the finite element model does not yield satisfactory results for these requirements. For that purpose, linear and rotational springs are introduced to the finite element models to match the measured deflections, bottom chord extension forces and natural frequencies. Hanagan (1994) and Rottmann (1996) also used linear and rotational springs in their finite element models to match their experimental data.

The rotational and translational springs shown in Figure 2.17 were used to match the stiffness test results for the bare joists and joists with cured concrete, for all bottom chord extension configurations. The SAP2000 finite element models of bare single span and three span footbridges are shown in Figures 2.18 and 2.19. In Figure 2.20 the deflected shapes of three span footbridge joists are displayed under wet concrete loading. The deflected shape of a composite three span footbridge under 20 psf distributed loading is shown in Figure 2.21.

The finite element modeling technique discussed above was used in the analyses of the footbridges under static loading (Chapter 3) and dynamic loading (Chapter 4).

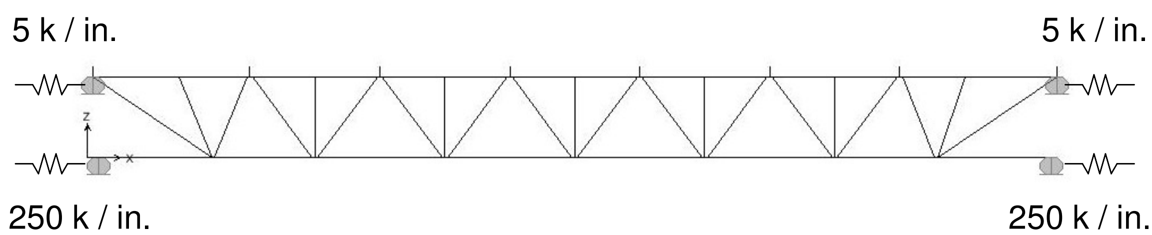

(a) Single Span Footbridge Model

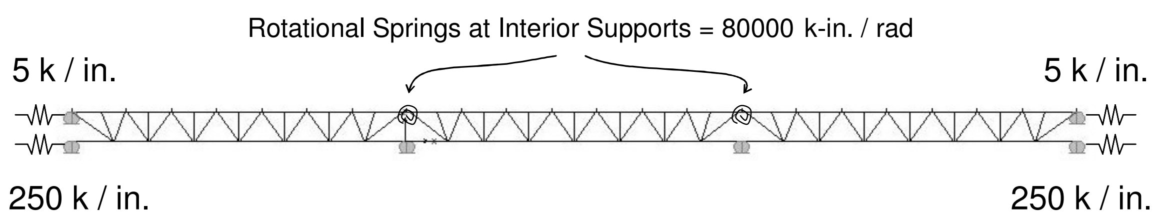

(b) Three Span Footbridge Model

Figure 2.17 Final Finite Element Models for Laboratory Footbridges

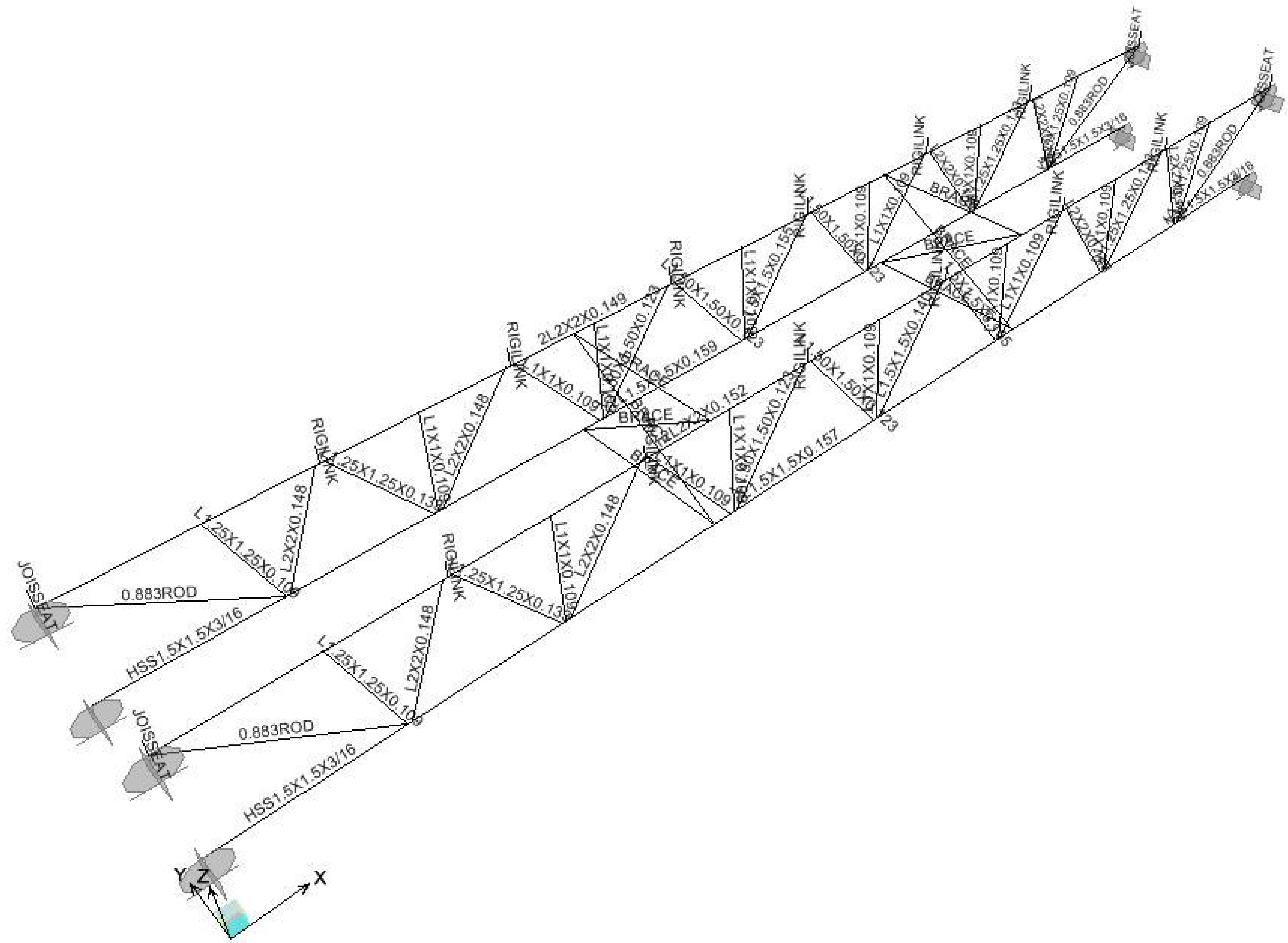

Figure 2.18 Single Span Laboratory Footbridge in SAP2000

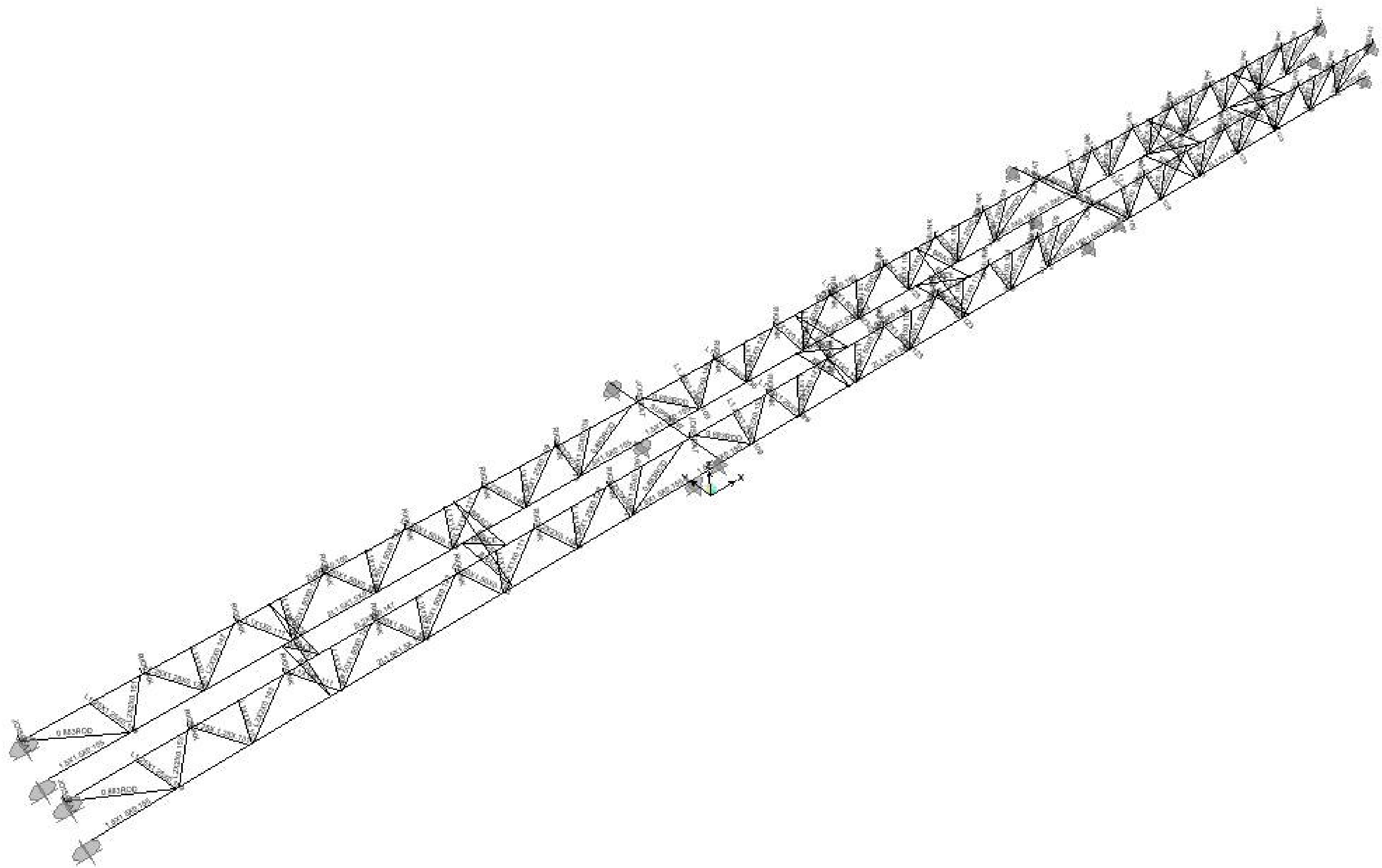

Figure 2.19 Three Span Laboratory Footbridge in SAP2000

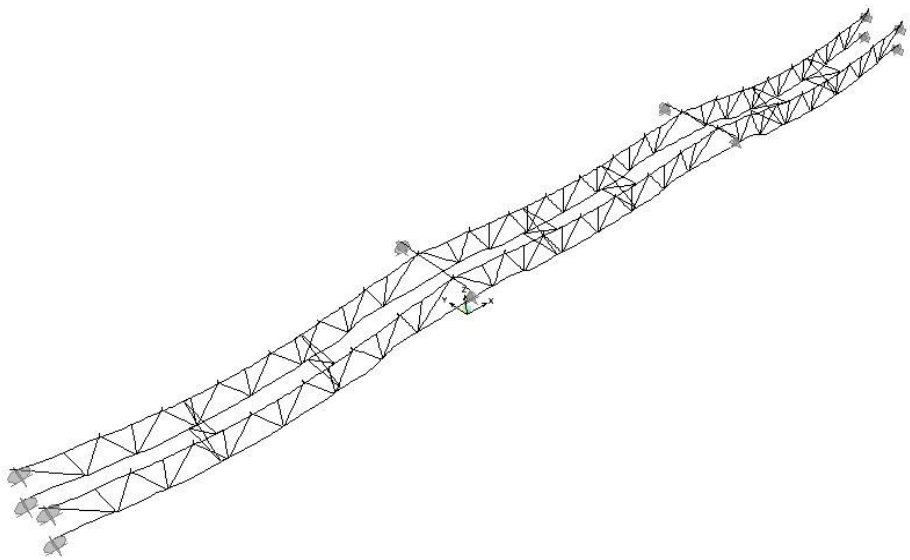

Figure 2.20 Three Span Laboratory Footbridge- Bare Joists Under Wet Concrete Loading

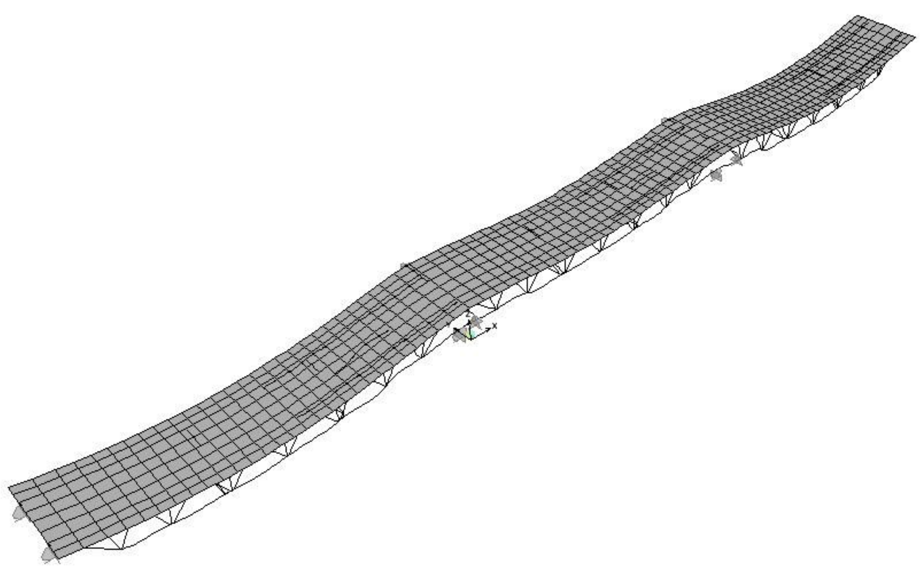

Figure 2.21 Three Span Laboratory Footbridge- Cured Concrete- 20 psf Distributed Loading

CHAPTER 3
STATIC TESTING: STIFFNESS TEST RESULTS

3.1 Introduction

The effective moment of inertia is one of the variables that affects the natural frequency and acceleration response characteristics of joist supported floor systems. The objective of stiffness testing is to determine the effective moment of inertia of the joist members with different bottom chord extension configurations with and without the concrete slab. For that purpose the footbridges were loaded with point and uniformly distributed loads.

3.2 Stiffness Testing Procedure

To experimentally determine the properties of the bare joists, the joists were loaded at midspan as shown in Figure 3.1. Rectangular steel plates were placed in stacks to simulate "point" loading and vertical deflections were measured by dial gages placed under the bottom chords at the joist midspans (Figure 3.2). The deflections and bottom chord extension forces were monitored and recorded at 100 lb increments up to 600 lb on each joist.

For both of the footbridges, the concrete was poured (Figure 3.3) with all the bottom chord extensions in place. The wet concrete was equivalent to a uniformly distributed load pattern on the bare joists. Midspan deflections and bottom chord extension forces due to the weight of the wet concrete were measured and recorded.

Figure 3.1 Midspan Point Loading- Bare Joists

Figure 3.2 Deflection Measurements

Figure 3.3 Three Span Footbridge- Concrete Pour

When the concrete was cured, the midspan point loading tests were repeated with all bottom chord extensions in place (Figure 3.4). Then, a 20 psf uniformly distributed load was applied to the footbridges. Steel bars (1.0 in. diameter) were used for loading. The steel bars were welded to each other in groups of eight to facilitate handling. The number and pattern of the steel bars were arranged to produce a 20 psf uniformly distributed loading. An overhead crane was used to place the steel bars for the single span footbridge; a forklift was used for the three span footbridge since it was built outdoors (Figures 3.5 and 3.6). Deflections and bottom chord extension forces were recorded.

Figure 3.4 Midspan Point Loading- Cured Concrete

Figure 3.5 Three Span Footbridge- A Forklift was used for 20 psf Uniformly Distributed Loading

Figure 3.6 Three Span Footbridge- 20 psf Uniformly Distributed Loading

The above procedures for point loading and distributed loading were repeated for all the bottom chord extension configurations as described in Section 2.3 and summarized in Figures 2.12 and 2.13.

3.3 Analytical Predictions and Comparison of Results

3.3.1 Single Span Footbridge

To determine the effect of the bottom chord extensions on joist stiffness, the stiffness test results are compared to the finite element model results and predictions from basic mechanics. When the joist bottom chord extensions are not in place, the joist member is assumed to behave like a simply supported beam as shown in Figures 3.7a and 3.7b. When the bottom chord extensions are in place, the member is expected to have more stiffness and approach the fixed-fixed conditions shown in Figures 3.7c and 3.7d.

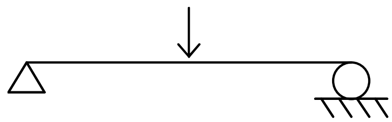

$$\Delta_{Midspan} = \frac{PL^3}{48EI}$$

a) Simple Span- Point Load

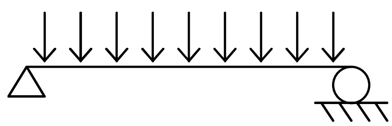

$$\Delta_{Midspan} = \frac{5wL^4}{384EI}$$

b) Simple Span- Uniform Loading

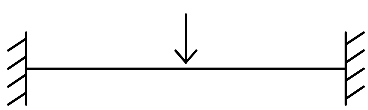

$$\Delta_{Midspan} = \frac{PL^3}{192EI}$$

c) Fixed-Fixed Span- Point Load

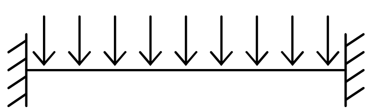

$$\Delta_{Midspan} = \frac{wL^4}{384EI}$$

d) Fixed-Fixed Span - Uniform Loading

Figure 3.7 Single Span Beam- Midspan Deflections from Mechanics

In Figure 3.8, midspan point load versus vertical midspan deflection results are compared to mechanics and finite element model predictions for various load stages for the single span footbridge. The cross sectional property calculations (bare and composite joists) are displayed in Appendix B. The mechanics deflections were calculated using the Design

Guide 11 procedure using C_r=0.8455 as determined from the original C_r research (Band 1996).

Figures 3.8a and 3.8b show results from the bare joist concentrated load tests, along with the analytical predictions. Since the North and South joists have slightly different properties, measured and finite element results are shown for each joist. The average of the calculated moments of inertia was used for the mechanics predictions.

Figure 3.8a shows excellent agreement between the measured and predicted deflections for the South joist. The measured North joist deflections are approximately 13% larger than the mechanics prediction and also 6 % larger than the finite element prediction at maximum loading.

Figure 3.8b shows that the deflections decreased somewhat with the bottom chord extensions installed, but nowhere near those for the fixed end condition. The measured deflections are approximately 80% of the mechanics predicted simple span deflection and 320% of the corresponding fixed condition. It is noted that the measured deflections of the North and South joists are nearly identical.

Figures 3.8c, 3.8d and 3.8e show the average measured and predicted deflections for midspan loading tests after the concrete was poured and cured. With the bottom chord extensions in place, the measured deflections are 76% of the mechanics simple span deflections and 88 % of the finite element deflections. With the bottom chord extensions removed, there is excellent agreement between the three sets of predictions, although the mechanics predictions are slightly less at maximum loading.

Figure 3.8e shows the deflections for a test after the footbridge was jacked up approximately 0.5 in. and the bottom chord extensions re-installed. There is excellent agreement between the measured and the finite element predicted deflections. The measured deflections at the maximum loading are approximately 88% of the mechanics deflections.

In summary, the deflections at maximum loading increased from 0.025 in. to 0.037 in. (48% increase) when the bottom chord extensions were removed and decreased to 0.029 in. when they were re-installed. For reference, the corresponding predicted mechanics fixed end deflection is 0.008 in.

Figures 3.9a, 3.9b and 3.9c show the average measured and predicted deflections for 20 psf uniform loading tests after the concrete was poured and cured. The behavior is similar to the midspan point loading case. Figure 3.9a shows the case where the bottom chord extensions were installed prior to the concrete pour. With the bottom chord extensions in place, the measured deflections are 77% of the mechanics simple span deflections and 93% of the finite element deflections. The measured deflections are nearly four times the predicted fixed-fixed deflections.

Figure 3.9b shows that, with the bottom chord extensions removed, there is excellent agreement between the measured deflections and mechanics predictions. The finite element model results are slightly less at maximum loading. It is also shown in Figure 3.9b that when the bottom chord extensions are taken out, the deflections increase around 24 % with respect to Figure 3.9a.

Figure 3.9c shows the deflections for a test after the footbridge was jacked up approximately 0.5 in. and the bottom chord extensions re-installed. There is excellent agreement between the measured and the finite element predicted deflections. The measured deflections at the maximum loading are approximately 80% of the mechanics deflections.

In summary, the deflections at maximum loading increased from 0.0545 in. to 0.0675 in. (24% increase) when the bottom chord extensions were removed and decreased to 0.057 in. when they were re-installed. For reference, the corresponding predicted mechanics fixed end deflection is 0.014 in.

It is realized that re-installing the bottom chord extensions (system jacked-up) to the joists of the single span footbridge with cured concrete helps to reduce the uniform load deflections to some extent (Figure 3.9c), but not as much as placing the bottom chord extensions before the concrete pour (Figure 3.9a).

From both point and uniform stiffness test results of the single span footbridge, it was found that installing the bottom chord extensions before the concrete pour results in less deflection than when they are installed after the concrete is cured. But it is nowhere near the fixed end case.

In Figures 3.10a and 3.10b, data from instrumented bottom chord extension, one end of the South joist is shown. Midspan point loading versus bottom chord extension force compared to finite element model and mechanics predictions is displayed. It is seen that the measured data is linear and the force in the bottom chord extensions before the members are removed is close to the force after re-installing the members. The force in the bottom chord extension is approximately 25% greater than the predicted force at the maximum loading. Also, the measured force at maximum loading is approximately 68% of the mechanics force for both Figures 3.10a and 3.10b.

In Figures 3.11a and 3.11b, 20 psf uniform loading versus bottom chord extension force compared to finite element model and mechanics predictions is displayed. It is seen that the force in the bottom chord extensions before the members are removed is greater than the force after re-installing the members. At the maximum loading, the force in the bottom chord extension is approximately 24% greater than the predicted force in Figure 3.11a, while it is almost the same as the predicted force in Figure 3.11b. Also, at the maximum loading, the force in the bottom chord extension is approximately 65% of the mechanics force in Figure 3.11a, while it is approximately 52% of the mechanics force in Figure 3.11b.

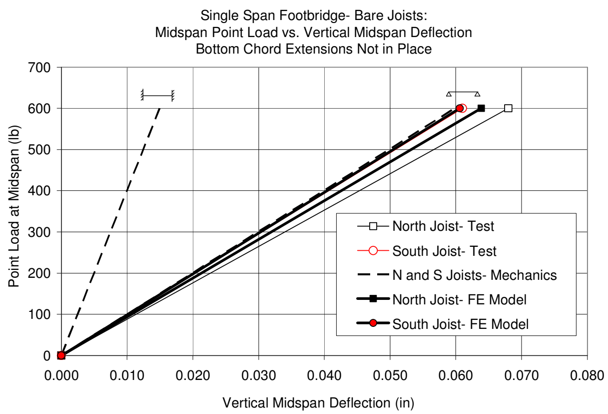

a) Bare Joists- No Bottom Chord Extensions in Place

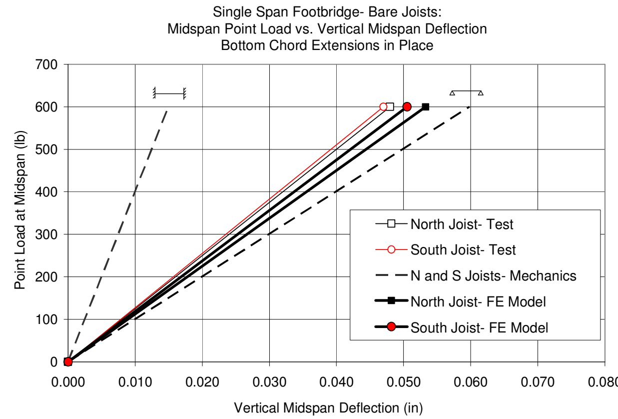

b) Bare Joists- Bottom Chord Extensions Installed

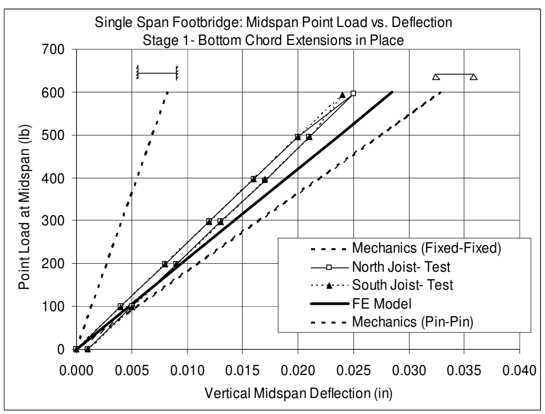

c) Cured Concrete- Stage 1: Bottom Chord Extensions In Place

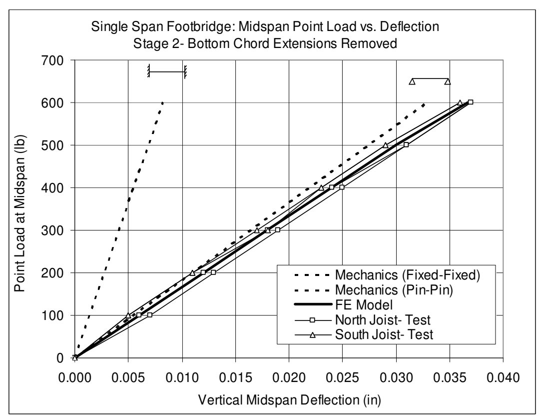

d) Cured Concrete- Stage 2: Bottom Chord Extensions Removed

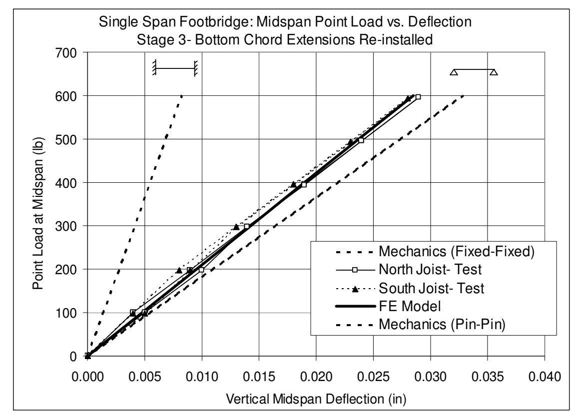

e) Cured Concrete- Stage 3: Bottom Chord Extensions Re-installed

Figure 3.8 Single Span Footbridge- Midspan Point Loading versus Midspan Deflection

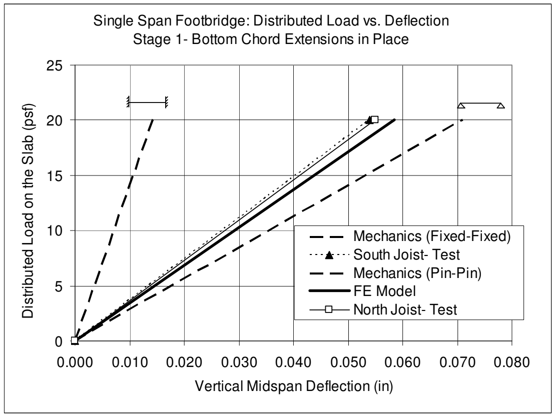

a) Cured Concrete- Stage 1: Bottom Chord Extensions In Place

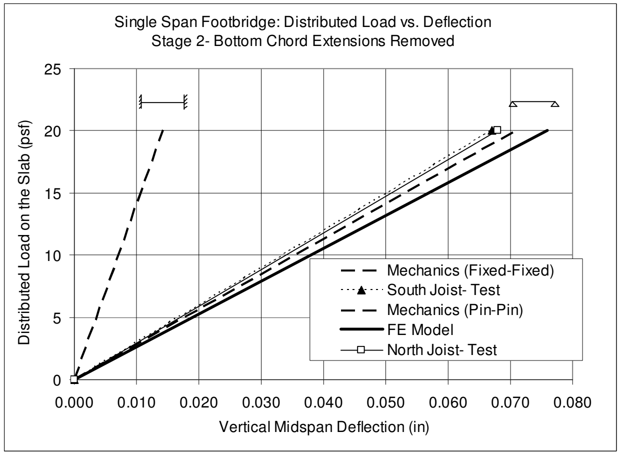

b) Cured Concrete- Stage 2: Bottom Chord Extensions Removed

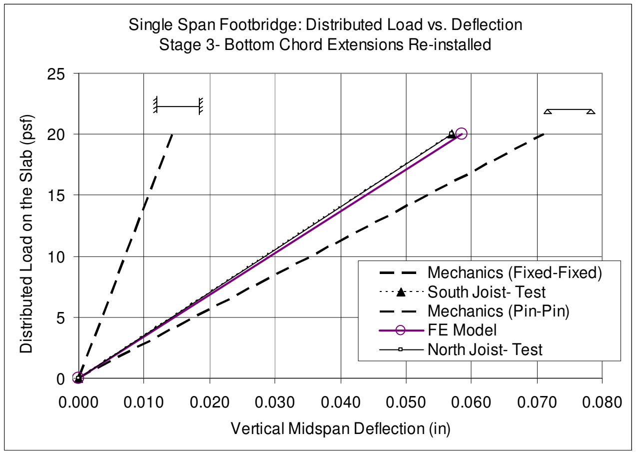

c) Cured Concrete- Stage 3: Bottom Chord Extensions Re-installed

Figure 3.9 Single Span Footbridge- Uniform Loading versus Midspan Deflection

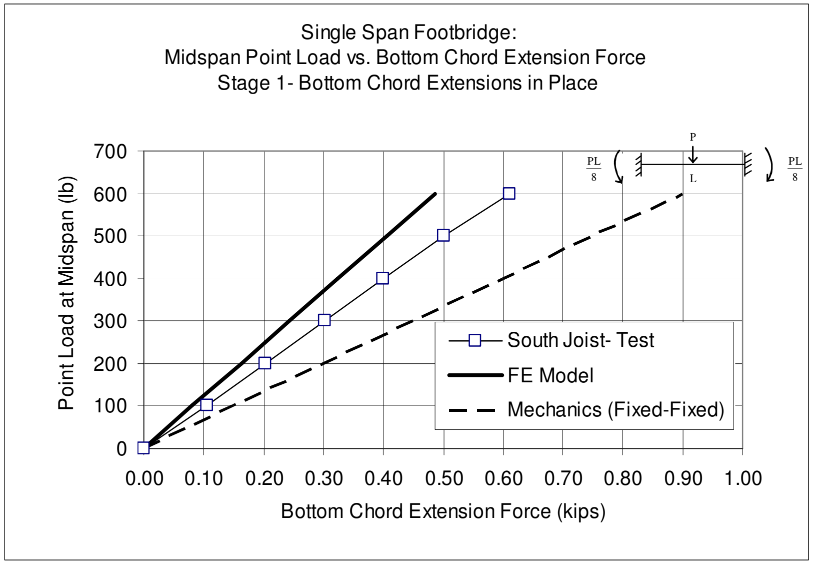

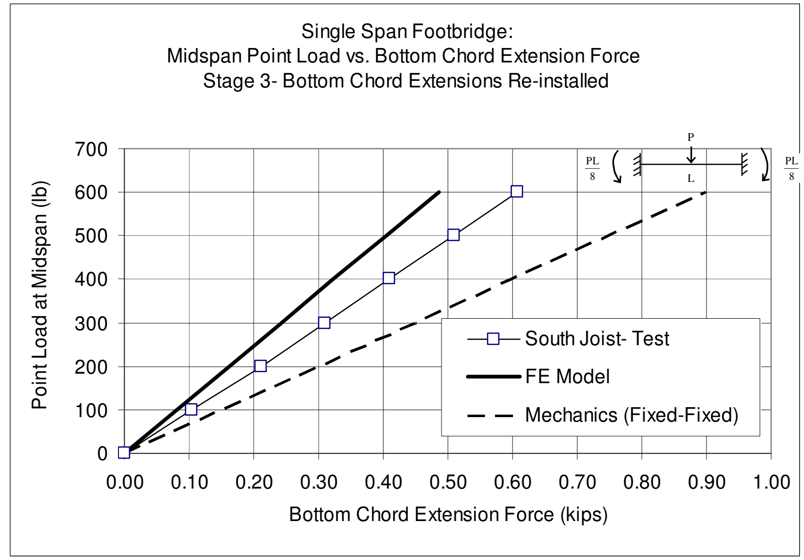

a) Cured Concrete- Stage 1:
Bottom Chord Extensions In Place

b) Cured Concrete- Stage 3:
Bottom Chord Extensions Re-installed

Figure 3.10 Single Span Footbridge- Midspan Point Loading versus Bottom Chord Extension Force

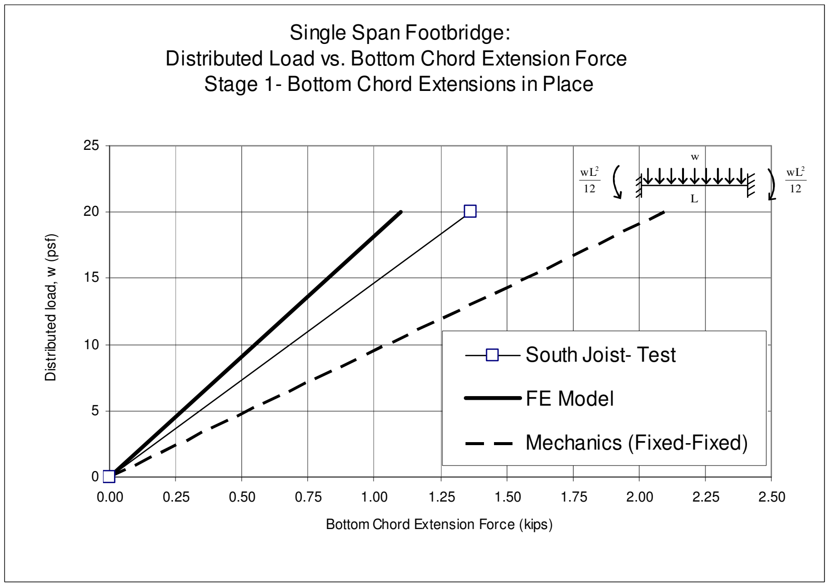

a) Cured Concrete- Stage 1:
Bottom Chord Extensions In Place

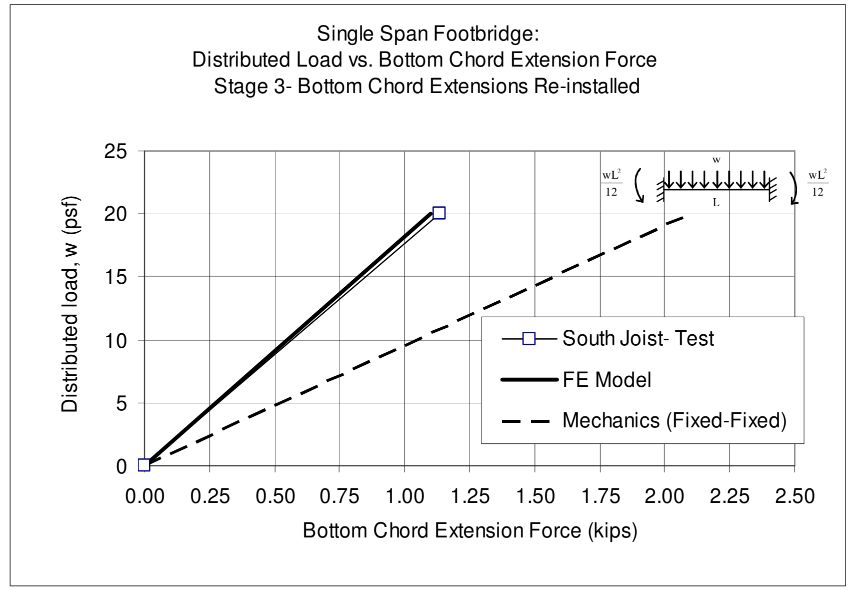

b) Cured Concrete- Stage 3:
Bottom Chord Extensions Re-installed

Figure 3.11 Single Span Footbridge- Uniform Loading versus Bottom Chord Extension Force

3.3.2 Three Span Footbridge

Stiffness test results for the three span footbridge are found in Appendix C and summarized in Figures 3.12 through 3.20. Locations of the twelve instrumented bottom chord extensions (N1 through N6 and S1 through S6) and joists are shown in Figure 2.12. The effect of bottom chord extensions on midspan point loading deflections is displayed in Figures 3.12 to 3.14. It is realized that the deflections due the midspan point loading are reduced around 20% when both exterior and interior bottom chord extensions are in place. The effect of bottom chord extensions on 20 psf uniformly distributed loading deflection are shown in Figures 3.15 to 3.17. The deflections due to the 20 psf UDL loading are reduced around 30% on the outside bays and about 10% on the interior bay when both exterior and interior bottom chord extensions are in place. Finite element results for the point and 20 psf loading are presented in Figures 2.21 to 26.

In Figures 3.18 to 3.20, 20 psf uniformly distributed loading versus bottom chord extension force are shown for Stages 1 and 5. The bottom chord extension forces were observed to be unstable during the distributed loading tests for the three span footbridge. Considering the fact that distributed loading of the three span footbridge took more time than for the point loading case and involved two graduate students constantly walking and moving the steel bars on the bridge (Figure 3.5), the amount of load on the bottom chord extensions did not remain constant. Since the structural system of the footbridge involves many members (truss web members), the distribution of the applied and removed loads in the system also affected the collected data. This is why the monitored load on the bottom chord extensions did not return to zero after the removal of the distributed load, in Figures 3.18-3.20 and other load cell plots in Appendix C.

It is found that re-installing the bottom chord extensions to the joists of the three span footbridge helps to reduce the deflections, since the force monitored on the bottom chord extensions after the re-installation has almost the same stiffness slope as the ones in the stages where the chord extensions were in place before the concrete placement (Figures

3.18-3.20). However, placing the bottom chord extensions before the concrete pour is observed to be a better solution.

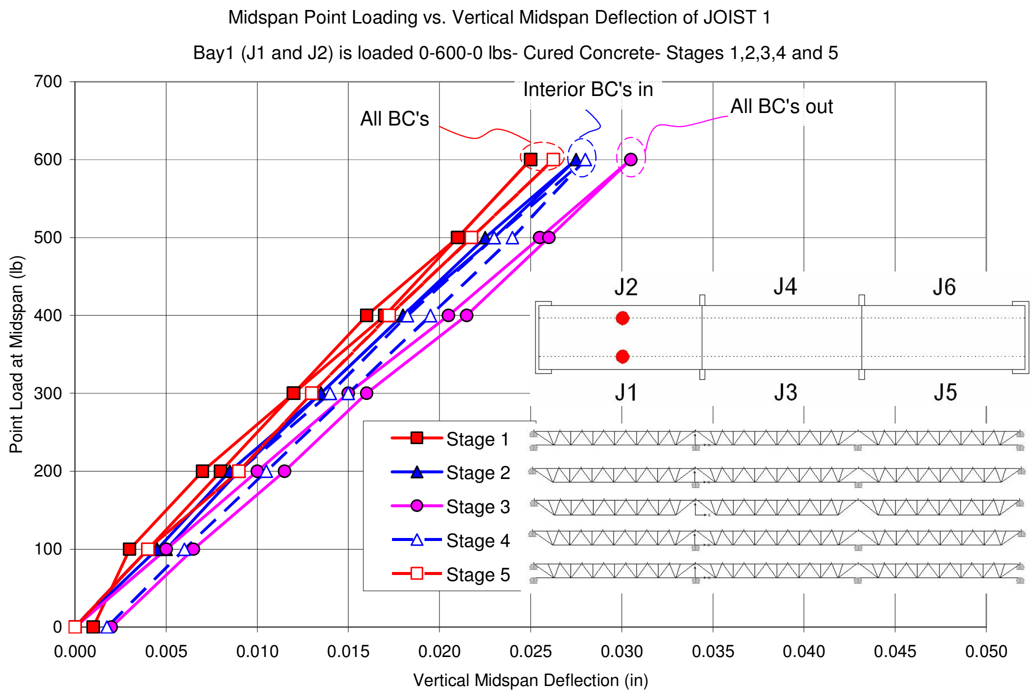

Figure 3.12 Three Span Footbridge- Midspan Point Loading versus Midspan Deflection- Joist 1

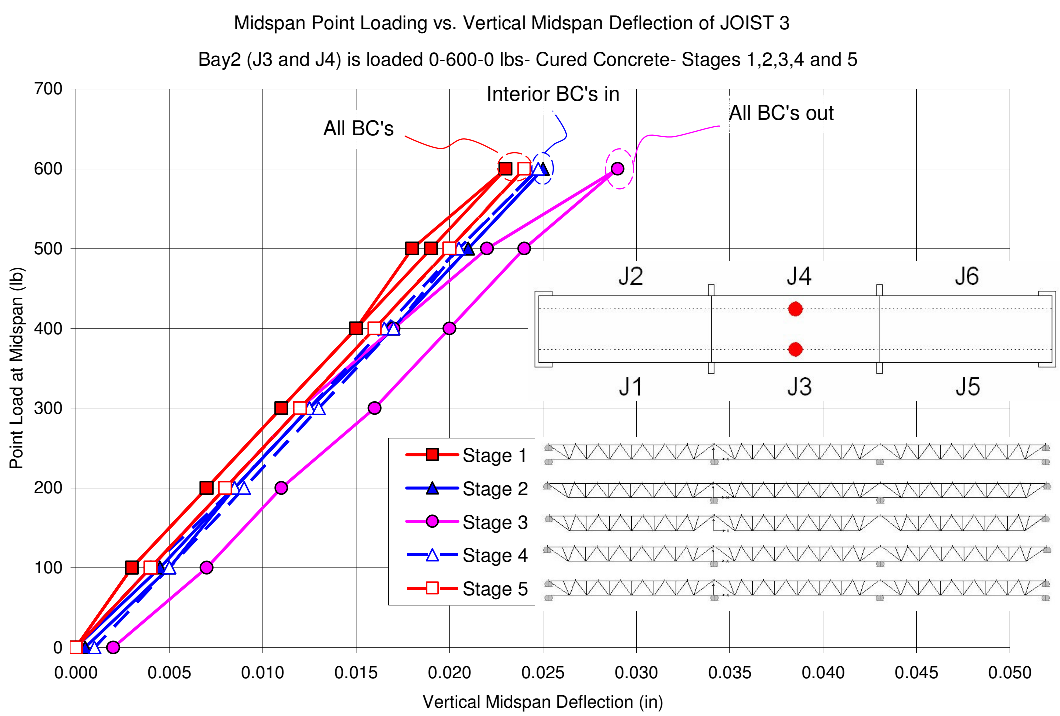

Figure 3.13 Three Span Footbridge- Midspan Point Loading versus Midspan Deflection- Joist 3

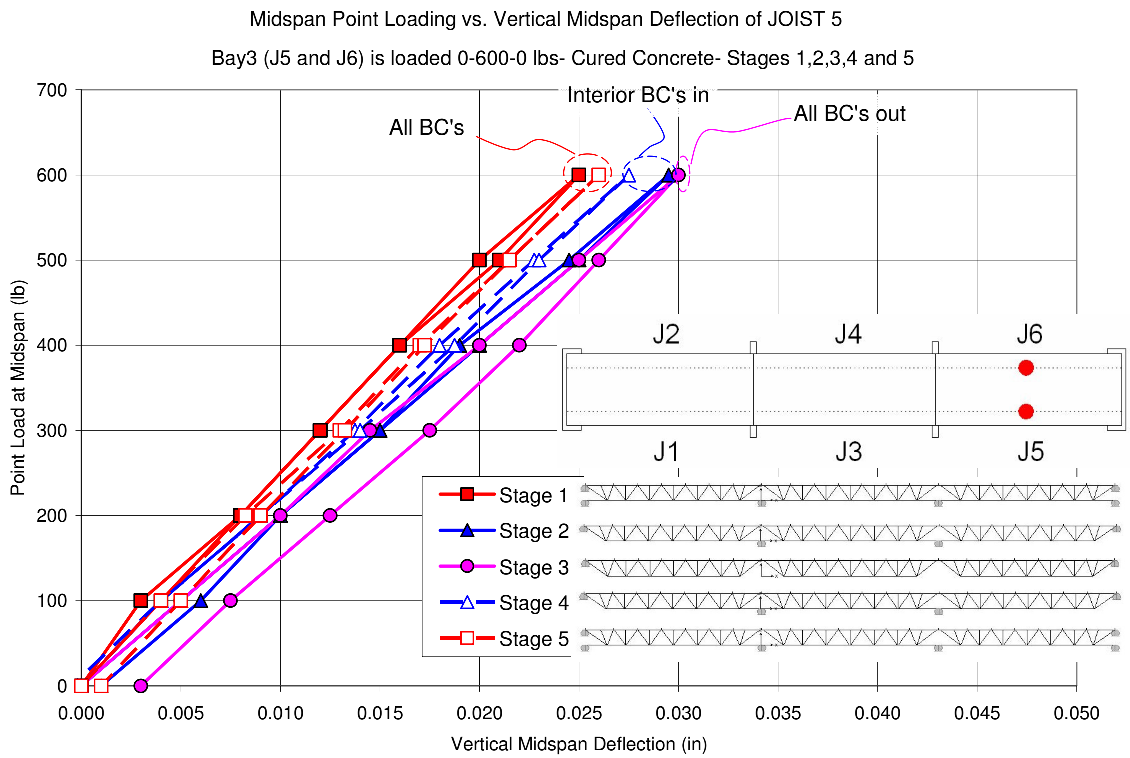

Figure 3.14 Three Span Footbridge- Midspan Point Loading versus Midspan Deflection- Joist 5

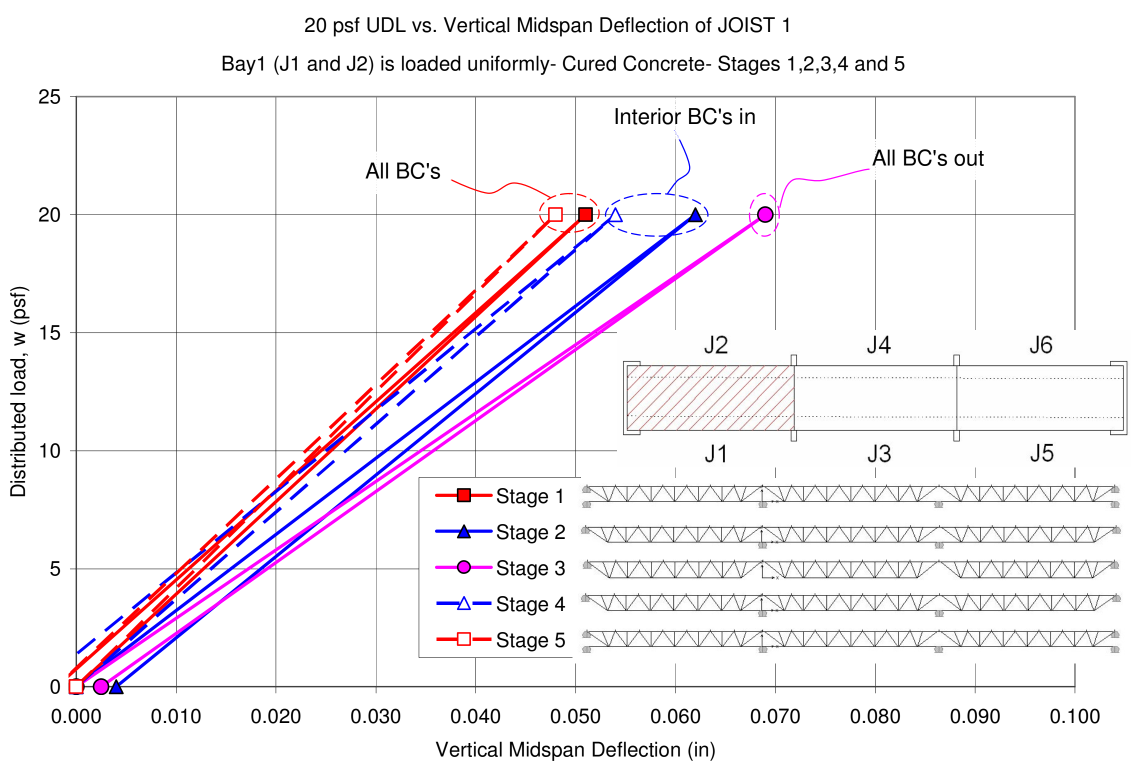

Figure 3.15 Three Span Footbridge- UDL versus Midspan Deflection- Joist 1

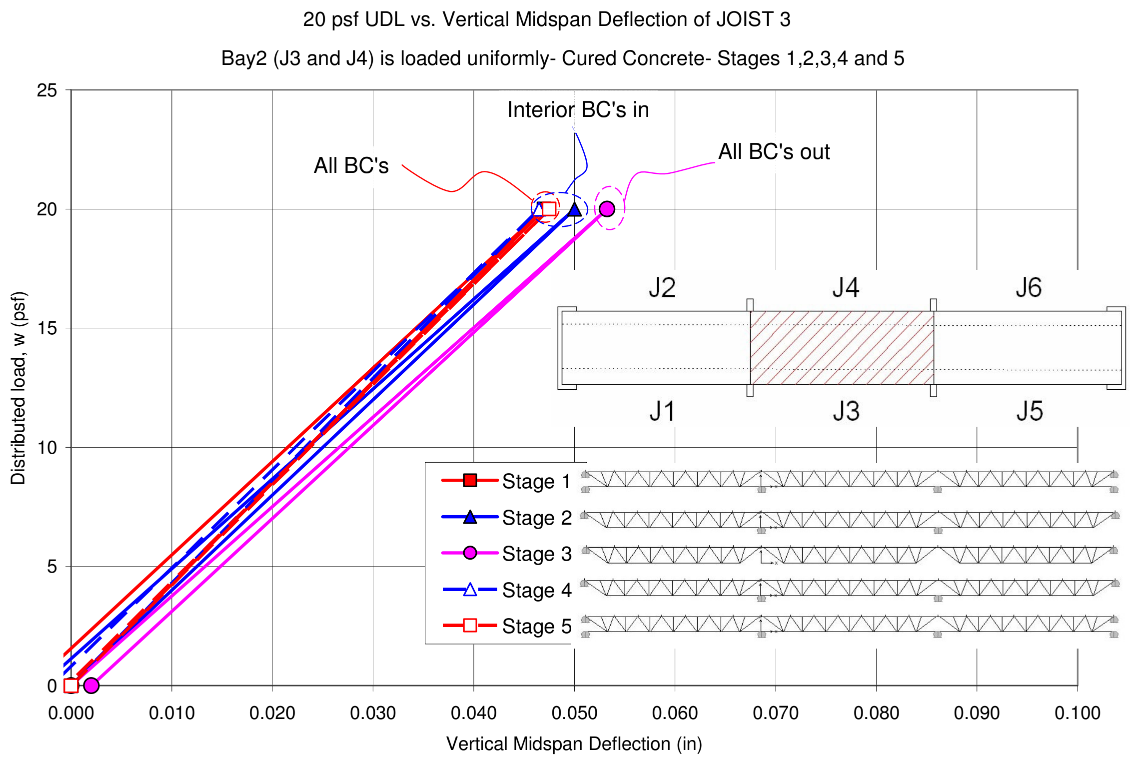

Figure 3.16 Three Span Footbridge- UDL versus Midspan Deflection- Joist 3

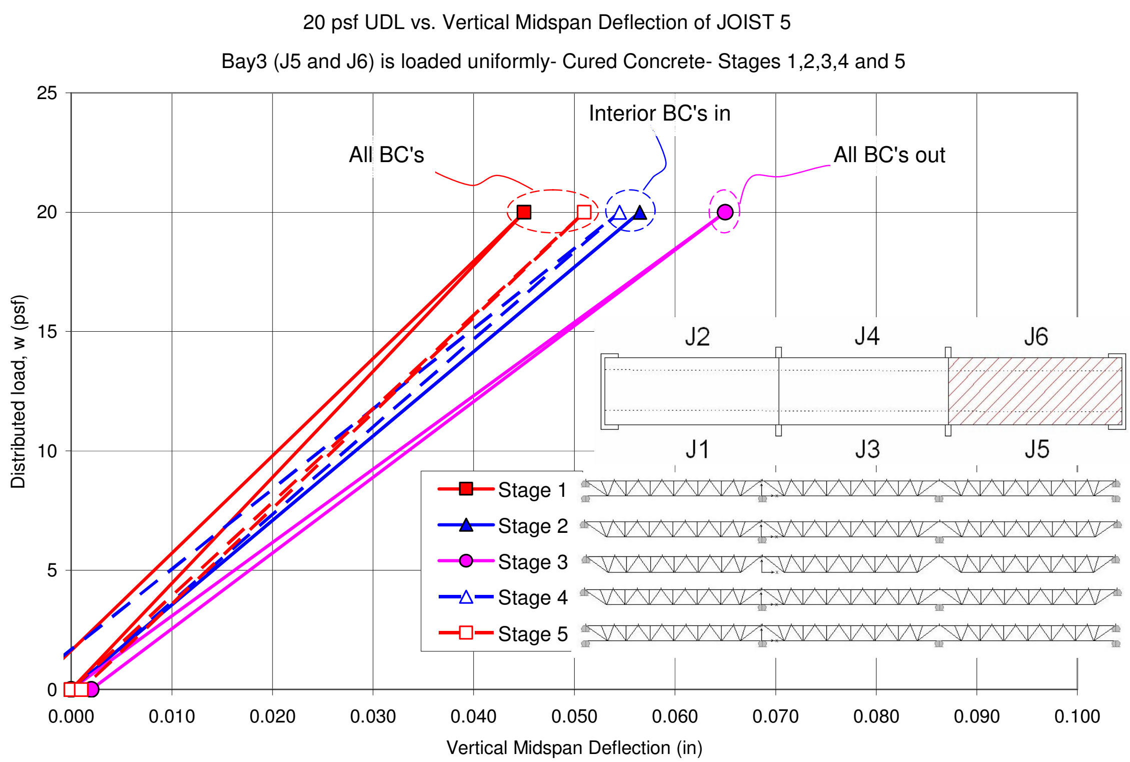

Figure 3.17 Three Span Footbridge- UDL versus Midspan Deflection- Joist 5

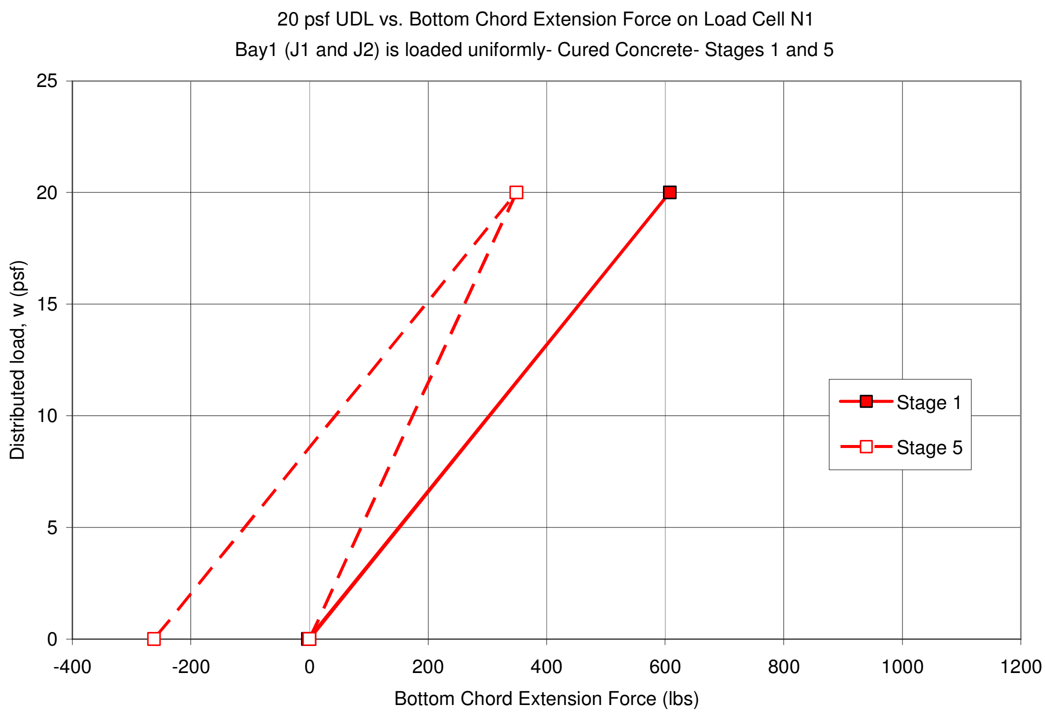

Figure 3.18 Three Span Footbridge- UDL versus Bottom Chord Extension Force- Load Cell N1

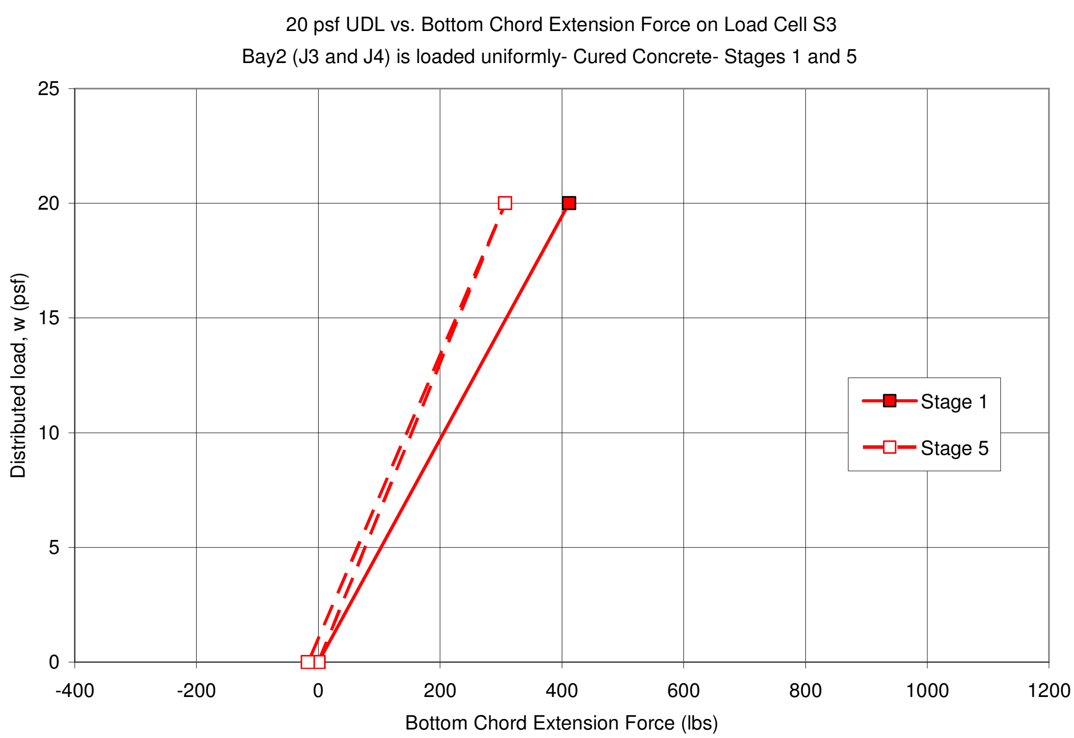

Figure 3.19 Three Span Footbridge- UDL versus Bottom Chord Extension Force- Load Cell S3

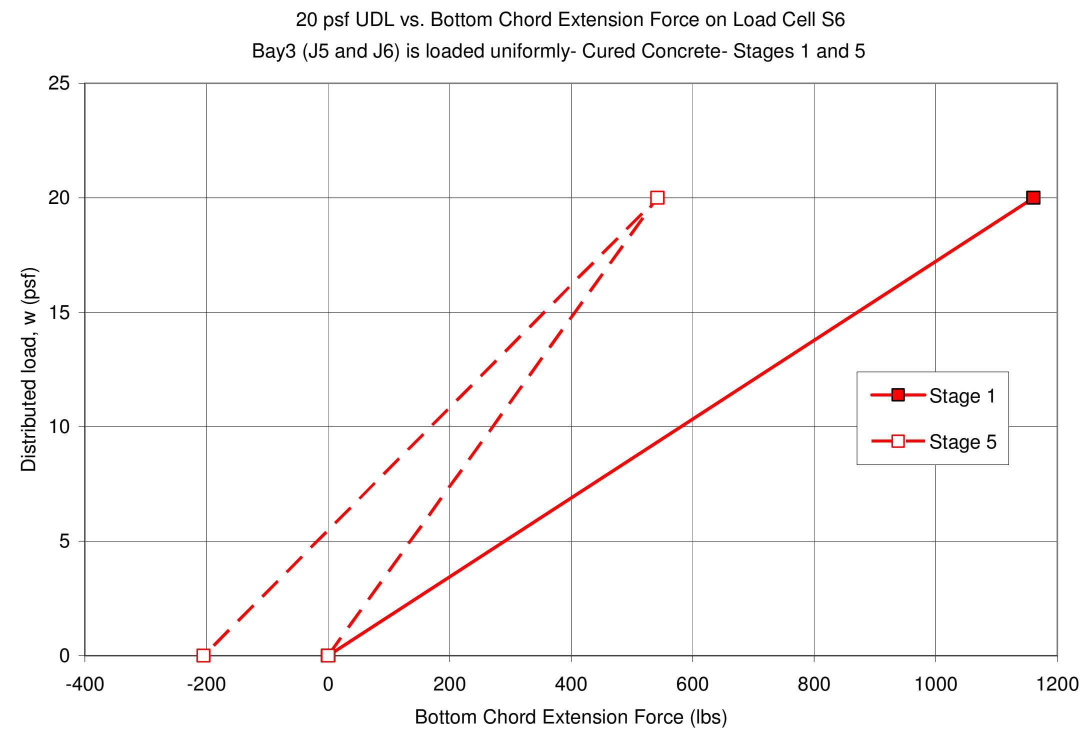

Figure 3.20 Three Span Footbridge- UDL versus Bottom Chord Extension Force- Load Cell S6

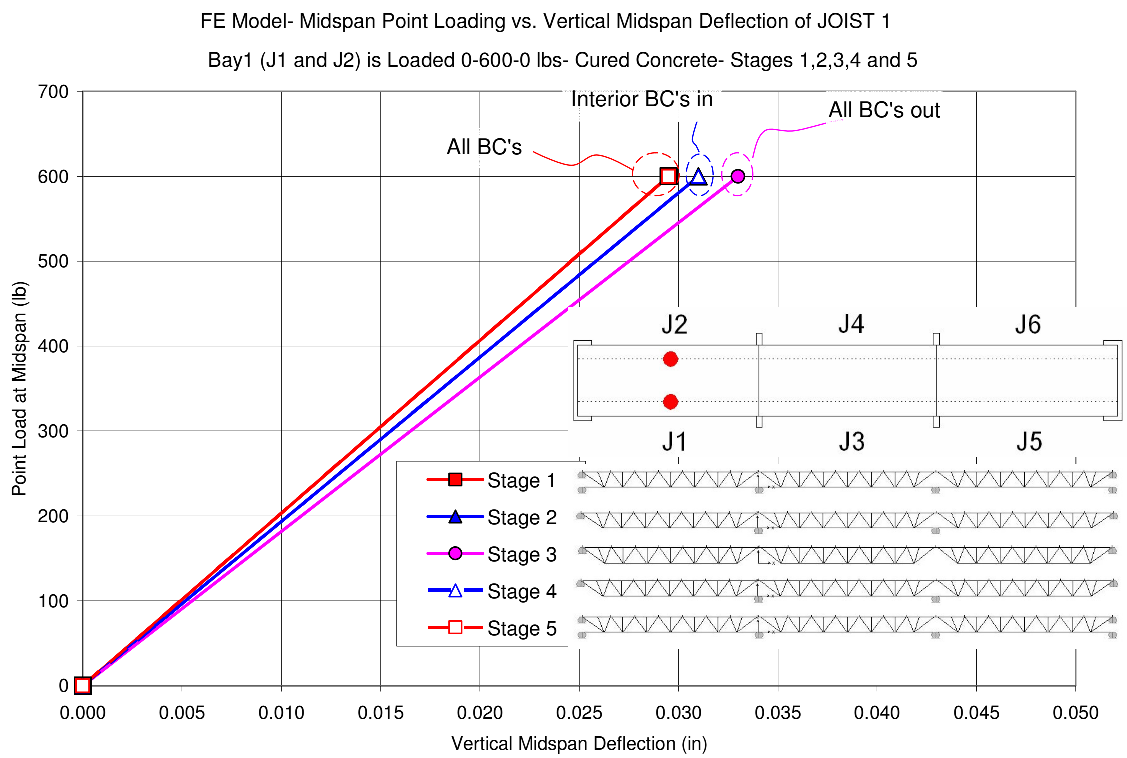

Figure 3.21 FE Model- Three Span Footbridge- Midspan Point Loading versus Midspan Deflection- Joist 1

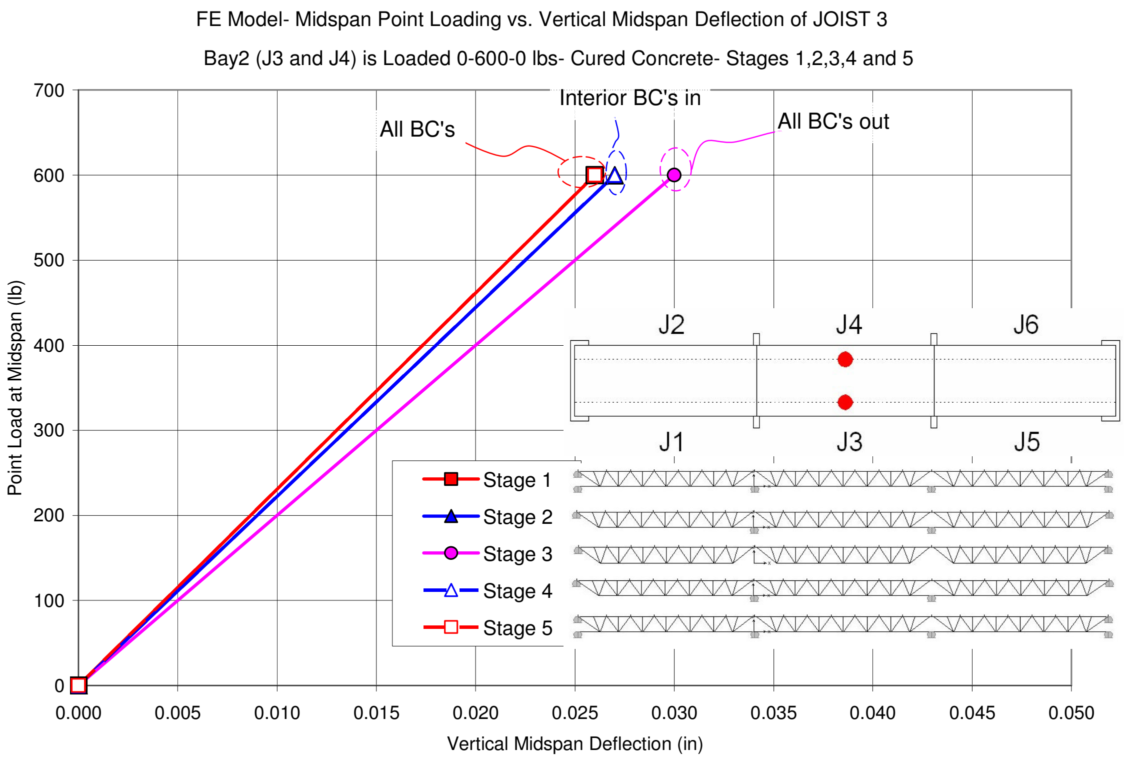

Figure 3.22 FE Model- Three Span Footbridge- Midspan Point Loading versus Midspan Deflection- Joist 3

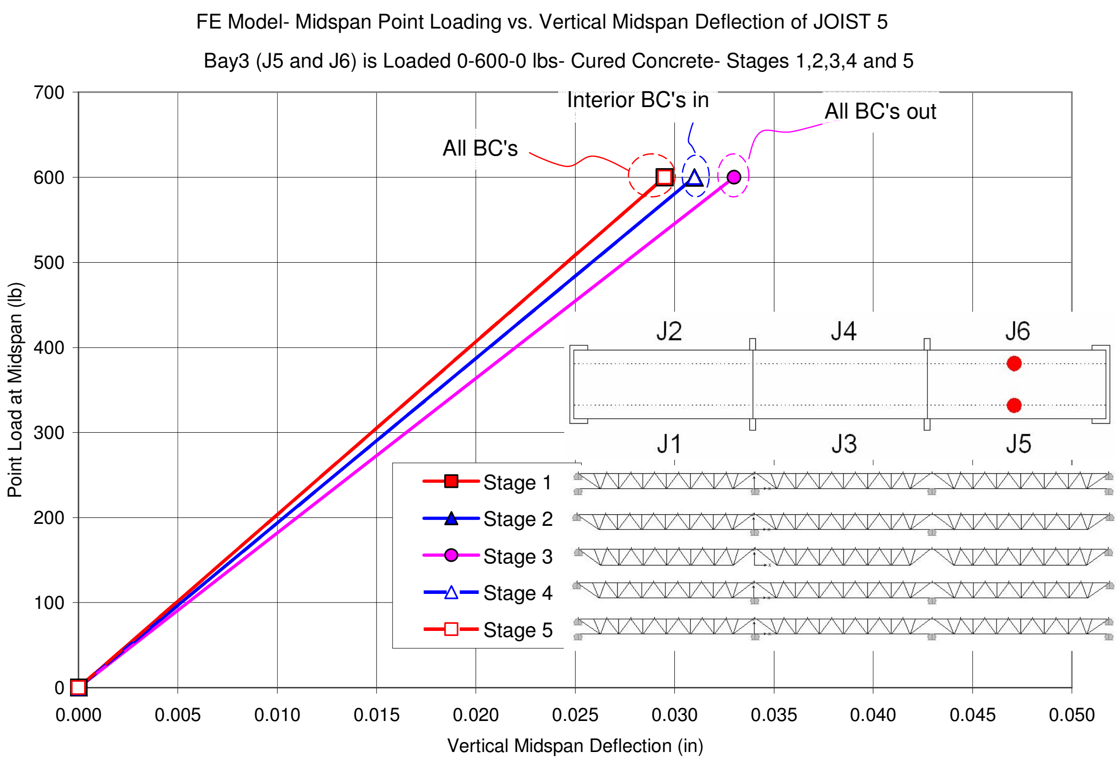

Figure 3.23 FE Model- Three Span Footbridge- Midspan Point Loading versus Midspan Deflection- Joist 5

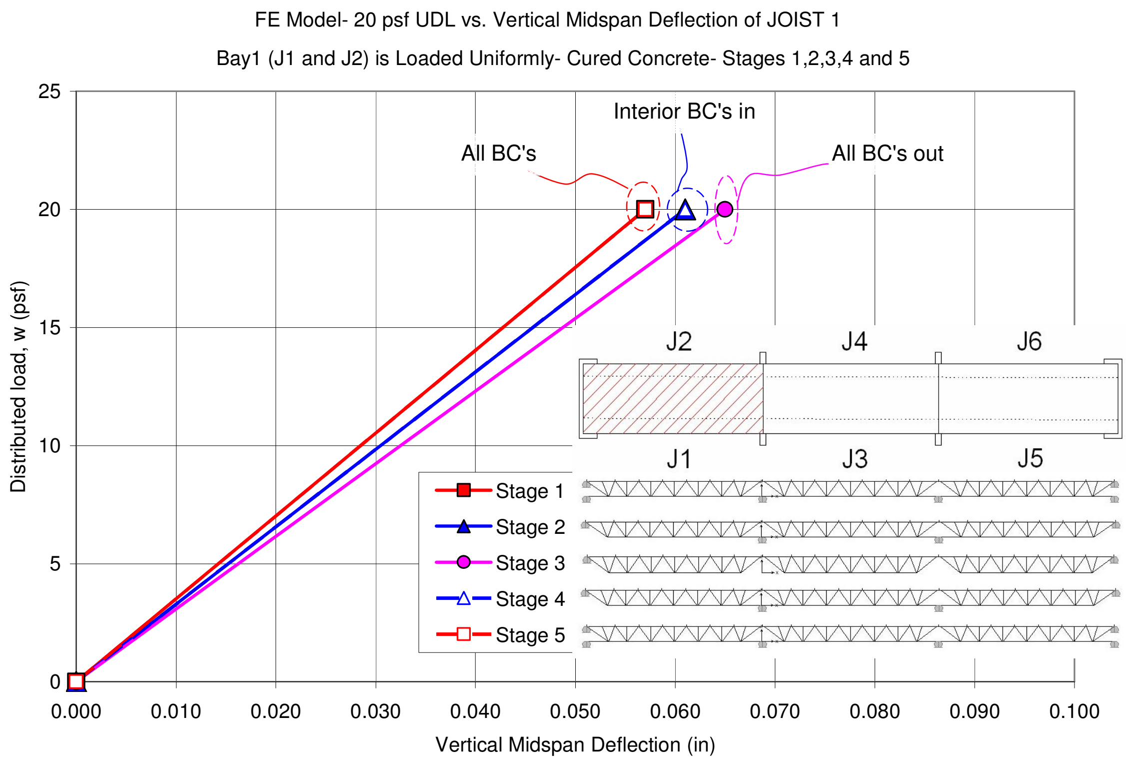

Figure 3.24 FE Model- Three Span Footbridge- UDL versus Midspan Deflection- Joist 1

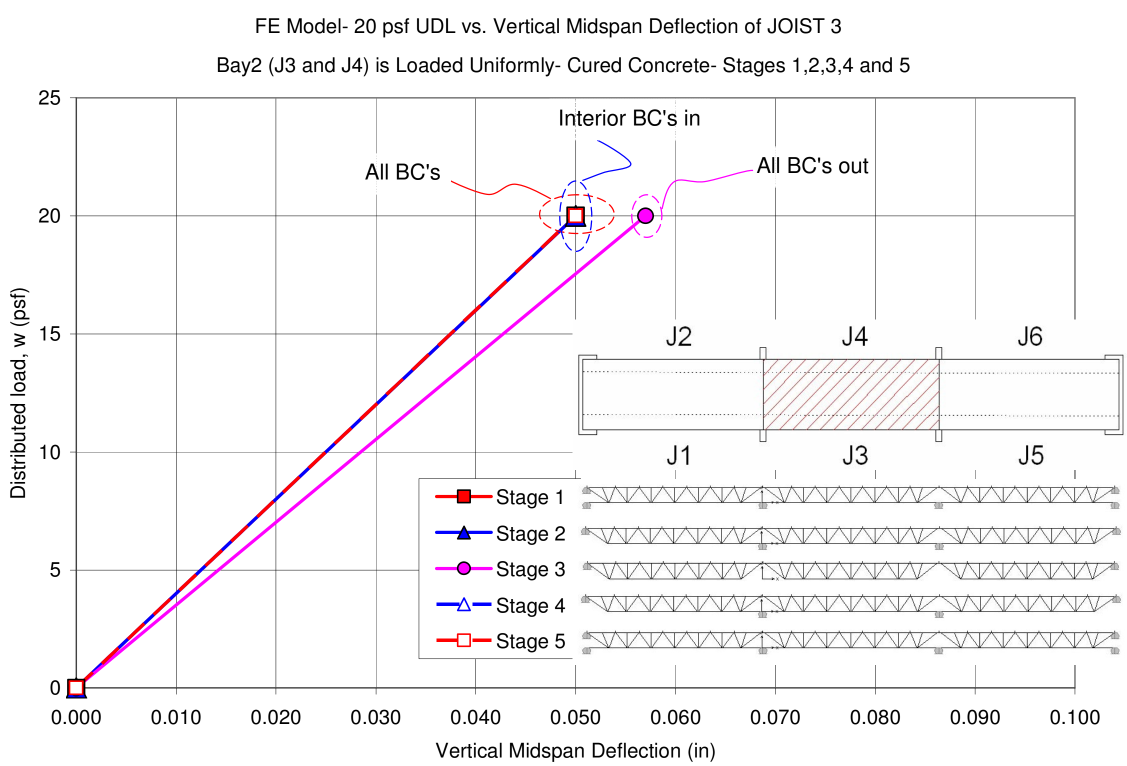

Figure 3.25 FE Model- Three Span Footbridge- UDL versus Midspan Deflection- Joist 3

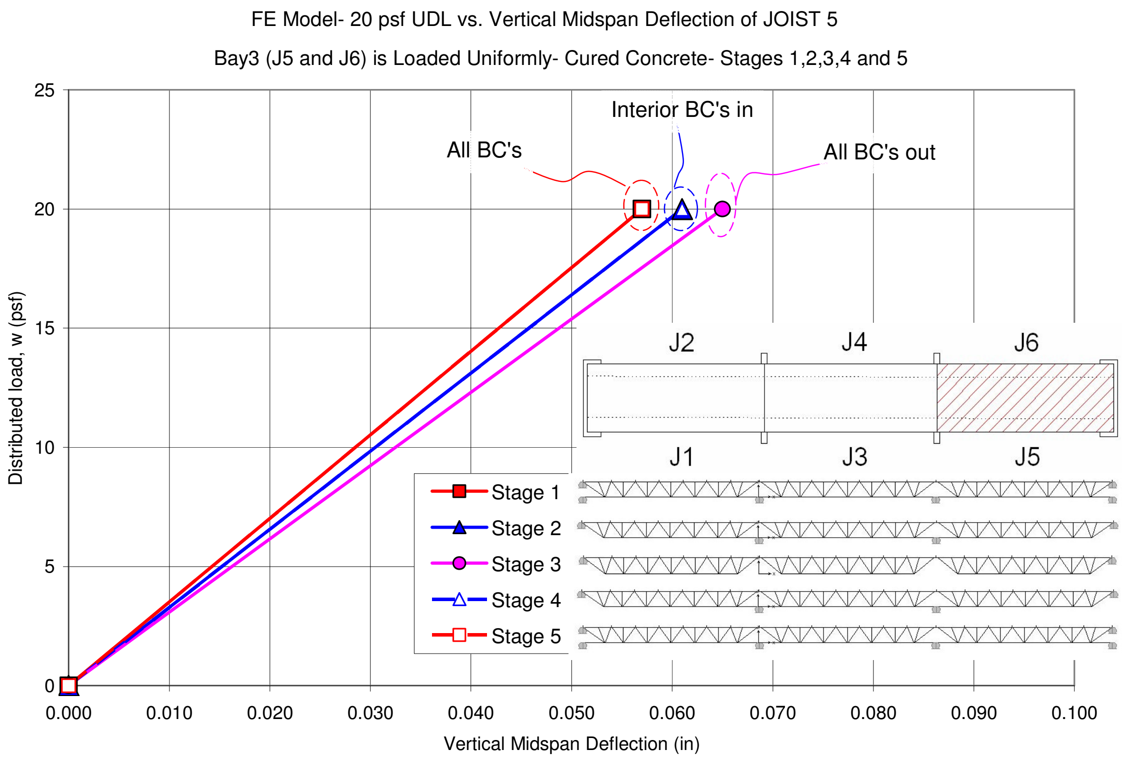

Figure 3.26 FE Model- Three Span Footbridge- UDL versus Midspan Deflection- Joist 5

CHAPTER 4
DYNAMIC TESTING: VIBRATION TEST RESULTS

4.1 Experimental Modal Analysis and Digital Signal Processing

Modal analysis is the procedure of determining dynamic characteristics (resonant frequencies, damping ratios and mode shapes) of a structural system by vibration testing. Resulting modal data is used to formulate a mathematical model (modal model) to represent the dynamic behavior of the structure. Finite element models are mathematical models in structural dynamics applications which are expected to represent the dynamic behavior of structural systems; however considering the complexity, nonlinearity and uncertainty of structures, it is unrealistic to expect finite element models to simulate complete structural behavior (He and Fu 2001). The philosophy behind experimental modal analysis is vibration testing the structure and updating the finite element model, minimizing the discrepancies between them for better design and response predictions. When the test data match analytical model predictions, the model is verified and can be used in design with some confidence (Inman 2000).

Every engineering structure has natural vibrating frequencies, corresponding mode shapes and damping ratios. A natural frequency is the frequency at which a structure naturally tends to vibrate, so that minimum energy is required to produce a forced vibration or to continue vibration at that frequency. While the structure vibrates at a natural frequency, its deformation tends to follow a specific pattern. The specific shape of a structural mode at a particular natural frequency is called the mode shape of the structure. Every vibrating mode has a mode shape. Every vibrating mode also has a corresponding damping ratio which is a dynamic property related to dissipation of oscillatory or vibratory energy with motion or with time. Modal analysis is the study of these dynamic properties.

Natural frequencies of a structure are very important because when the system is excited with forcing frequencies at or near any natural frequency, the magnitude of the structural response increases rapidly (Figures 4.1 and 4.2). This phenomenon is called resonance and it is one of the fundamental concepts in vibrations. As the excitation frequency hits the resonance frequency, the phase of the response shifts by 180° with the value of the phase angle being 90° (Figure 4.3).

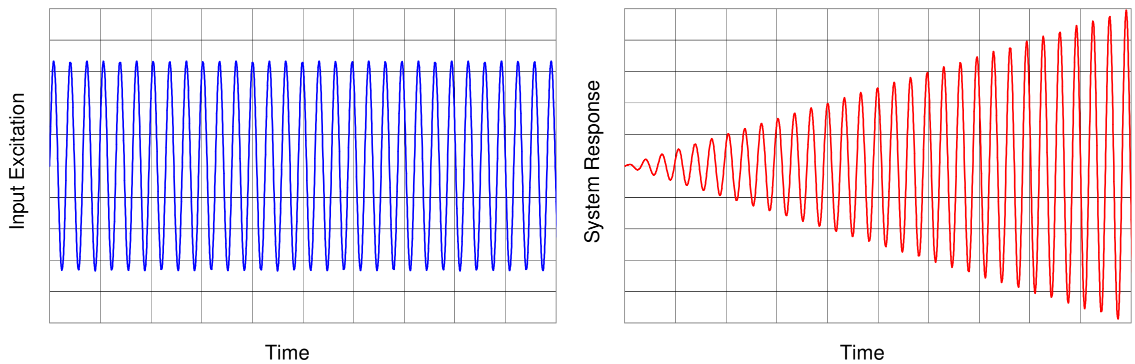

Figure 4.1 Input Excitation at Resonant Frequency and System Response (Undamped System)

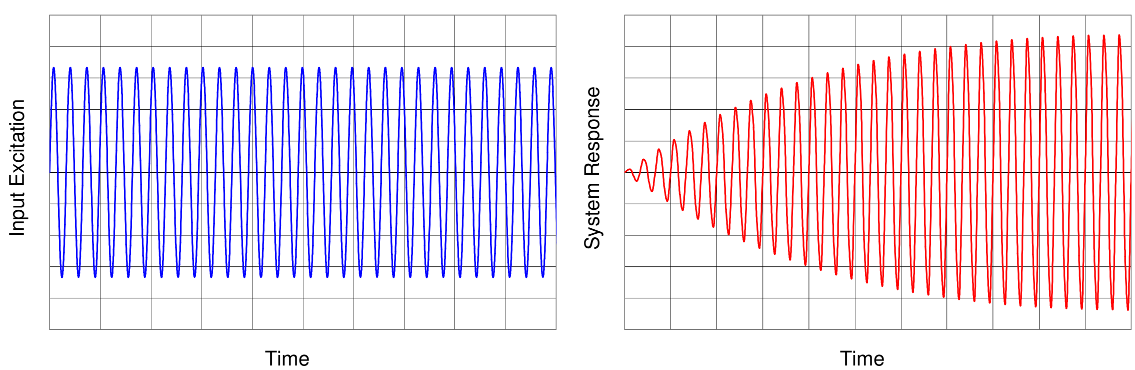

Figure 4.2 Input Excitation at Resonant Frequency and System Response (Damped System)

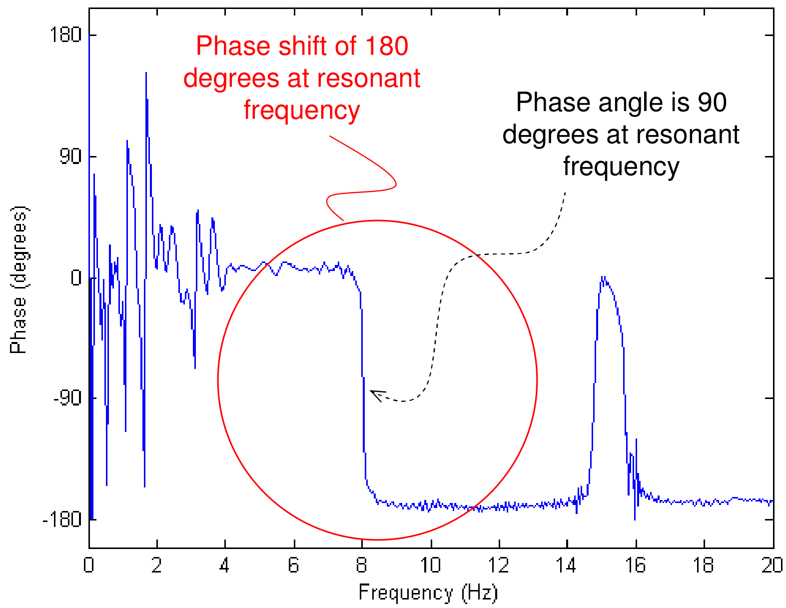

Figure 4.3 Phase Shift and Phase Angle at Resonance

The essential idea of modal analysis is that the overall vibration response of a system can be represented by a combination of natural modes of vibration. Each mode has its own physical (mass, stiffness, damping) and modal (natural frequency, damping ratio and mode shape) properties, and the response of a system to any excitation can be represented by a combination of these modes. The structure is excited at one location (input to the system) and the vibration response is measured at another location (output of the system). The response of the system can be measured in displacement, velocity or acceleration. The relationship between the input and output is known as the frequency response function (FRF),

$$FRF = \frac{Output}{Input} = \frac{FFT(response)}{FFT(force)} \tag{4.1}$$

Modal analysis involves measuring FRFs and extracting dynamic properties of the structural system using them.

The input to the system is usually a force excitation and it is measured by a load cell. For floor vibrations, a shaker (Figure 4.4) or a person who is going to perform a heel drop (or marching) stands on the load cell (force plate) so that the applied excitation force is measured and recorded. The applied force is converted to an electrical signal to produce a voltage proportional to the force applied to the system. The force plate used in this research is a triangular aluminum plate supported by three cantilevered load cells at each corner as shown in Figure 4.5. It is connected to a summing amplifier (power box), Figure 4.6, which controls the gain on the signal before the signal enters the signal analyzer, Figure 4.7. SigLab DSP units were used as a digital signal analyzer. They are connected to a computer with SigLab software (a MatLab based software) on it. The analyzer has four input channels and two output channels. The summing amplifier of the force plate is connected to the first input channel of the DSP unit, while all the accelerometers are connected to the rest of the input channels. Thus, there are three accelerometer channels available when only one DSP unit was used; seven accelerometer channels were available when two DSP units were used.

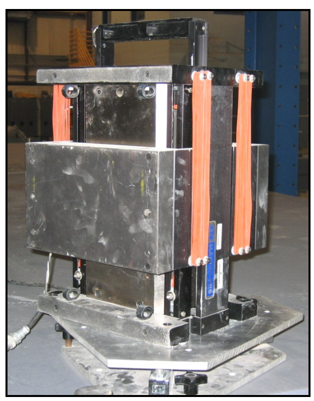

Figure 4.4 Shaker on the Force Plate

Figure 4.5 Force Plate

Figure 4.6 Summing Amplifier

Figure 4.7 Signal Analyzer (SigLab Unit)

An APS Dual-Mode Amplifier, Model 144 (Figure 4.8), was used to send voltage signals to the shaker. The electromagnetic shaker is an APS Electro-Seis (Model 400) with a dynamic mass of 67.4 lb suspended from its support frame by rubber bands. With a core weight of 170.6 lb, the total weight of the shaker is 238 lbs. It has a frequency range of 0-200 Hz and the force rating for the 0.10-20 Hz range (the frequency range generally used for floor vibration measurements) is about 100 lbs. The electro-magnetic shaker allows the user to apply a variety of excitations (harmonic or random) with different ranges of frequencies.

Figure 4.8 APS Dual-Mode Amplifier

Chirp signals (a sinusoidal function with adjustable frequency) and sinusoidal excitations are common harmonic excitations used in modal analysis. Chirp signals are defined as

$$F(lb) = (A)Sin\left[2\pi\left(\frac{(f_{\max} - f_{\min}).t}{T} + f_{\min}\right).t\right] \tag{4.2}$$

where

F	=	chirp (lb)
A	=	amplitude of chip signal (lb)
f_{min}	=	frequency of chirp signal at time zero (Hz)
f_{max}	=	frequency of chirp signal at time T (Hz)
t	=	time (sec)
T	=	number of periods or time intervals (sec)

In Figures 4.9 and 4.10 theoretical time history, applied chirp time histories and associated auto-spectrum are displayed. Auto-spectrum is the average of the power of the individual frequency components over a number of instantaneous spectra showing the variation of the frequency content of the collected vibration data. A theoretical sine wave excitation is displayed in Figure 4.11.

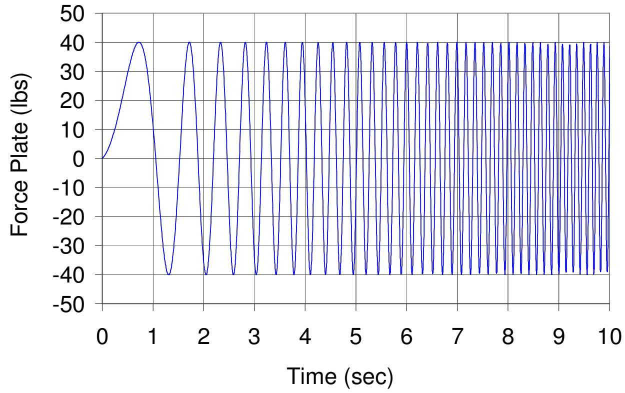

Figure 4.9 Theoretical Chirp Excitation Signal

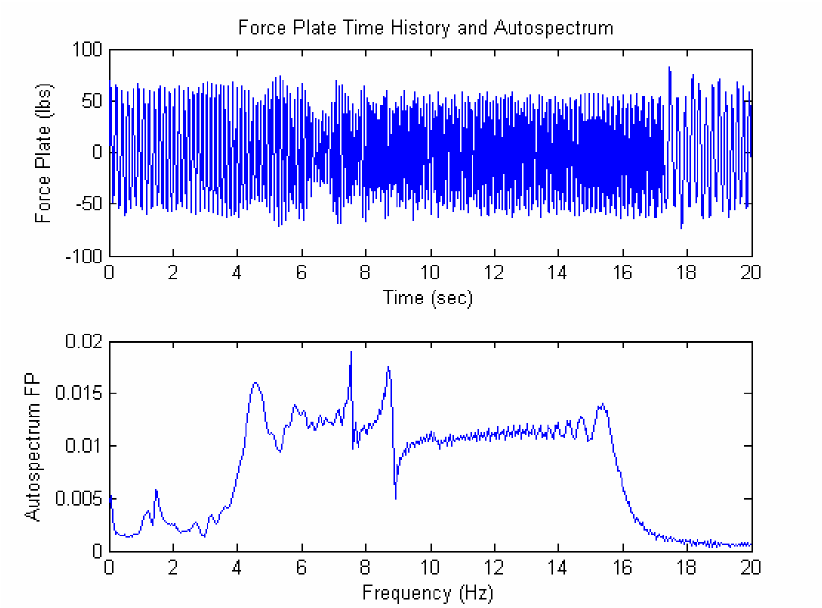

Figure 4.10 Chirp Input Signal (4-16 Hz) From an Actual Test and Associated Auto-spectrum

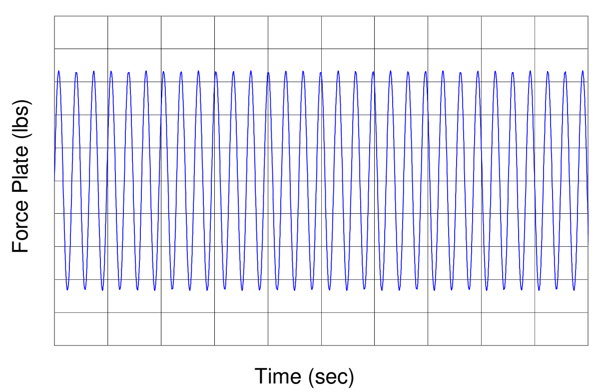

Figure 4.11 Typical Sine Excitation Signal

Piezo-based PCB 393C accelerometers were used to measure the acceleration response of the floors, Figure 4.12. The accelerometers have a sensitivity of 1V/g and 0.025-800 Hz frequency range. The acceleration response of the structure is converted to an electrical signal to produce a voltage proportional to the acceleration measured on the system and sent to the analyzer.

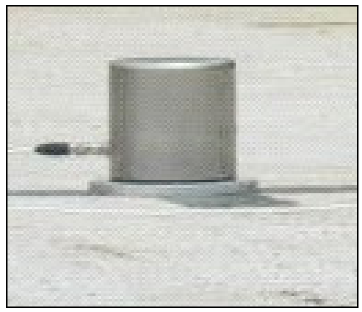

Figure 4.12 PCB 393C Accelerometer

The measurement system diagram is shown in Figure 4.13. The input and output data are collected in the time domain and processed in the signal analyzer. Analog voltages of input (force excitation) and output (displacement, velocity or acceleration) are filtered, digitized and transformed into the frequency domain in the signal analyzer to produce the frequency response functions. The standard transformation method for this purpose is the digital Fast Fourier Transformation. The basis of Fourier transformation is that any arbitrary periodic function can be represented by a summation of sine and cosine functions (Bracewell 2000). This mathematical operation enables a time series to be resolved into a series of numbers that characterize the relative amplitude and phase components of the signal as a function of the frequency. In digital signal processing this method is used to convert an analog signal $x(t)$ into the frequency domain by using Fourier series equations and Fourier coefficients.

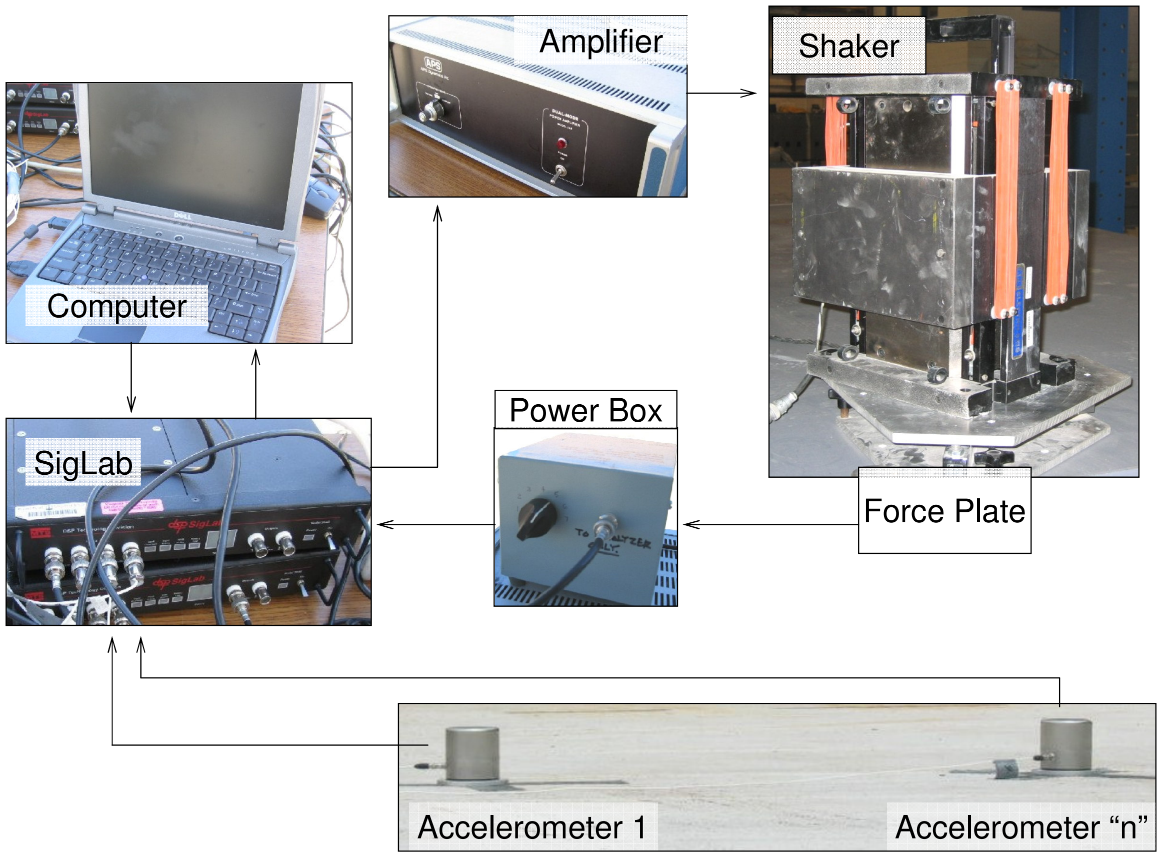

Figure 4.13 Experimental System Diagram

The sampled data is in the analog signal format $x(t)$, which is sampled in equally spaced time intervals to produce the digital record. This process is called analog-to-digital (A/D) conversion:

$$\{x(t_1), x(t_2), \ldots\ldots x(t_N)\}$$

where

N is the number of samples taken (a power of 2), and at any time t_k, $x(t_k)$ is the discrete value of the analog signal $x(t)$.

A/D conversion can be thought in a way that the signal is sampled every Δt seconds and both sampling time and the corresponding signal $x(t_k)$ are recorded at the same instant. Sampling time should be set properly so that the details of the analog signal are caught. If the sampling rate is too slow, then the high frequency signals are going to be interpreted as a low frequency, which is called aliasing- a common error in signal processing (Figure 4.14). To avoid aliasing, usually the sampling interval Δt is chosen small enough to capture at least two samples per cycle of the maximum frequency to be measured. There are also anti-aliasing filters available in commercial signal analyzers to filter the frequency content higher than half of the maximum frequency of interest, Nyquist frequency (Ifeachor and Jervis 2002).

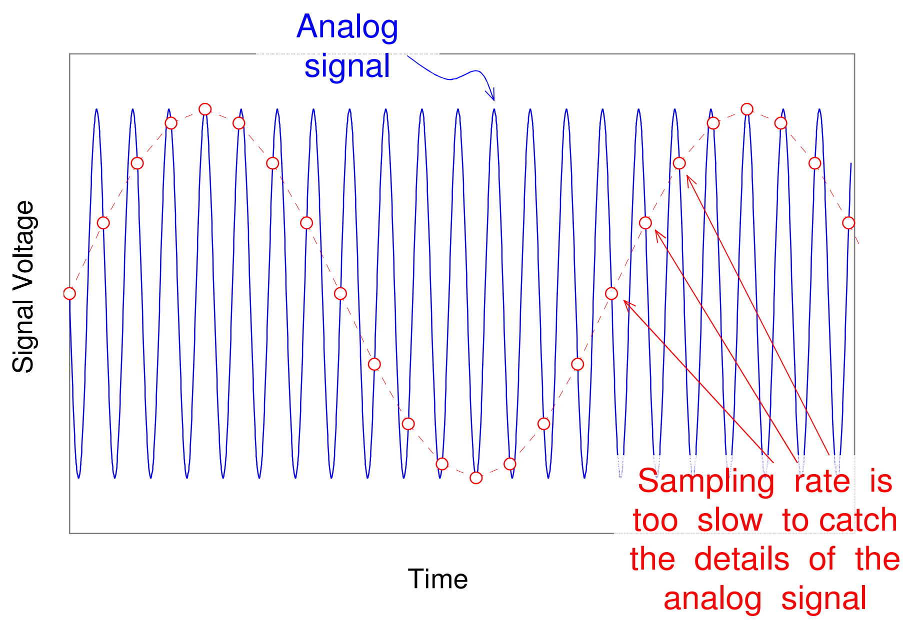

Figure 4.14 Aliasing- A Common Error in Signal Processing

Because the Fourier transform assumes that the signal is periodic, the actual frequency is going to "leak" into other fictitious frequencies when the signal has high frequency content. This is called leakage and can be prevented by windowing on sampled data. However windowing can change the original characteristics of the data, which might result in misinterpretation of dynamic system properties (e.g., increased damping).

For an ideal test, input and output signals are completely clean. There is no noise or uncorrelated content in the signals and coherence is 1.0. Then, FRF is basically the ratio of the two:

$$H(\omega) = \frac{X(\omega)}{F(\omega)} \tag{4.3}$$

Figure 4.15 shows the input/output model for an ideal system. It is difficult to analyze the collected signals since the data will always contain noise. For that purpose, the random signal analysis is used in digital signal processing instead of the deterministic approach. For all measurements, there is going to be some uncorrelated content in both the input and output (Figure 4.16). Around resonant frequencies the vibration response is so significant that the noise in the output can be ignored. Also around anti-resonant frequencies the excitation voltage is so significant that the noise in the input can be ignored. For other frequency contents the noise is always going to be present in the FRF estimations, so getting the most accurate FRF in the presence of noise is the main issue.

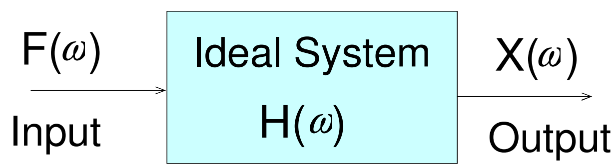

Figure 4.15 Ideal Input/ Output Model

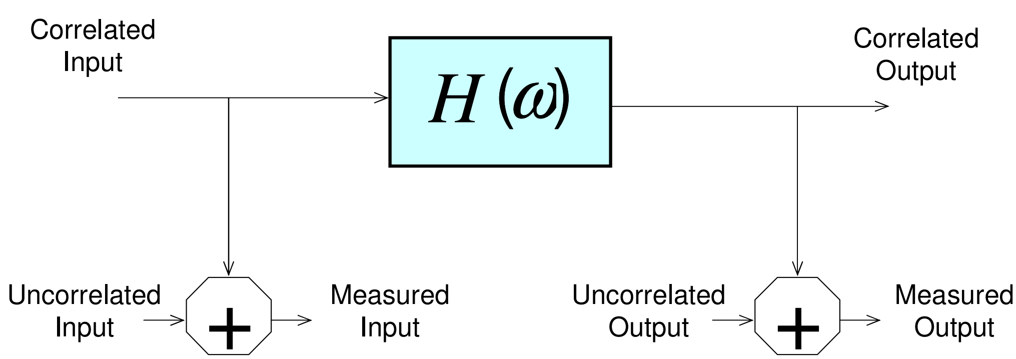

Figure 4.16 General Input/ Output Model

Several sets of input time histories and output time histories are averaged for frequency response functions. From these averages, correlation functions are produced which are then transformed into power spectral densities (PSDs). FRF magnitudes are calculated from the PSDs.

In random signal analysis an FRF can also be defined as the "cross-spectrum of excitation and response" divided by the auto-spectrum of the excitation:

$$H_1(\omega) = \frac{S_{fx}(\omega)}{S_{ff}(\omega)} \tag{4.4}$$

where $S_{fx}(\omega)$ is the cross-spectrum of the excitation and response, and $S_{ff}(\omega)$ is the autospectrum of the excitation.

Also, the ratio of the auto-spectrum of the response $S_{xx}(\omega)$ and the "cross-spectrum of the excitation and response ($S_{xf}(\omega)$)" is defined as

$$H_2(\omega) = \frac{S_{xx}(\omega)}{S_{xf}(\omega)} \tag{4.5}$$

where $S_{xf}(\omega)$ is the cross-spectral density function and $S_{xx}(\omega)$ is the power spectral density of the output signal $x(t)$.

$H_1(\omega)$ assumes that uncorrelated content is only in the output, while $H_2(\omega)$ assumes the uncorrelated content is only in the input. For an ideal case where there is no noise,

$$H(\omega) = H_1(\omega) = H_2(\omega) \tag{4.6}$$

For acceleration measurements,

$$H_{ik}(\omega) = \frac{\ddot{X}_i}{F_k} = \sum_{r=1}^{R} \frac{(j\omega)^2({}_r\phi_i)({}_r\phi_k)}{(-\omega^2 + \omega_r^2 + j2\zeta\omega\omega_r)[M_r]} \tag{4.7}$$

where

$x_i(j\omega)$ = displacement function at the spatial location i

$f_k(j\omega)$ = forcing function at the spatial location k

Equation 4.7 is called inertance or accelerance. Usually the commercial DSP analyzers provide either $H_1(\omega)$ or $H_2(\omega)$ and most of the time it is $H_1(\omega)$. Although the phase information is the same for both of these functions, the magnitudes may differ for some parts of the frequency domain (Ewins 2000). To measure this difference, the coherence function γ^2 is defined as the ratio of these equations and gives an idea about the consistency of the collected data:

$$\gamma^2 = \frac{H_1(\omega)}{H_2(\omega)} = \frac{\dfrac{S_{fx}(\omega)}{S_{ff}(\omega)}}{\dfrac{S_{xx}(\omega)}{S_{xf}(\omega)}} = \frac{\left|S_{xf}(\omega)\right|^2}{S_{xx}(\omega)S_{ff}(\omega)} \tag{4.8}$$

The coherence value lies between 0 and 1. It indicates how good the measurement is. For noise free measurements it is 1.0 and for pure noise it is 0. Usually there is a drop in the coherence function near resonant and anti-resonant frequencies. Near resonant frequencies the output noise can be ignored since the correlated output is almost equal to measured output. However for $H_1(\omega)$, the input signal hence $S_{ff}(\omega)$ becomes vulnerable to errors around resonant frequencies because $H_1(\omega)$ assumes that there is no noise in the input signal. Near anti-resonant frequencies the input noise can be ignored since the correlated input is almost equal to measured input. However for $H_2(\omega)$, the output signal hence $S_{xx}(\omega)$ becomes vulnerable to errors around anti-resonant frequencies because $H_2(\omega)$ assumes there is no noise in the output signal. In both cases there is a drop in the coherence function. In cases of coherence less than 0.75 the test should be repeated (Inman 2000). All FRF plots should be presented with coherence plots in addition to phase plots to display the confidence on collected modal data (Figure 4.17).

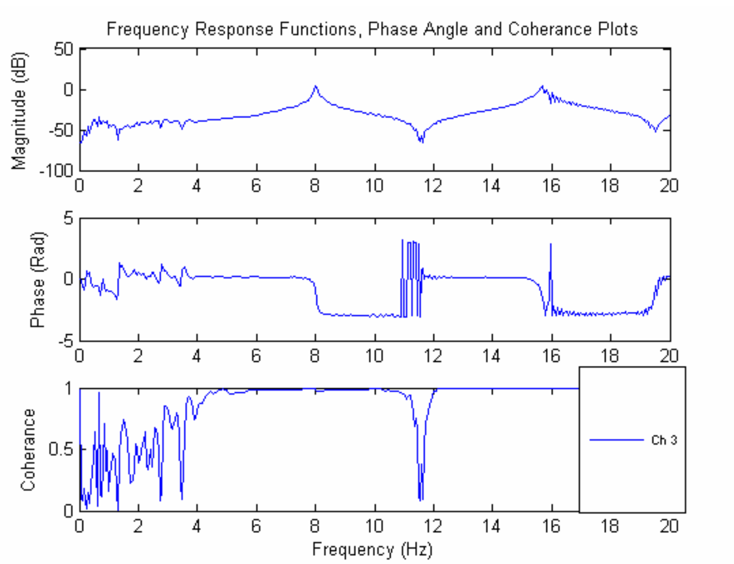

Figure 4.17 FRF Plot With Phase and Coherence Information

The fundamental idea of modal testing is to find the natural frequencies, damping ratios, mode shapes and response amplitudes through frequency response functions. The DSP analyzers manipulate the time domain data of input and output signals to calculate and produce the plots of frequency response functions, auto-spectrum functions, and phase and coherence plots in the frequency domain. The driving excitation and response time history data are also recorded. Typical plots are shown in Figure 4.18.

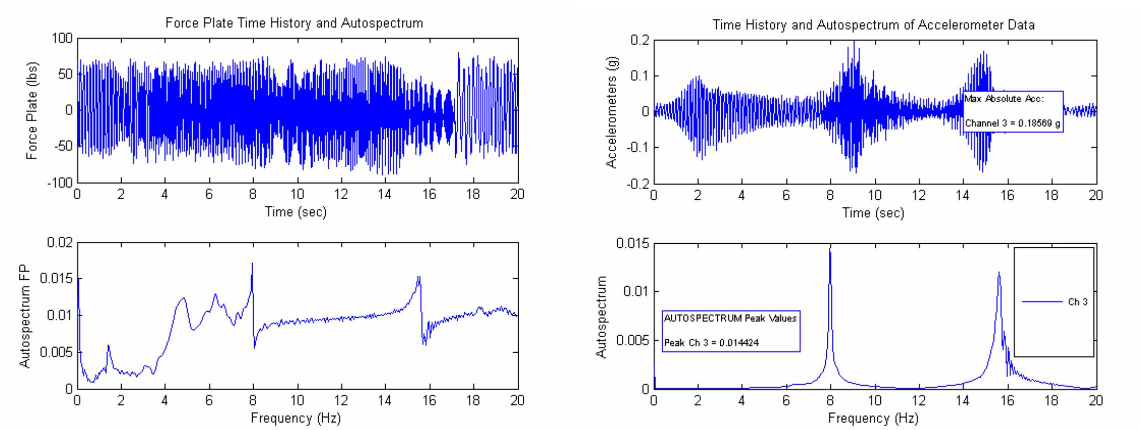

a) Input (Force Plate) **b) Output (Acceleration Response)**

Figure 4.18 Time History Data and Autospectra

Frequency response functions provide information about the relationship between the excitation force at one point and the reaction at the same or another point on the structure. Typical FRF plots are shown in Figure 4.19. The peaks on the FRF plots (resonant peaks) show that the response of the structure becomes very high for certain frequencies (resonant frequencies) when the structure is excited with enough energy and frequency content. Each peak corresponds to a mode and includes information about that mode. For instance, two natural frequencies are evident around 8 Hz and 16 Hz in Figure 4.19. Modal damping information can also be extracted from each FRF peak using the peak picking method. In the frequency domain, the half power method is used for damping estimations considering the fact that the width of each modal peak is directly proportional to modal damping. The peaks and corresponding half power points of frequency response functions are used in this method and the damping ratio is determined from

$$\beta = \zeta = \frac{f_b - f_a}{2 f_r} \tag{4.9}$$

where

f_r = natural frequency of the r[th] mode

f_a and f_b = half power point frequencies located on each side of the identified ω_r with amplitudes $\frac{1}{\sqrt{2}}$ of the peak amplitude.

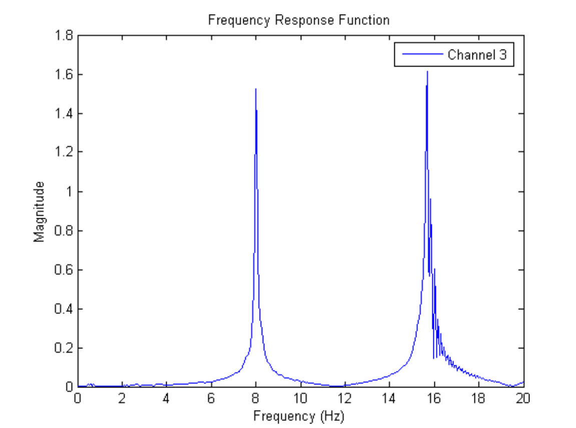

a) y-axis in Linear Scale

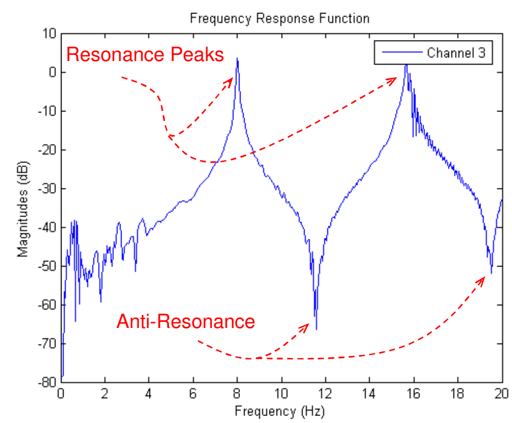

b) y-axis in Logarithmic Scale

Figure 4.19 Typical Frequency Response Function (FRF) Plots

Because FRFs are complex functions, sometimes they are shown with real and imaginary parts in addition to magnitude (Figure 4.20).

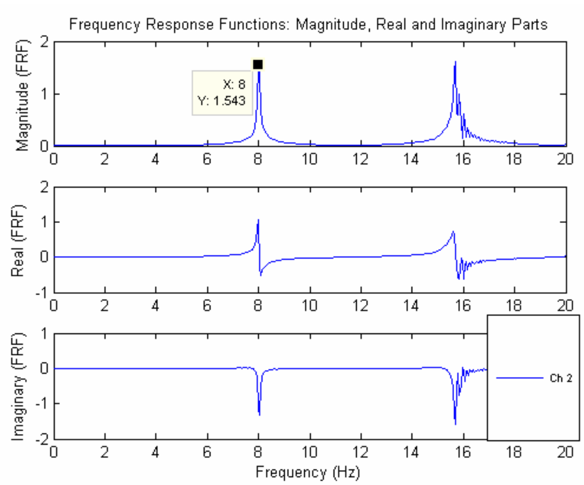

Figure 4.20 Typical FRF Plots: Magnitude, Real and Imaginary Parts

Each successive peak can be treated as a SDOF system since around each peak (and around each natural frequency) the FRF is dominated by that specific mode. At the natural frequencies, the phase of the response shifts by 180° with the value of the phase angle being 90° (Figure 4.3, 4.17 and 4.21). Accuracy of the FRF measurements is shown with coherence plots (Figure 4.22).

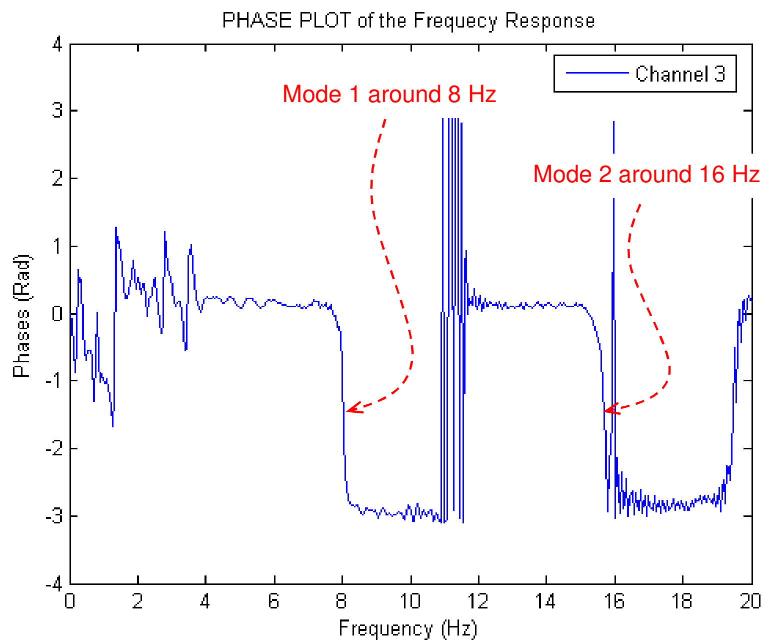

Figure 4.21 A Typical Phase Plot

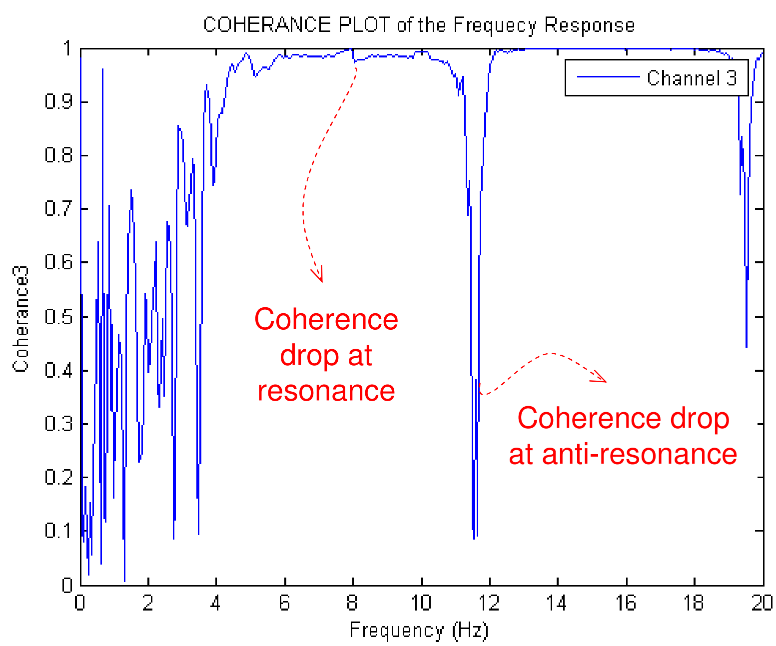

Figure 4.22 A Typical Coherence Plot

4.2 Vibration Test Results

4.2.1 Introduction

The objective of vibration testing conducted in this study was to experimentally determine the natural frequency, damping, mode shape and effective mass properties of the laboratory footbridges and to determine the effect of bottom chord extensions for each configuration. The ratio of acceleration response of the footbridge to the excitation force (FRF) is the key to identify the effect of bottom chord extensions on the acceleration response.

Four types of excitations, chirp, sinusoidal, heel drop and walking, were used to excite the footbridges, as the acceleration response of the footbridges was measured. Chirp and sinusoidal excitations were done using a shaker located on a force plate. Heel drop and walking excitations were done by graduate students. For chirp, sine and heel drop excitations, frequency response functions were measured and recorded. Heel drops were conducted on a force plate, however it was not possible to conduct walking on the force plate. Since the input to the system can not be measured for walking excitations, frequency response functions are not available for walking excitations. Alternatively, acceleration time histories of walking excitations were used for comparison of bottom chord extension effects in the different configurations.

In the literature, the heel drop excitation is defined as the loading caused by a 190 lb person standing on the balls of his feet (while the heels are approximately 2.5 inches above the floor) and suddenly releasing the heels to fall and create an impact on the floor (Figure 4.23). It was first measured and approximated by Ohmart and Lenzen (1968) as a linearly decreasing ramp function as shown in Figure 4.24.

Figure 4.23 Heel drop Excitation

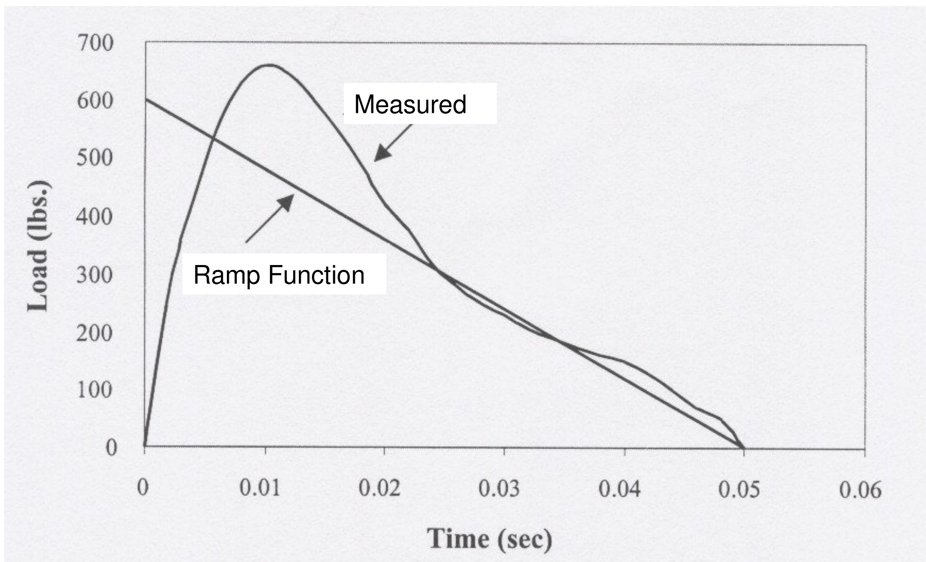

Figure 4.24 Heel drop Functions

For vibration tests, the shaker and force plate assembly was placed in different locations on the footbridge and chirp signals were used to sweep a frequency range of 4-20 Hz for each bottom chord extension configuration. Natural frequencies for different modes were determined from the frequency response functions. Then sinusoidal excitations at system natural frequencies were used to put the system into resonance, and measurement of the response at resonance was made.

During the tests, all the chirp data were collected in *.vna format in SigLab software (Figure 4.25). After the tests were completed, all the files were converted to *.blk format and input to MEScope software (Figure 4.26) for curve fitting of all collected data and determination of the natural frequencies, modal damping and mode shapes for each bottom chord extension configuration. Once the mode shapes were known, then the effective masses for different modes were calculated for each stage.

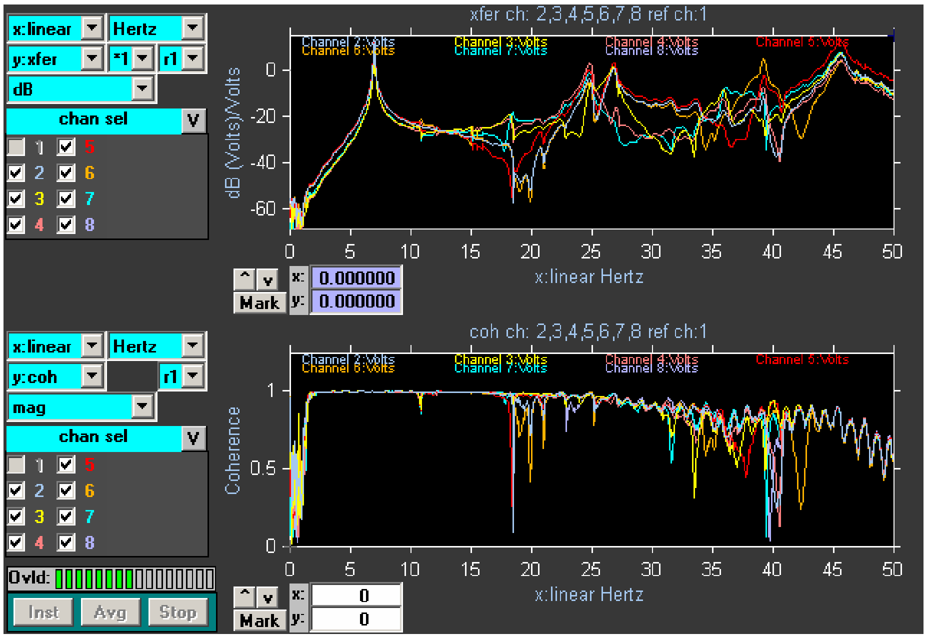

Figure 4.25 The *.vna file format in Siglab

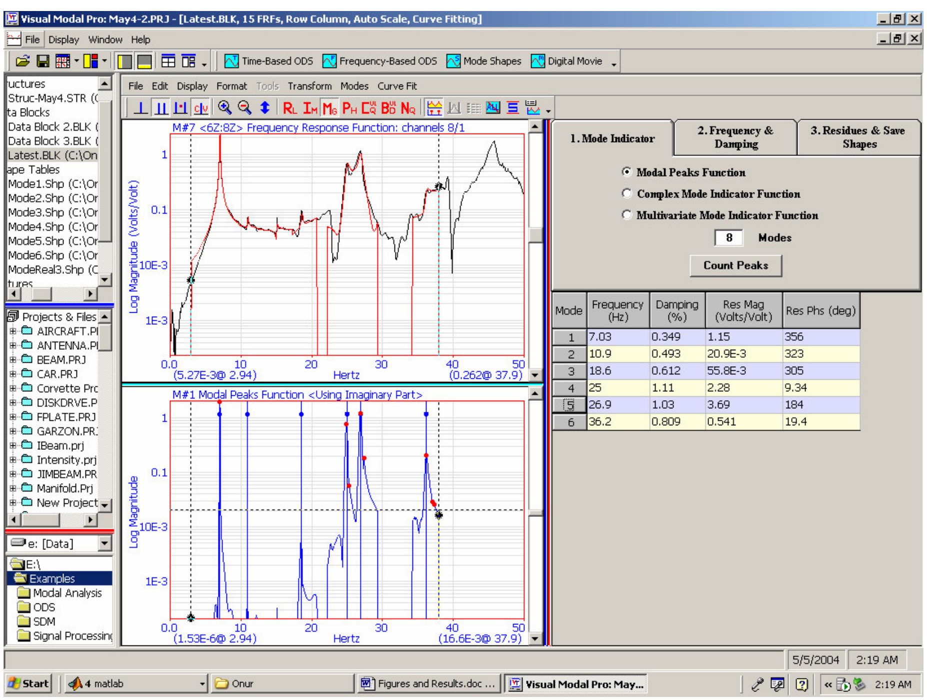

Figure 4.26 MEScope Curve Fitting Window

4.2.2 Single Span Laboratory Footbridge

The shaker and force plate assembly was placed at the inside and outside quarter points on the single span footbridge, and chirp signals were used to sweep a frequency range of 4-20 Hz for all three bottom chord extension configurations. Acceleration response data was collected at the points shown in Figure 4.27. First bending mode (Figure 4.28) natural frequencies, determined from the frequency response functions, are shown in Table 4.1. When the single span footbridge was excited with a chirp signal at the central midspan location, some drops in coherence values were observed at the first bending natural frequency for each bottom chord extension configuration. Consequently, the chirp FRF comparisons between Stages 1, 2 and 3 were made for the outside quarter point excitation location as shown in Figure 4.29. The results of the accelerometer placed next to the shaker are shown in Figure 4.29(a) while the results of the accelerometer placed at the footbridge center are displayed in Figure 4.29(b).

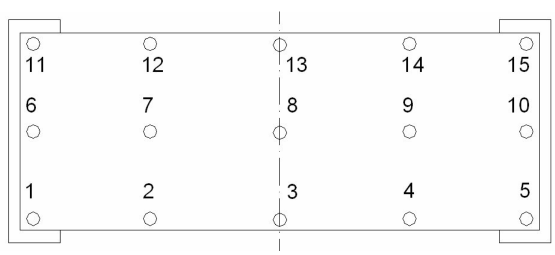

Figure 4.27 Accelerometer Locations- Single Span Footbridge

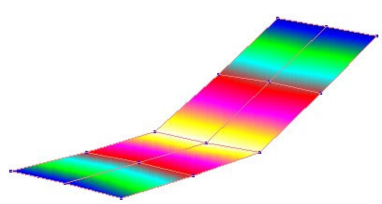

Figure 4.28 First Bending Mode- Single Span Footbridge

Table 4.1 First Bending Mode Natural Frequencies for Single Span Footbridge

FRF Observations	First Bending Mode, f_n (Hz)
Stage 1	8.00
Stage 2	6.95
Stage 3	7.80

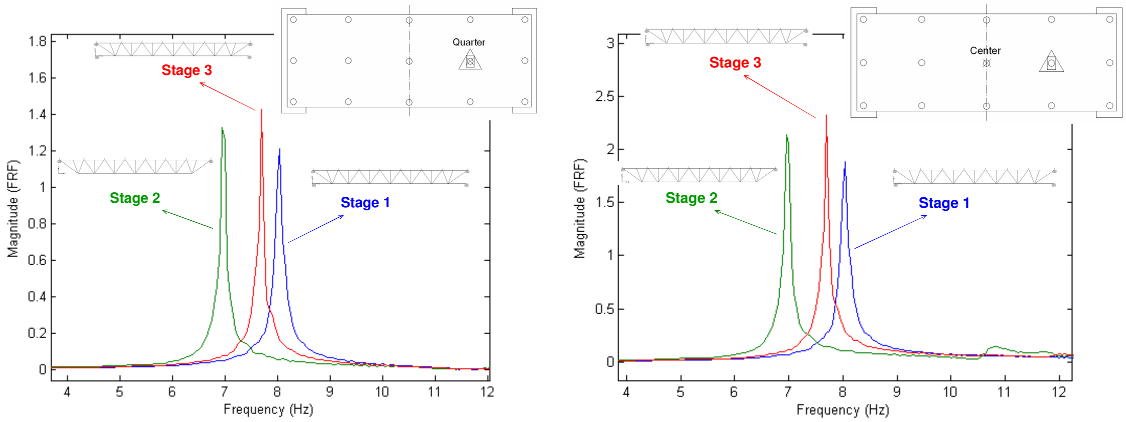

a) Accelerometer at Outside Quarter Point **b) Accelerometer at Center Point**

Figure 4.29 Chirp FRF comparisons for Quarter Point Excitation- Single Span Footbridge

As mentioned earlier, the bottom chord extensions were placed before the concrete was placed (Stage 1). It is shown in Figure 4.29 that removing bottom chord extensions from the system (Stage 2) caused a 13% drop (8.0 Hz to 6.95 Hz) in the natural frequency and about a 10% increase in the frequency response function magnitude. Re-installing the bottom chord extensions by jacking up the footbridge (Stage 3) increased the natural frequency of Stage 2 about 12% (6.95 Hz to 7.80 Hz) but it did not bring the natural frequency back to the original value of Stage 1. The frequency response function magnitudes increased about 8% when the bottom chord extensions were re-installed.

The single span footbridge was excited sinusoidally at the footbridge center for each bottom chord extension configuration. The excitation frequency was the first bending mode natural frequency of the system found from the chirp excitations. The first bending frequency was the main concern since it is in the range of human sensitivity for the single span footbridge. The second bending mode and the torsional modes did not play an important role in the acceleration response of the single span footbridge. Before the entire chirp FRF data was input and curve fitted in MEScope, the natural frequencies of the first bending modes of the three different bottom chord extension configurations were determined by the "peak picking method" directly from the frequency response function peaks (Table 4.1). However, MEScope resulted in slightly different natural frequency values since the curve fitting operation includes all collected chirp data. Modal damping ratios were also computed using MEScope (Table 4.2). The finite element model natural frequency predictions are also shown in Table 4.2. The curve fitted MEScope and FE model frequency predictions are within 1% with each other for Stages 1 and 2, while the FE model natural frequency is 4% higher than the MEScope predictions for Stage 3. First bending mode shapes from the FE models are shown in Figures 4.30 and 4.31.

Table 4.2 First Bending Mode Natural Frequencies and Damping Ratios for Single Span Footbridge

	MEScope Results		FE Model
	f_n (Hz)	Modal Damping Ratio (%)	f_n (Hz)
Stage 1	8.08	0.451	7.99
Stage 2	6.95	0.448	7.03
Stage 3	7.65	0.409	7.99

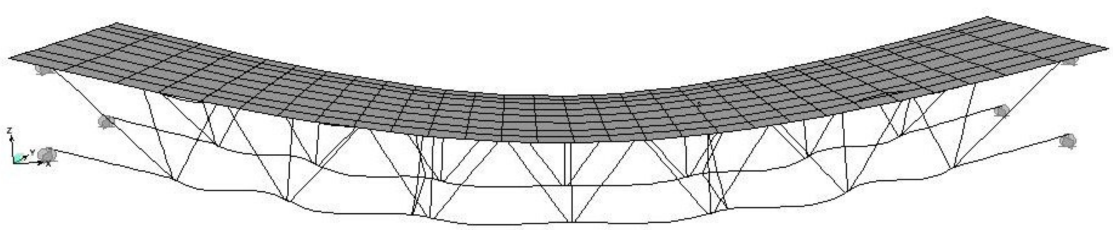

Figure 4.30 FE Model First Bending Mode Shape for Stages 1 and 3- Single Span Footbridge

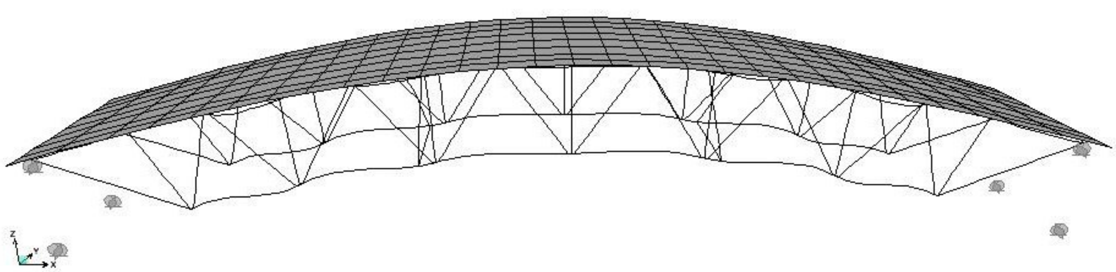

Figure 4.31 FE Model First Bending Mode Shape for Stage 2- Single Span Footbridge

Sinusoidal excitations were used to put the system into resonance and measure the response at resonance. In Figures 4.32 and 4.33, input and output time history and autospectra for the Stage 2, the simply supported beam case, are shown for 6.95 Hz sinusoidal excitation with the shaker placed at the center of the footbridge; the response data is from an accelerometer placed adjacent to the shaker. The force plate sinusoidal excitation amplitude was 7.59 lb. The FRF magnitude of the sinusoidal test excitations displayed in Figures 4.29 and 4.30 is 1.576 (0.01576 g/lbs) which is the ratio of output (11.96% g) to the input (7.59 lbs) at 6.95 Hz. In Figure 4.34, the frequency response function plot is magnified to see the FRF magnitude at 6.95 Hz. It must be noted that the FRF plot of Figure 4.34 is calculated based on the raw input and output signal voltages without converting them into force and acceleration (i.e. no calibration factors). The magnitude at 6.95 Hz is 3.534 which is the ratio of the output peak autospectrum to the peak input autospectrum of the raw signal voltage calculated by SigLab software during the test.

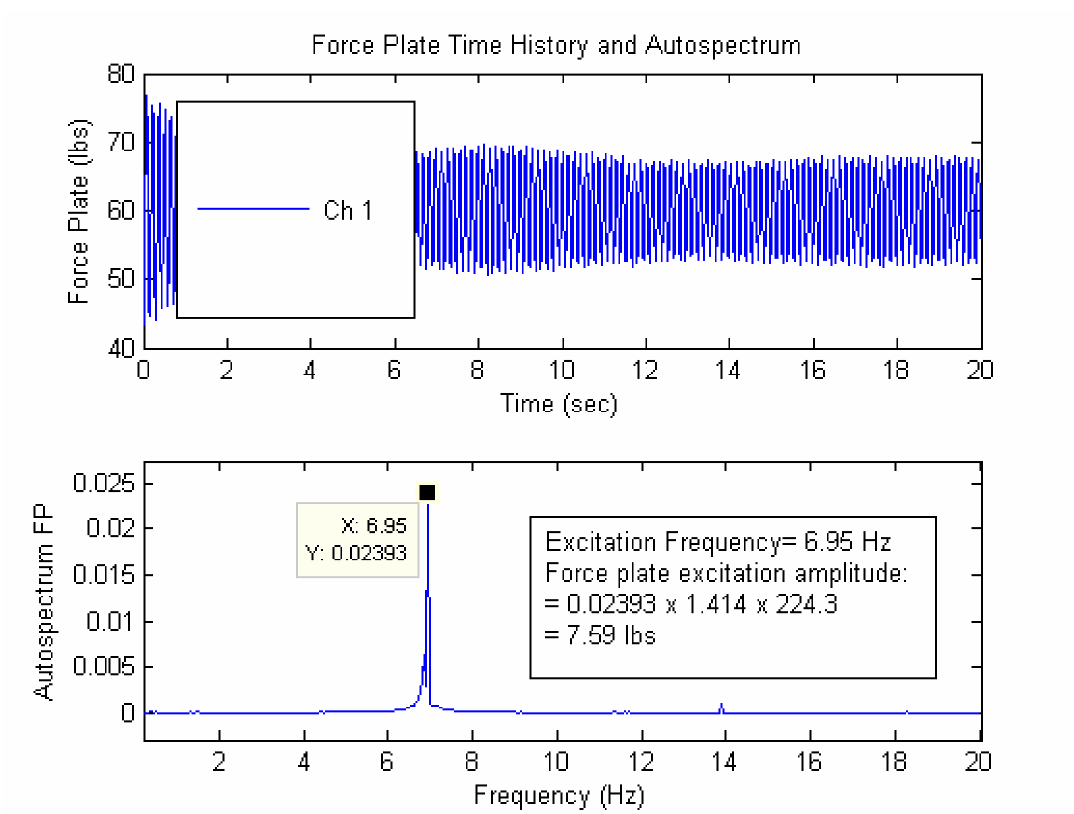

Figure 4.32 Input Time History and Associated Autospectrum- 6.95 Hz Sine Excitation at Footbridge Center

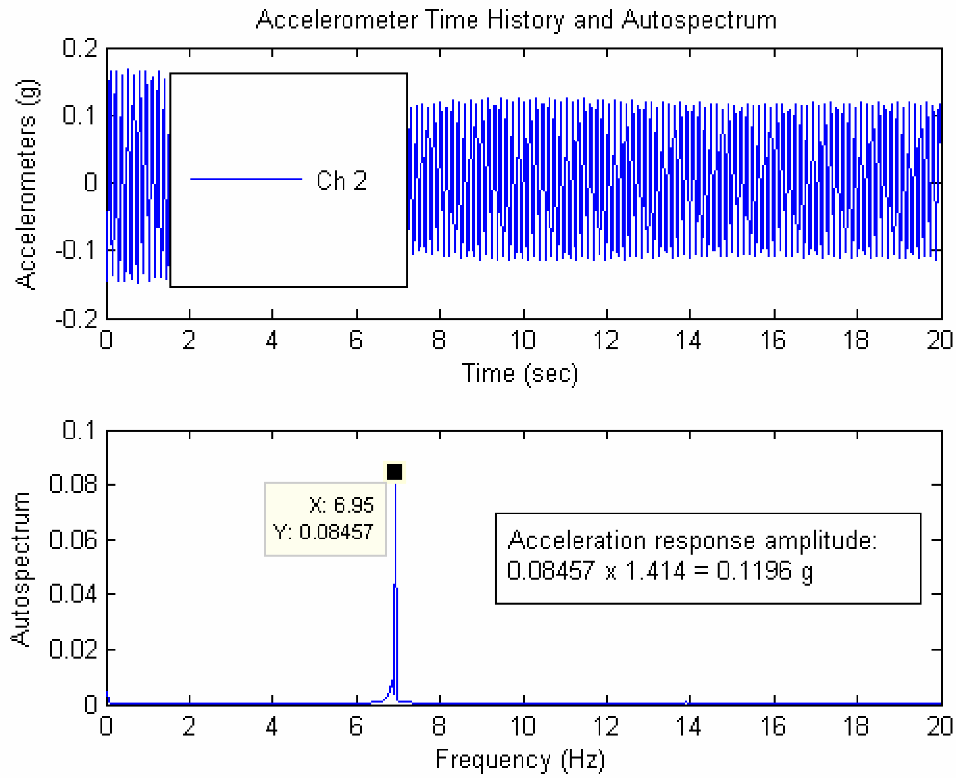

Figure 4.33 Output Time History and its Autospectrum- 6.95 Hz Sine Excitation at Footbridge Center

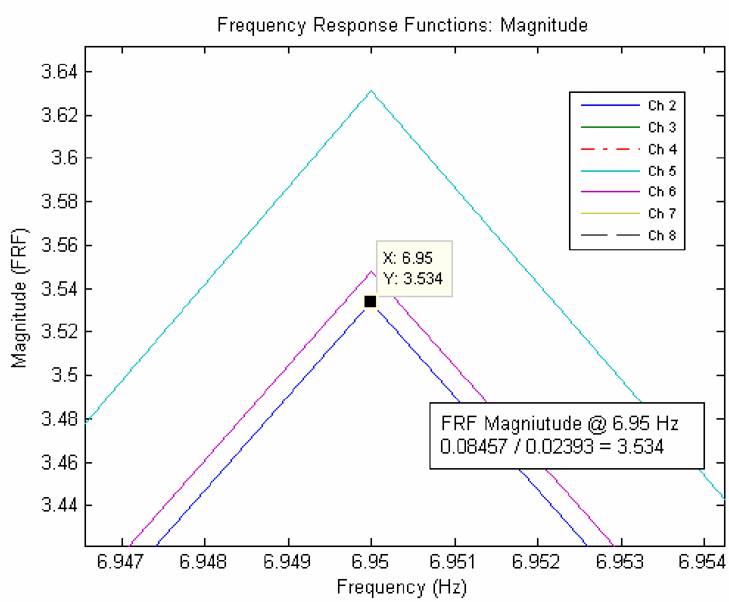

Figure 4.34 Frequency Response Function Based on the Raw Input and Output Signal Voltages - Magnified- 6.95 Hz Sine Excitation

For the Stage 2- simply supported beam case, the measured first bending mode natural frequency is 6.95 Hz. The Design Guide 11 calculation yields a natural frequency of 7.24 Hz (Appendix B) while the corresponding SAP model natural frequency is 7.03 Hz (Table 4.2). The DG-11 natural frequency value is 4% higher than the measured natural frequency while the SAP natural frequency is about 1% higher than the measured frequency. In DG-11, ideal walking excitation is a sine wave with an amplitude of $P_0 e^{-0.35 f_n}$, where P_0 is the recommended DG-11 "constant force" and f_n is the natural frequency. Estimated peak acceleration due to this excitation is,

$$\frac{a_p}{g} = \frac{P_0 e^{-0.35 f_n}}{\beta W} \tag{4.10}$$

where

f_n = system natural frequency

β = First bending mode damping ratio for Stage 2 = 0.00448 = 0.448%

W = Single span footbridge total weight= 13986 lbs

P_0 = Recommended DG11 "constant force" for indoor and outdoor footbridges = 92 lbs

The term $P_0 e^{-0.35 f_n}$ is the ideal walking excitation sine wave amplitude. The amplitudes of the excitations (input) for the measured, DG11, and finite element predicted natural frequencies, the corresponding estimated peak accelerations (output) and frequency response function magnitudes (output/input) are shown in Table 4.3.

Table 4.3 First Bending Mode Sinusoidal Excitation Amplitudes- Single Span Footbridge

Parameter	First Bending Mode		
f_n	6.95 Hz (measured)	7.235 Hz (DG11)	7.029 Hz (FE)
$P_0 e^{-0.35 f_n}$	8.079 lbs	7.312 lbs	7.860 lbs
$\frac{a_p}{g} = \frac{P_0 e^{-0.35 f_n}}{\beta W}$	12.9% g	11.7% g	12.5% g
FRF (Output / Input)	1.597	1.600	1.590

The FRF magnitude of the sinusoidal test excitations displayed in Figures 4.32 and 4.33 is 1.576 at the measured natural frequency of 6.95 Hz, which is in excellent agreement with the theoretical FRF magnitudes shown in Table 4.3. The same test is simulated in the FE model (Figure 4.35) with an excitation frequency of 7.029 Hz (first bending mode of the SAP model) and excitation amplitude of $P_0 e^{-0.35.(7.029)}$ =7.860 lbs and a modal damping ratio of 0.448% (MEScope). (The damping ratios are also hand-calculated by half-power method from the chirp frequency response functions. The average of the damping ratios from different chirp excitations resulted in 0.453%, which is within 1% of MEScope calculated damping ratio). The resulting peak acceleration and FRF magnitude are 12.6%g and 1.60, respectively; which are very close to the test results of Figures 4.32 and 4.33 and DG-11 predicted numbers of Table 4.3.

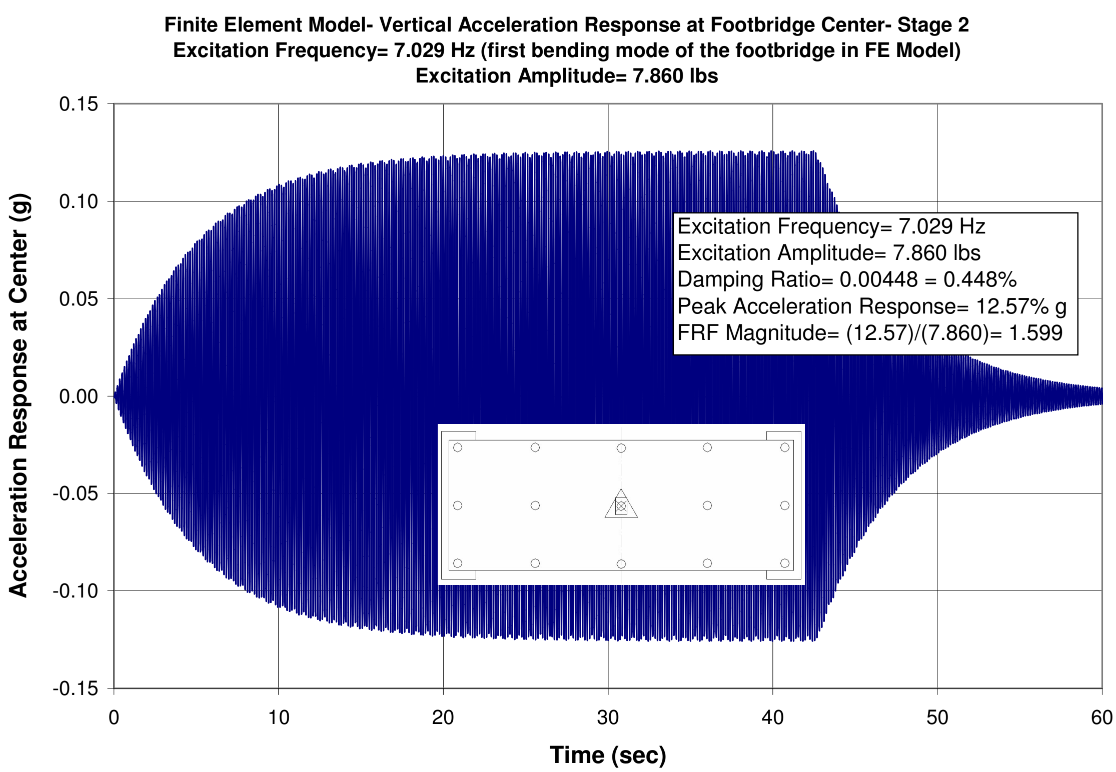

Figure 4.35 Output Time History of SAP Model- 7.029 Hz Sine Excitation at Footbridge Center- Stage 2

The acceleration response at the center of the footbridge is plotted with respect to excitation force amplitude in Figure 4.36. It is realized that the system behavior is very close to linear above excitation amplitudes of approximately 12 lb. However, for an excitation amplitude below 12 lb, the system behavior is nonlinear. This nonlinearity can also be seen in the frequency response (measured acceleration / input force of the raw signal) magnitudes in Figure 4.37. As the excitation amplitude increases, the frequency response decreases, which is attributed to the apparent amplitude dependent damping of the footbridge structure. That is, as the vibration amplitude increases, the damping ratio also increases. This is why the sinusoidal excitation test results agree well with the finite element model predictions for low excitation amplitudes when the modal damping ratios in Table 4.2 are used. The finite element model acceleration predictions are higher than the test results as the modal damping ratio is underestimated in the FE model for higher excitation amplitudes. For example, when a sinusoidal excitation with 12.4 lbs amplitude was applied at the footbridge center (Stage 1- Bottom chord extensions in place) the resulting acceleration response was around 14%g in an actual test (FRF = 14/12.4= 1.13). However, when the same test is simulated in SAP with a modal damping ratio of 0.451%, the resulting acceleration response is around 19.2%g (FRF = 19.2/12.4 = 1.55) as shown in Figure 4.38. The damping ratios are also hand-calculated by half-power method from the chirp frequency response functions. The average of the damping ratios from different chirp excitations resulted in 0.639%, which is within 40% higher than that of MEScope calculated damping ratio. When damping ratio of 0.639% is used in the FE model, the acceleration response was predicted as 13.6%g which is very close to the acceleration measured during the test (14%). It is realized that the damping ratio was underestimated by MEScope for this stage.

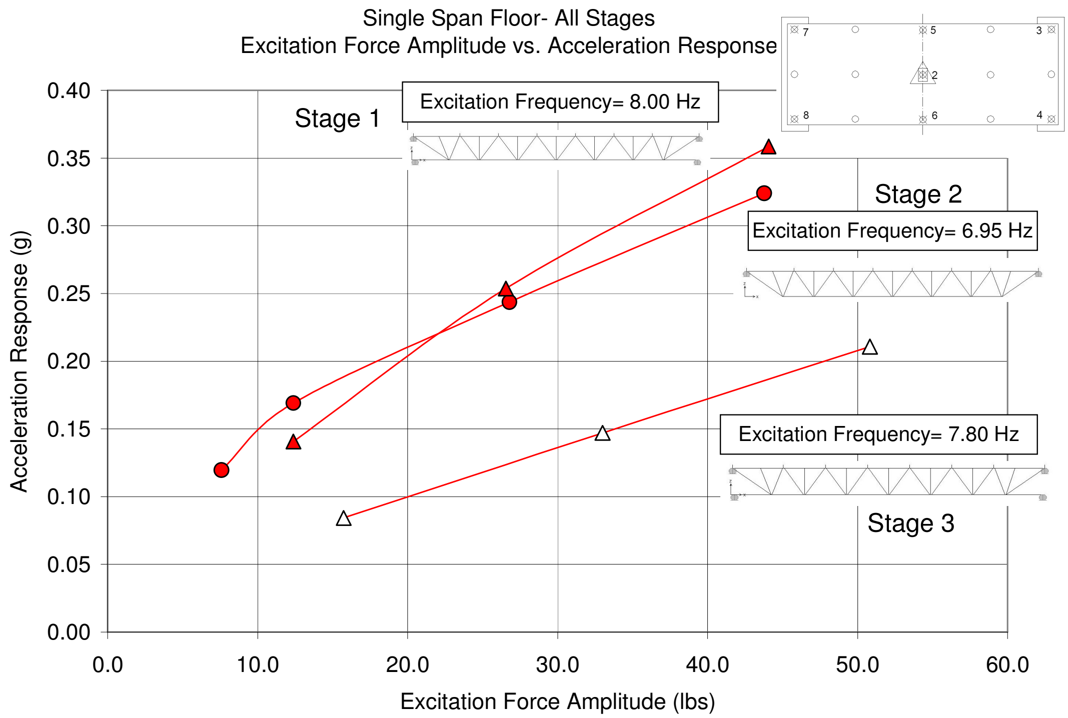

Figure 4.36 Excitation Force Amplitude vs. Acceleration Response at Footbridge Center

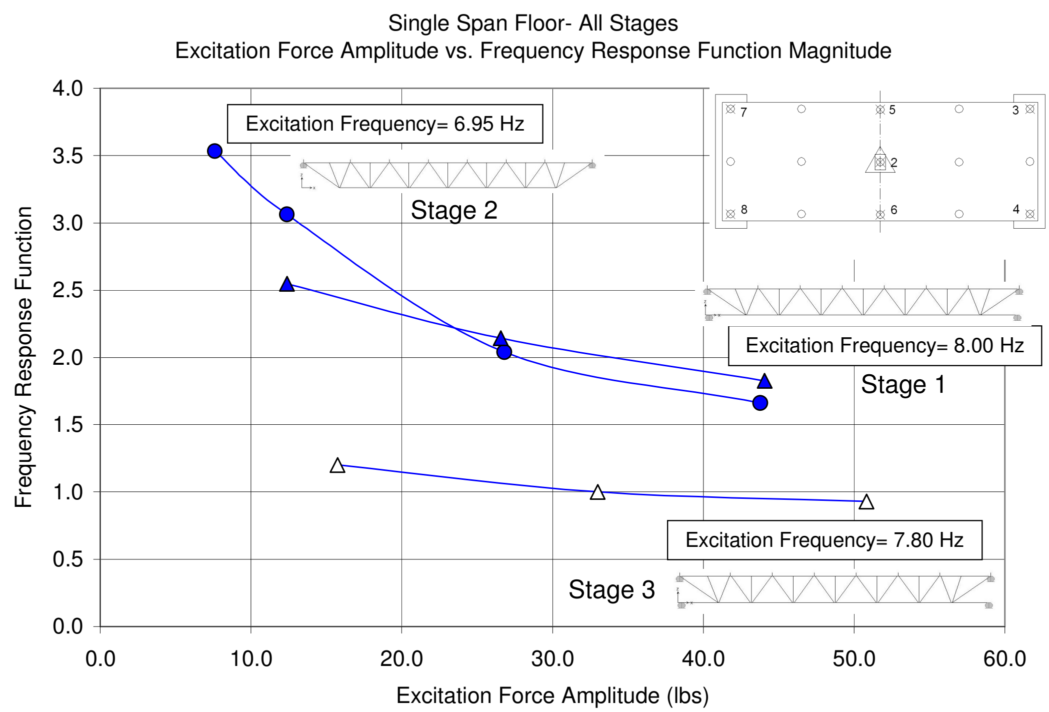

Figure 4.37 Excitation Force Amplitude vs. Frequency Response Function at Footbridge Center

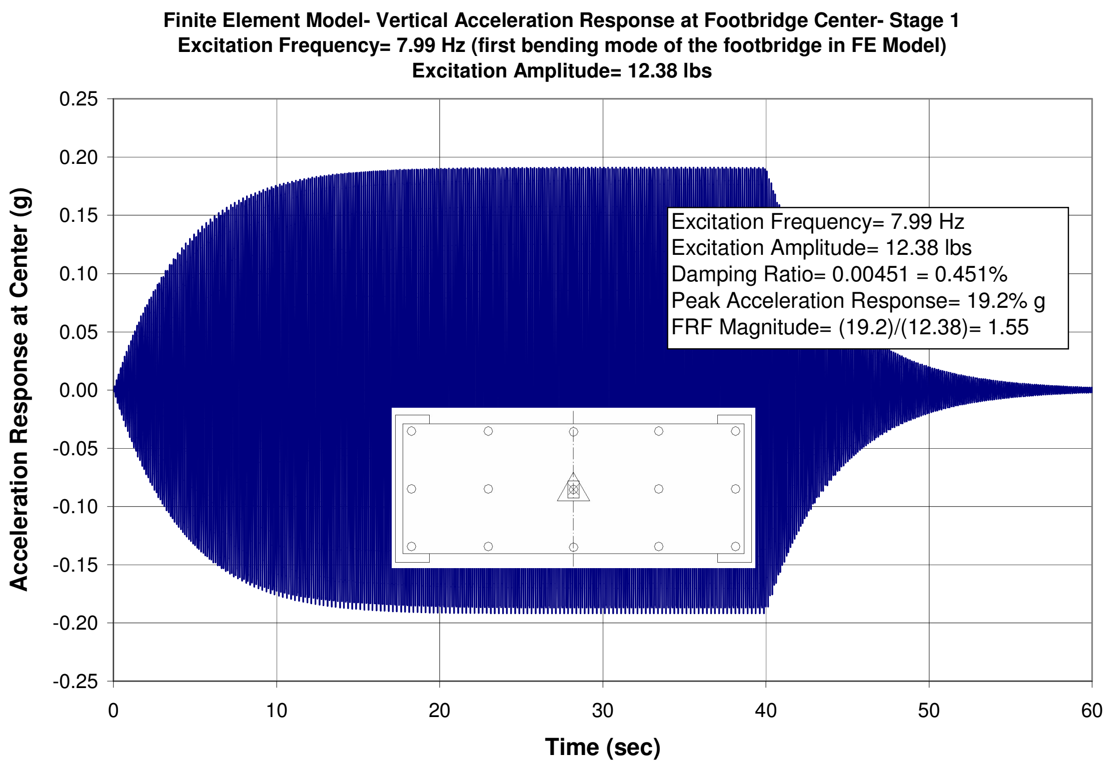

Figure 4.38 Output Time History of SAP Model- 7.99 Hz Sine Excitation at Footbridge Center- Stage 1

The discrepancy between the MEScope and FRF half-power method damping ratios might be related to amplitude dependent damping phenomenon. Amplitude dependent damping is a very common aspect in mechanical engineering applications and the earthquake engineering field of civil engineering applications. With increasing vibration amplitude, the damping ratio also increases (Leonard and Eyre 1975). However it has not been studied extensively in floor vibration applications.

It has also been reported that in addition to amplitude dependent damping, the natural frequencies may also be amplitude dependent due to change of stiffness and coupling with other eigenmodes (Bachmann et al. 1995).

It is observed that for Stages 1 and 2, the system was at resonance with sinusoidal excitations, however for Stage 3 the system was excited at 7.80 Hz (peak picking method directly from FRF measurements) while the actual natural frequency was 7.65 Hz

(MESope curve fitting). So, the system was not in full resonance for Stage 3 (Figures 4.36 and 4.37). When Stage 1 and Stage 2 are compared, it is realized that the frequency response function magnitudes are very close for excitation amplitudes of 27 lb and 44 lb. However for the 12 lb excitation amplitudes, the frequency response function value is 20% higher in Stage 2 than in Stage 1 (Figure 4.37).

To further investigate the footbridge, heel drop excitations were performed on the force plate, which was placed at the center and quarter point locations of the footbridge. Heel drop data was recorded for all three bottom chord extension configurations. The FRF comparisons between Stages 1, 2 and 3 for the center (Figure 4.39(a)) and quarter point (Figure 4.39(b)) locations are shown in Figure 4.39.

From the quarter point data in Figure 4.39(a), removing the bottom chord extensions from the system (Stage 2) caused a 34% drop in the frequency response function magnitude. Re-installing the bottom chord extensions (Stage 3) increased the frequency response function magnitudes about 11%. From the center point data in Figure 4.39(b), removing bottom chord extensions from the system (Stage 2) caused a 37% drop in the frequency response function magnitude. Re-installing the bottom chord extensions (Stage 3) decreased the frequency response function magnitude about 7%.

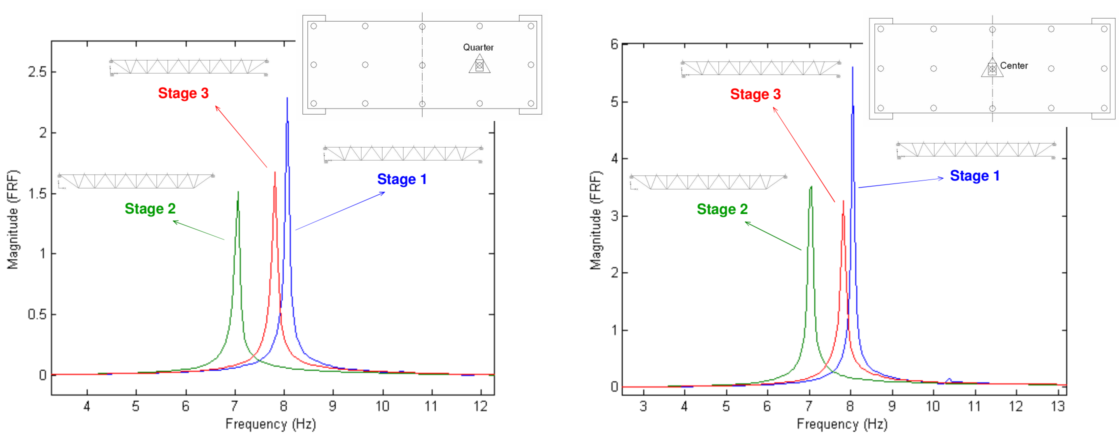

a) Accelerometer at Quarter Point **b) Accelerometer at Center Point**

Figure 4.39 Heel drop FRF Comparisons for Quarter and Central Point Excitation- Single Span Footbridge

As seen in Figures 4.29, 4.37 and 4.39, the effect of bottom chord extensions in Stages 1 and 2 does not follow a specific pattern in the levels of frequency response function magnitudes. The stiffness tests showed that Stage 1 was the stiffest configuration and the question was whether the bottom chord extensions will effect the frequency response of the footbridge or not. From the heel drop and chirp tests, it is realized that the frequency response function magnitudes do not decrease in Stage 1 when compared to Stage 2. In Figure 4.39 it is seen that Stage 2 has even lower frequency response function magnitudes although no bottom chord extensions are in place for this case. For sinusoidal excitations, when Stage 1 and Stage 2 are compared, it is realized that the frequency response function magnitudes are very close to each other for excitation amplitudes of 27 lb and 44 lb. However, for the 12 lbs excitation amplitudes, the frequency response function value is 20% higher in Stage 2 than in Stage 1 (Figure 4.37). That means having the bottom chord extension in place before the concrete pour (Stage 1) improved the acceleration response of the footbridge 20% for sinusoidal resonance excitations for the first bending mode as compared to Stage 2.

After the heel drop tests, walking excitations were performed with different walking pace frequencies. Because the input excitation can not be measured for walking excitations, frequency response functions are not available. Acceleration versus time traces of walking excitations as well as RMS and $\sqrt{2}$ RMS values, were used for comparison of bottom chord extension effects. Acceleration time histories from walking of one pedestrian (162 lb) at 1/3rd of the measured first bending mode natural frequency of the single span footbridge are shown in Figure 4.40. The associated autospectra of the time history data with RMS and $\sqrt{2}$ RMS records are also shown in Figure 4.41 (1 Volt = 1 g). It can be seen in autospectra that the first bending mode of each stage was excited by the walking.

Comparing the results of Stage 1, as constructed with the bottom chord extensions in place, to Stage 2, it is clear that extending the bottom chords does not reduce the walking acceleration response of the footbridge. The RMS value of Stage 1 walking data dropped 11% when the bottom chord extensions were removed from the system for Stage 2. Re-installing the bottom chord extensions for Stage 3 did not result in improvements for acceleration response for walking excitations either. The RMS value of Stage 2 increased about 10% with the re-installation of the bottom chord extensions for Stage 3.

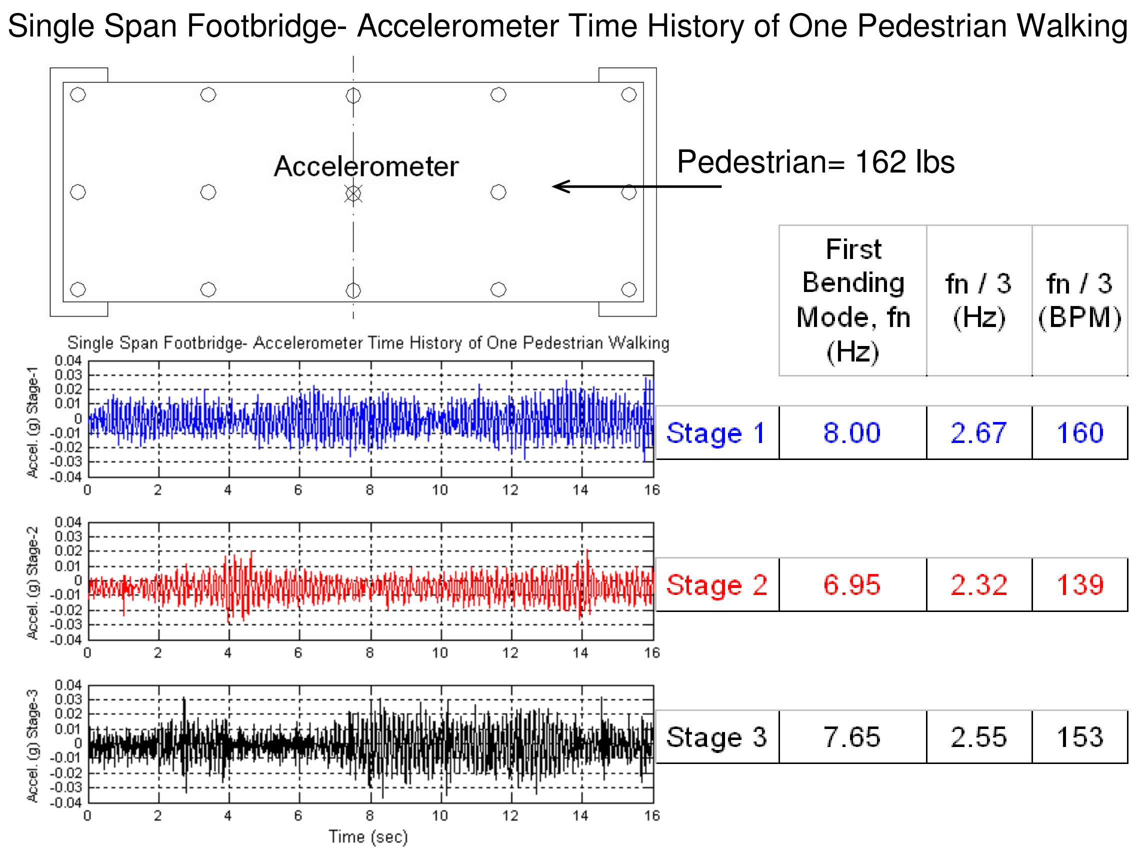

Figure 4.40 Accelerometer Time History of One Pedestrian Walking on Single Span Footbridge

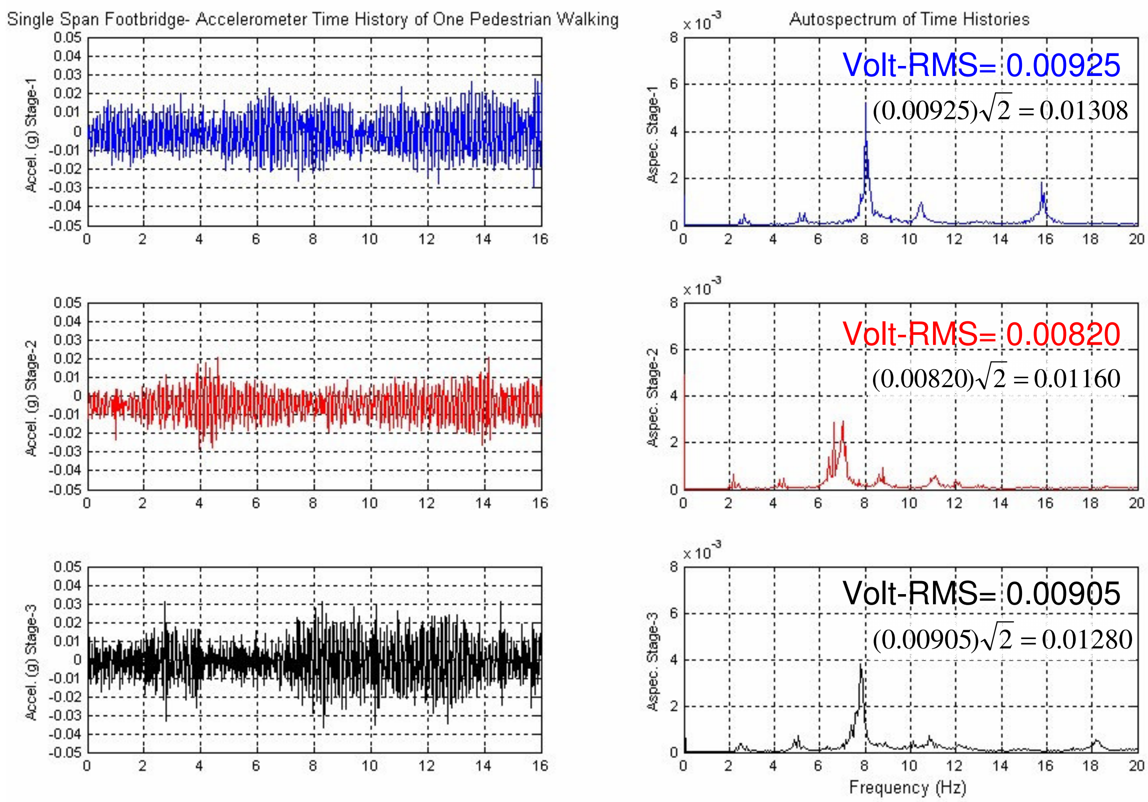

Figure 4.41 Accelerometer Time History of One Pedestrian Walking on Single Span Footbridge and Associated Autospectra

4.2.3 Three Span Laboratory Footbridge

The excitation forces applied to the single span footbridge were repeated for the three span footbridge. The shaker and force plate assembly were placed at several locations. Acceleration response data was collected at the points shown in Figure 4.42. Chirp signals were input to MEScope and the first three bending modes were determined (Figure 4.43) for all five bottom chord extension configurations. The first three bending mode natural frequencies determined from the frequency response functions are shown in Table 4.4. The nonlinearity observed in the single span footbridge measurements was also seen in three span footbridge measurements. The natural frequency values and frequency response function magnitudes depending on the excitation amplitude and excitation location. This phenomenon was especially true for the third bending mode natural frequencies of Stages 2, 4 and 5 showed some deviations depending on excitation location. As the excitation amplitude increased, the natural frequency values decreased and the frequency response function magnitude decreased. The natural frequency values are also amplitude dependent due to change of stiffness and coupling with other eigenmodes (Bachmann et al 1995).

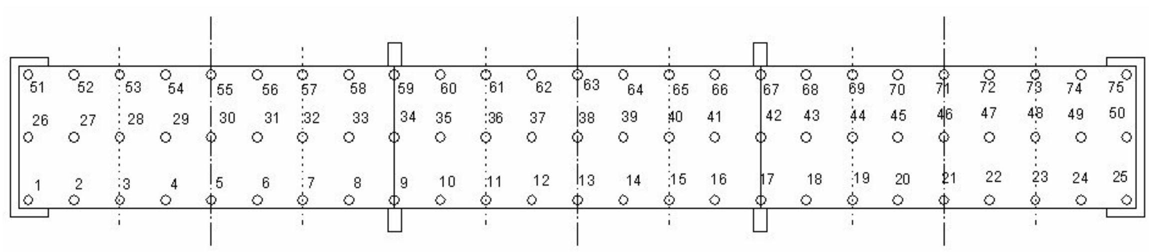

Figure 4.42 Accelerometer Locations- Three Span Footbridge

Table 4.4 First Three Bending Mode Natural Frequencies- Three Span Footbridge

FRF observations	First Bending Mode, f_n (Hz)	Second Bending Mode, f_n (Hz)	Third Bending Mode, f_n (Hz)
Stage 1	7.75	8.10	8.95
Stage 2	7.50	7.90	8.75-8.90
Stage 3	7.50	7.80	8.40
Stage 4	7.60	8.15	8.85-8.90
Stage 5	7.80	8.10	8.85-8.95

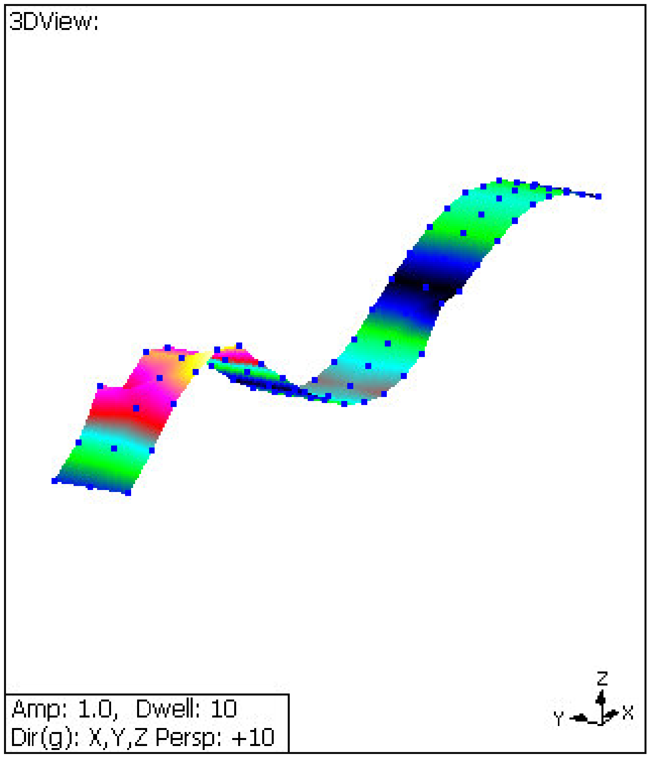

a) First Bending Mode

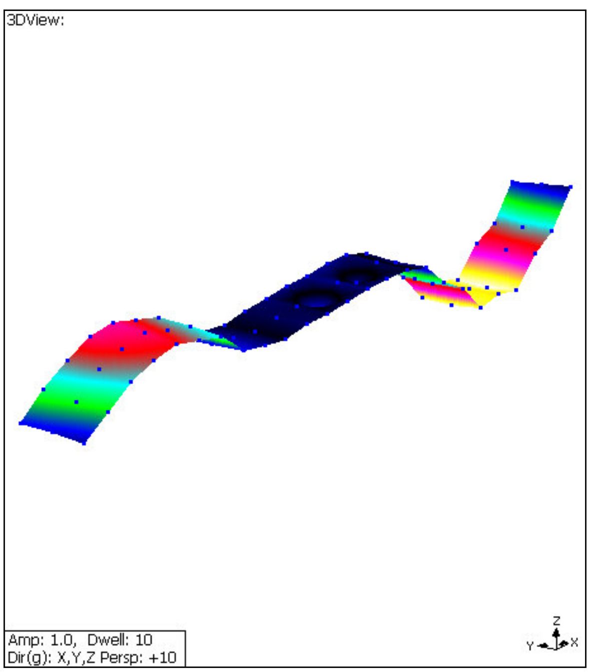

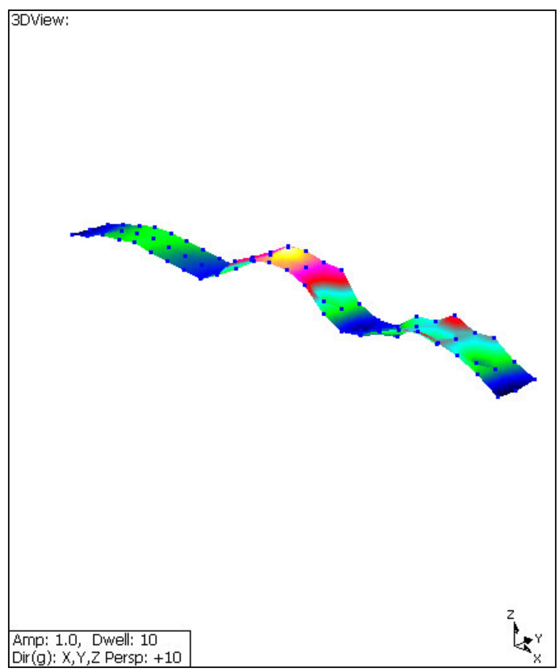

b) Second Bending Mode **c) Third Bending Mode**

Figure 4.43 Bending Modes- Three Span Footbridge

The chirp FRF comparisons between all five stages were made for central Bay 2 and central Bay 3 excitation points as shown in Figures 4.44, 4.45 and 4.46. In each figure, the FRF magnitudes are from accelerometers placed adjacent to the shaker since they have the best coherence values consistently for all measurement.

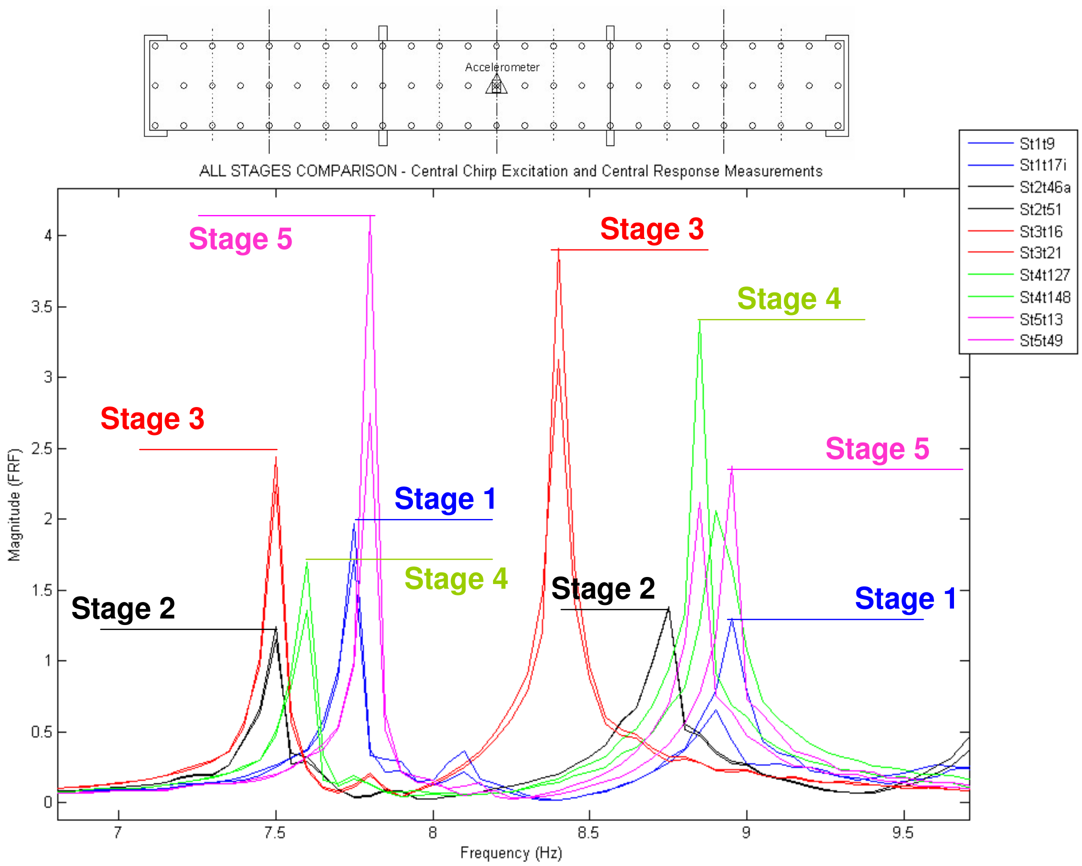

Figure 4.44 Chirp FRF Comparisons for Bay 2 Central Point Excitation- First and Third Bending Modes- Three Span Footbridge

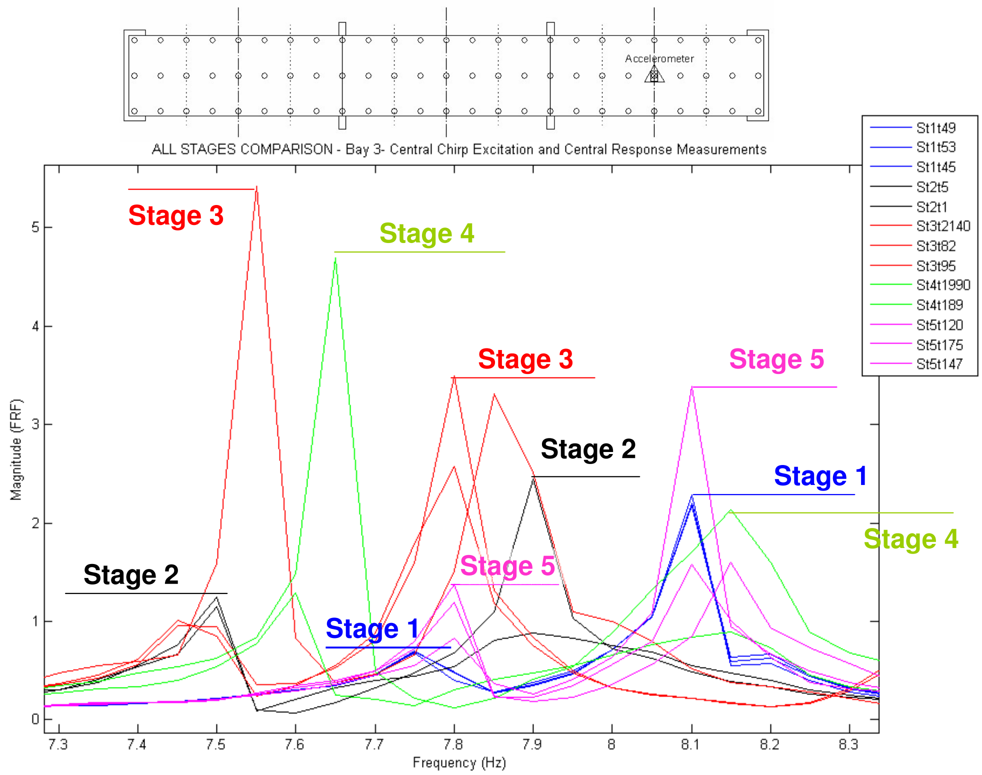

Figure 4.45 Chirp FRF Comparisons for Bay3 Central Point Excitation- First and Second Bending Modes- Three Span Footbridge

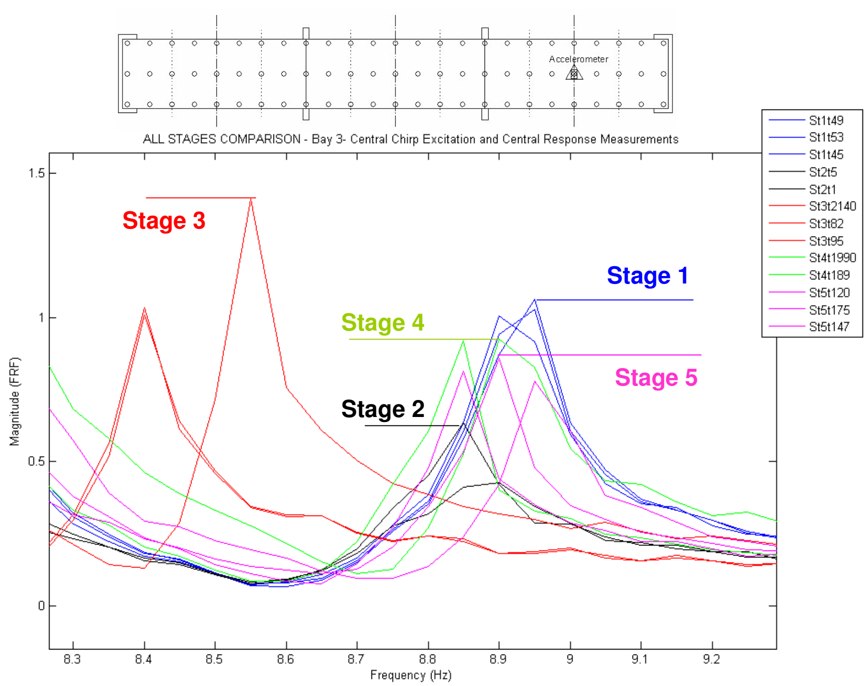

Figure 4.46 Chirp FRF Comparisons for Bay3 Central Point Excitation- Third Bending Mode- Three Span Footbridge

The results of the central Bay 2 chirp excitations are shown in Figure 4.44. For this excitation location it was not possible to excite the second bending mode since the shaker location is at the node point. Hence, the peaks in Figure 4.44 are the peaks of bending modes 1 and 3.

It is shown in Figure 4.44 that the first bending natural frequency of Stage 1 (7.75 Hz) decreased to 7.50 Hz and the corresponding FRF magnitude peak decreased about 37% when the exterior bottom chord extensions were removed from the system (Stage 2). Also, the third bending natural frequency of Stage 1 (8.95 Hz) decreased to 8.75 Hz and the FRF magnitude stays about the same when the exterior bottom chord extensions were removed from the system (Stage 2). Removing the interior bottom chord extensions (Stage 3) did not affect the first bending mode frequency (7.50 Hz), however it decreased the third bending mode frequency to 8.40 Hz from 8.75 Hz. The FRF magnitudes increased about 97% for the first bending mode and 182% for the third bending mode when the interior bottom chord extensions were removed from the system (Stage 3). Re-installing the interior bottom chord extensions (Stage 4) increased the first bending mode natural frequency to 7.60 Hz and the third bending mode natural frequency to 8.85-8.90 Hz. The FRF magnitudes decreased about 30% for the first bending mode and 13 % for the third bending mode when the interior bottom chord extensions were re-installed in the system (Stage 4). Re-installing the exterior bottom chord extensions (Stage 5) increased the first bending mode natural frequency to 7.80 Hz and the third bending mode natural frequency to 8.95 Hz. Also, the FRF magnitudes increased about 140% for the first bending mode and decreased about 30% for the third bending mode when the exterior bottom chord extensions were re-installed (Stage 5).

The results of the central Bay 3 chirp excitations are shown in Figure 4.45 and 4.46. At this excitation location it was possible to excite all the first three bending modes. Results of the first two modes are shown in Figure 4.45 with third mode results shown in Figure 4.46.

From Figure 4.45, the first bending natural frequency of Stage 1 (7.75 Hz) decreased to 7.50 Hz and the corresponding FRF magnitude peak increased about 72% when the exterior bottom chord extensions were removed from the system (Stage 2). Also, the second bending natural frequency of Stage 1 (8.10 Hz) decreased to 7.90 Hz and the FRF magnitude increased about 14% when the exterior bottom chord extensions were removed from the system (Stage 2). Removing the interior bottom chord extensions (Stage 3) slightly increased the first bending mode frequency (7.55 Hz); however, it decreased the second bending mode frequency to 7.80 Hz from 7.90 Hz. The FRF magnitudes increased more than 300% for the first bending mode and 40% for the second bending mode when the interior bottom chord extensions were removed from the system (Stage 3). Re-installing the interior bottom chord extensions (Stage 4) increased the first bending mode natural frequency to 7.65 Hz and the second bending mode natural frequency to 8.15 Hz. The FRF magnitudes decreased about 14% for the first bending mode and 39% for the second bending mode when the interior bottom chord extensions were re-installed to the system (Stage 4). Re-installing the exterior bottom chord extensions (Stage 5) increased the first bending mode natural frequency to 7.80 Hz and sets the second bending mode natural frequency at 8.10 Hz. The FRF magnitudes decreased about 71% for the first bending mode and increased about 59% for the second bending mode when the exterior bottom chord extensions were re-installed to the system (Stage 5).

The results of the third bending mode are shown in Figure 4.46. It is shown that the third bending mode natural frequency of Stage 1 (8.90-8.95 Hz) decreased to 8.85 Hz and the corresponding FRF magnitude peak decreased about 40% when the exterior bottom chord extensions were removed from the system (Stage 2). Removing the interior bottom chord extensions (Stage3) decreased the third bending mode frequency from 8.85 Hz to 8.40-8.55 Hz and the FRF magnitudes increased about 123% for the third bending mode when the interior bottom chord extensions were removed from the system (Stage 3). Re-installing the interior bottom chord extensions (Stage 4) increased the third bending mode natural frequency to 8.85-8.90 Hz from 8.40-8.55 Hz and the FRF magnitudes decreased about 34% for the third bending mode when the interior bottom chord extensions were re-installed to the system (Stage 4). Re-installing the exterior bottom chord extensions (Stage 5) did not affect the third bending mode much and sets it in the 8.85-8.95 Hz range. The FRF magnitudes decreased about 7% for the third bending mode when the exterior bottom chord extensions were re-installed in the system (Stage 5).

The three span footbridge was excited sinusoidally at the center of the bays for each bottom chord extension configuration. The excitation frequencies were the first three bending mode natural frequencies and some torsional mode frequencies of the system found from the chirp excitation FRFs. The first three bending modes were the main concern since they were in the range of human sensitivity for the three span footbridge. The torsional modes did not play an important role in the acceleration response of the three span footbridge. Before the entire chirp FRF data was input and curve fitted in MEScope, the natural frequencies of the first three bending modes of the five different bottom chord extension configurations were determined by the "peak picking method" directly from the frequency response function peaks (Table 4.4). However, MEScope resulted in slightly different natural frequency values since the curve fitting operation includes all collected chirp data. Modal damping ratios are also computed by MEScope (Table 4.5). The finite element model natural frequency predictions are also shown in Table 4.5. The curve fitted MEScope and FE model frequency predictions are within 1% of each other for the first bending mode and 3% for the second bending mode for all stages. For the third bending mode, the FE model predictions are 4-to-10% higher than the MEScope natural frequencies. The first three bending mode shapes from the FE model are shown in Figure 4.47.

It must be noted that for all Stage 5 measurements, the power box was not functioning with proper calibration during the modal testing. All Stage 5 data shown in this dissertation are re-calibrated data.

Table 4.5 First Three Bending Mode Natural Frequencies and Damping Ratios for Three Span Footbridge

	First Bending Mode			Second Bending Mode			Third Bending Mode		
	MEScope Results		FE Model	MEScope Results		FE Model	MEScope Results		FE Model
	f_n (Hz)	Modal Damping Ratio (%)	f_n (Hz)	f_n (Hz)	Modal Damping Ratio (%)	f_n (Hz)	f_n (Hz)	Modal Damping Ratio (%)	f_n (Hz)
Stage 1	7.76	0.265	7.76	8.11	0.255	7.88	8.93	0.332	9.76
Stage 2	7.51	0.272	7.49	7.90	0.361	8.10	8.81	0.539	9.63
Stage 3	7.49	0.281	7.49	7.81	0.402	7.78	8.37	0.213	8.70
Stage 4	7.60	0.273	7.49	8.14	1.440	8.10	8.78	0.203	9.63
Stage 5	7.80	0.178	7.76	8.13	0.235	7.88	8.89	0.571	9.76

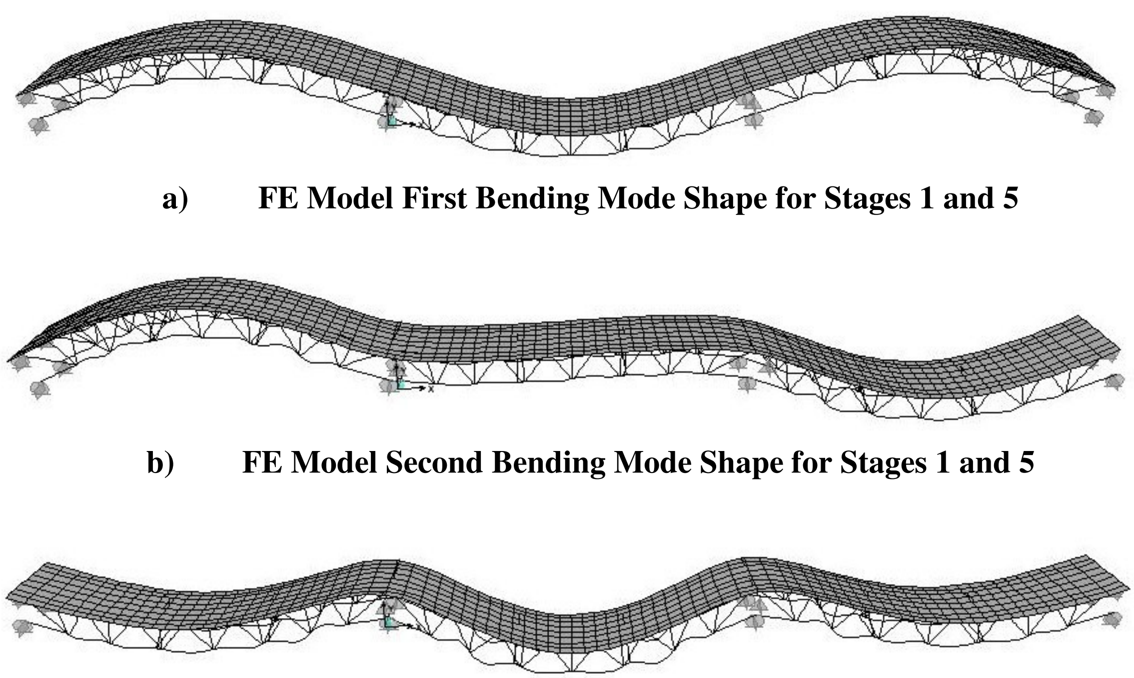

a) FE Model First Bending Mode Shape for Stages 1 and 5

b) FE Model Second Bending Mode Shape for Stages 1 and 5

c) FE Model Third Bending Mode Shape for Stages 1 and 5

Figure 4.47 FE Model Bending Mode Shapes- Three Span Footbridge

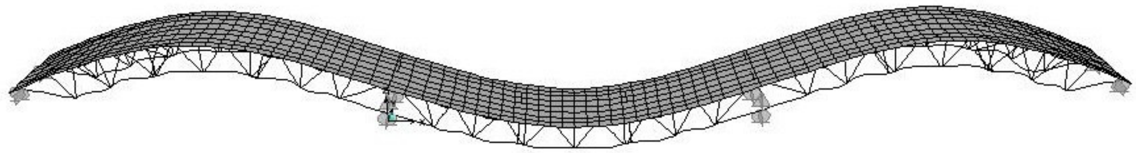

d) First Bending Mode Shape for Stages 2 and 4

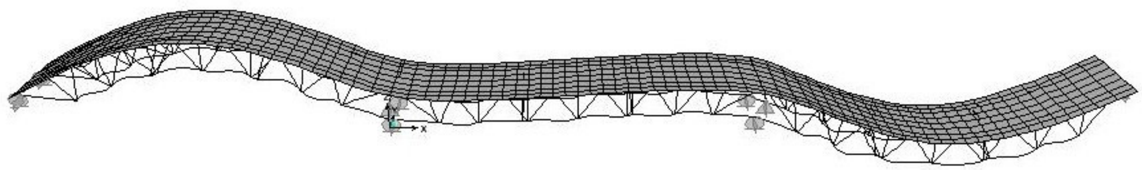

e) Second Bending Mode Shape for Stages 2 and 4

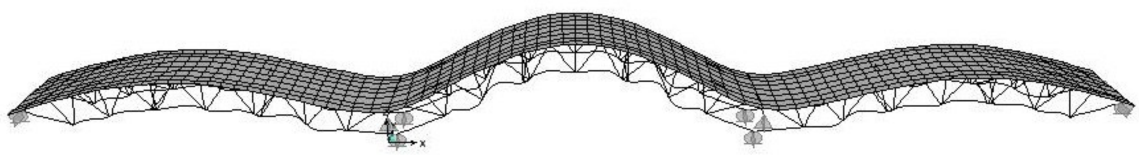

f) Third Bending Mode Shape for Stages 2 and 4

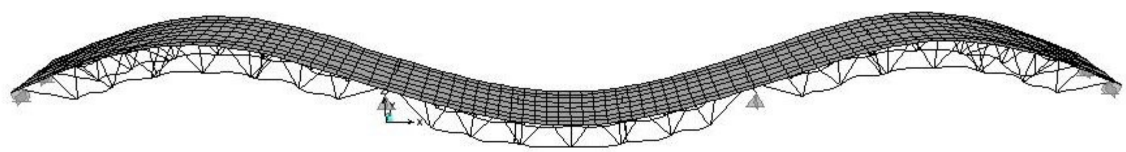

g) First Bending Mode Shape for Stage 3

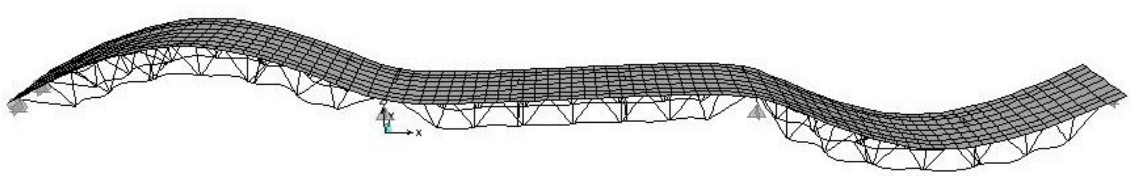

h) Second Bending Mode Shape for Stage 3

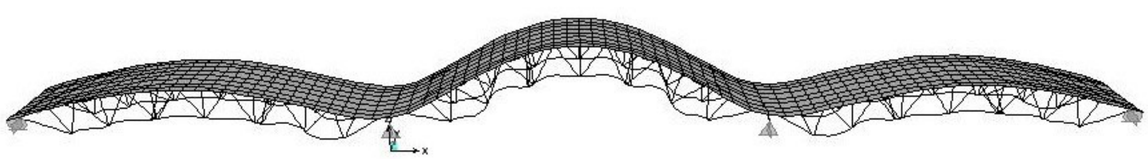

i) Third Bending Mode Shape for Stage 3

Figure 4.47 FE Model Bending Mode Shapes- Three Span Footbridge (Continued)

The sinusoidal excitations were used to put the system into resonance. The sinusoidal excitation FRF magnitude comparisons between all five stages were made for the first three bending modes for central Bay 2 and central Bay 3. The accelerometers were placed adjacent to the shaker, since they gave the best coherence values consistently, in the comparisons.

The results of the central Bay 2 first bending mode sine excitations are shown in Figure 4.48. It is shown that the first bending natural frequency of Stage 1 (7.75 Hz) decreased to 7.50 Hz and the corresponding sine excitation FRF magnitude peak decreased about 20% (from 1.03 to 0.82) when the exterior bottom chord extensions were removed from the system (Stage 2). Removing the interior bottom chord extensions (Stage 3) did not affect the first bending mode frequency (7.50 Hz); however, the FRF magnitudes decreased about 13% (from 0.82 to 0.71). Re-installing the interior bottom chord extensions (Stage 4) increased the first bending mode natural frequency to 7.60 Hz and decreased the FRF magnitudes about 6% (from 0.71 to 0.67). Re-installing the exterior bottom chord extensions (Stage 5) increased the first bending mode natural frequency to 7.80 Hz and increased the FRF magnitudes about 27% (from 0.67 to 0.85). It is concluded that having the bottom chord extensions in place increased the first bending mode natural frequency of the footbridge but does not significantly lower the frequency response of the footbridge for sinusoidal excitations at the first bending mode frequencies.

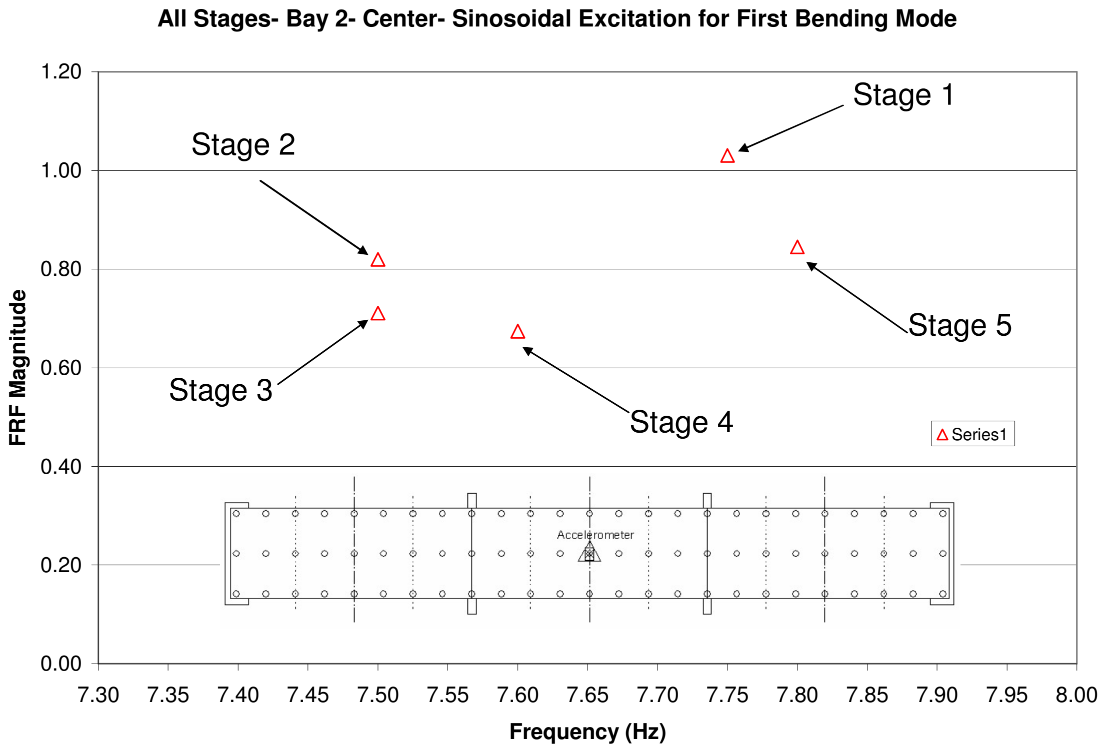

Figure 4.48 Frequency Response Function vs. Sinusoidal Excitation Frequency at Footbridge Center- First Bending Mode

The results of the central Bay 2 third bending mode sine excitations are shown in Figure 4.49. It is shown that the third bending natural frequency of Stage 1 (8.95 Hz) drops to 8.75 Hz and the corresponding sine excitation FRF magnitude peak increased about 16% (from 0.69 to 0.80) when the exterior bottom chord extensions were removed from the system (Stage 2). Removing the interior bottom chord extensions (Stage 3) decreased the third bending mode frequency about 4% (from 8.75 Hz to 8.40 Hz) and increased the FRF magnitudes about 59% (from 0.80 to 1.27). Re-installing the interior bottom chord extensions (Stage 4) increased the third bending mode natural frequency from 8.40 Hz to 8.90 Hz and decreased the FRF magnitudes about 20% (from 1.27 to 1.02). Re-installing the exterior bottom chord extensions (Stage 5) increased the third bending mode natural frequency to 8.95 Hz and increased the FRF magnitudes about 18% (from 1.02 to 1.20). The data in Figure 4.49 show that with bottom chord extensions in place (Stages 1, 2, 4 and 5) the third bending mode natural frequency of the footbridge is greater than the frequency of the footbridge when no bottom chord extensions are in place (Stage 3).

Having the bottom chord extensions in place before the concrete pour (Stages 1 and 2) helps to keep the third bending mode sinusoidal excitation FRF magnitudes down, but re-installing the extensions without jacking-up the system after the concrete pour (Stages 4 and 5) does not decrease the FRF magnitudes for the third bending mode sine excitations.

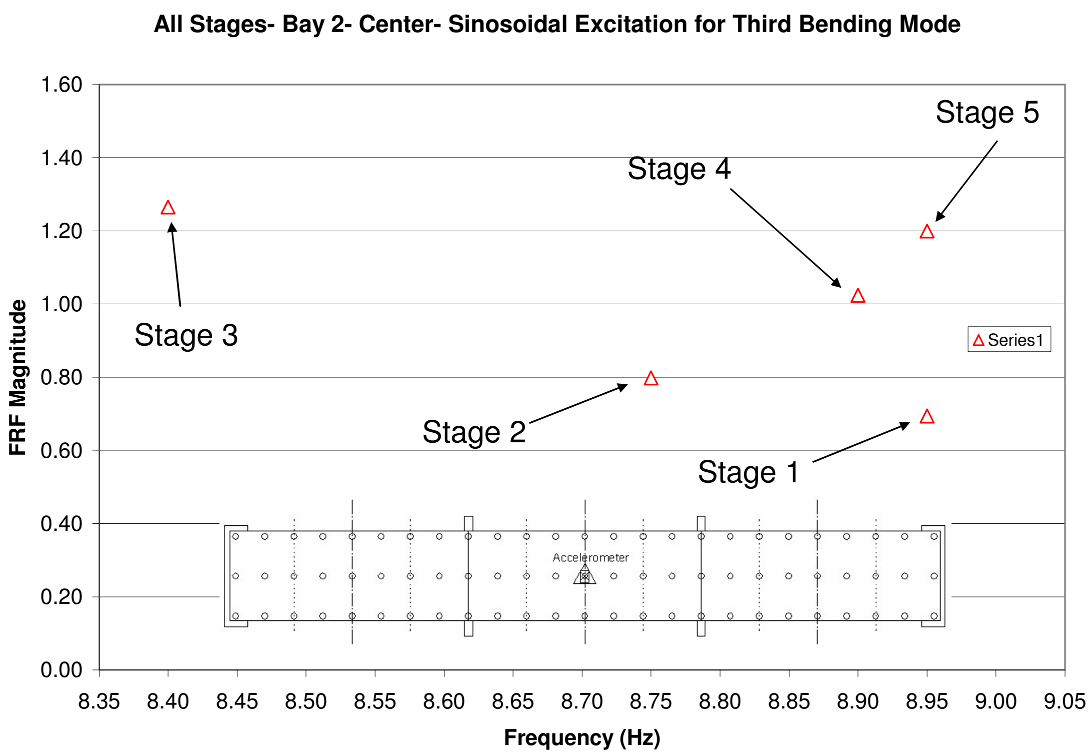

Figure 4.49 Frequency Response Function vs. Sinusoidal Excitation Frequency at Footbridge Center- Third Bending Mode

The results of the central Bay 3 first bending mode sine excitations are shown in Figure 4.50. It is shown that the first bending natural frequency of Stage 1 (7.75 Hz) decreased to 7.50 Hz and the corresponding sine excitation FRF magnitude peak increased about 45% (from 0.47 to 0.68) when the exterior bottom chord extensions were removed from the system (Stage 2). Removing the interior bottom chord extensions (Stage 3) does not affect the first bending mode frequency (7.50 Hz) but decreased the FRF magnitudes about 46% (from 0.68 to 0.37). Re-installing the interior bottom chord extensions (Stage 4) increased the first bending mode natural frequency from 7.50 Hz to 7.60 Hz and increased the FRF magnitudes about 86% (from 0.37 to 0.69). Re-installing the exterior bottom chord extensions (Stage 5) increased the first bending mode natural frequency to

7.80 Hz and decreased the FRF magnitudes about 43% (from 0.69 to 0.43). According to Figure 4.58, having the bottom chord extensions in place (Stages 1, 2, 4 and 5) again results in a higher first bending mode natural frequency.

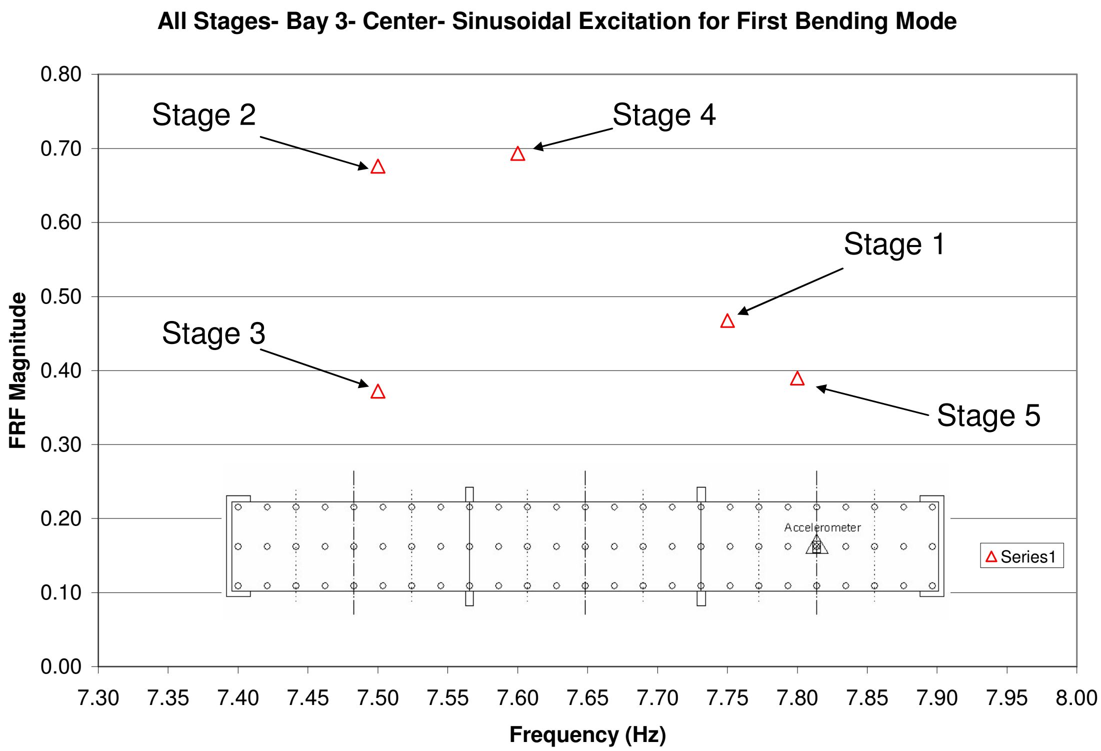

Figure 4.50 Frequency Response Function vs. Sinusoidal Excitation Frequency at Bay 3 Center- First Bending Mode

The results of the central Bay 3 second bending mode sine excitations are shown in Figure 4.51. It is shown that the second bending natural frequency of Stage 1 (8.10 Hz) decreased to 7.90 Hz and the corresponding sine excitation FRF magnitude peak decreased about 29% (from 1.03 to 0.73) when the exterior bottom chord extensions were removed from the system (Stage 2). Removing the interior bottom chord extensions (Stage 3) decreased the second bending mode frequency from 7.90 Hz to 7.80 Hz) and increased the FRF magnitudes about 133% (from 0.73 to 1.70). Re-installing the interior bottom chord extensions (Stage 4) increased the second bending mode natural frequency from 7.80 Hz to 8.15 Hz and decreased the FRF magnitudes about 58% (from 1.70 to 0.58). Re-installing the exterior bottom chord extensions (Stage 5) slightly decreased the second bending mode natural frequency to 8.10 Hz and decreased the FRF magnitudes about 4% (from 0.71 to 0.68). Again with the bottom chord extensions in place (Stages 1, 2, 4 and 5) the second bending mode natural frequency of the footbridge is higher and the frequency response function lower for the sinusoidal excitations.

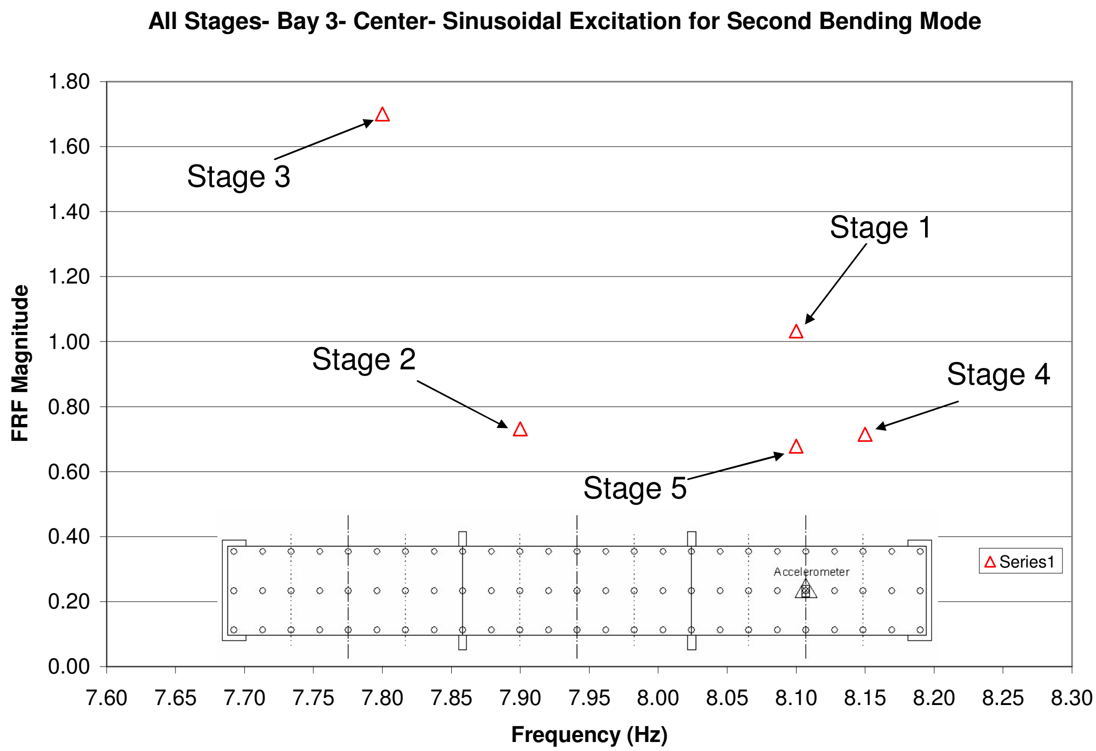

Figure 4.51 Frequency Response Function vs. Sinusoidal Excitation Frequency at Bay 3 Center- Second Bending Mode

The results of the central Bay 3 third bending mode sine excitations are shown in Figure 4.52. It is shown that the third bending natural frequency of Stage 1 (8.95 Hz) decreased to 8.90 Hz and the corresponding sine excitation FRF magnitude peak decreased about 51% (from 0.77 to 0.38) when the exterior bottom chord extensions were removed from the system (Stage 2). Removing the interior bottom chord extensions (Stage 3) decreased the third bending mode frequency about 6% (from 8.90 Hz to 8.40 Hz) and increased the FRF magnitudes about 82% (from 0.38 to 0.69). Re-installing the interior bottom chord extensions (Stage 4) increased the third bending mode natural frequency from 8.40 Hz to 8.85 Hz and decreased the FRF magnitudes about 26% (from 0.69 to 0.26). Re-installing the exterior bottom chord extensions (Stage 5) did not affect the third bending mode natural frequency but increased the FRF magnitudes about 24% (from 0.51 to 0.63).

According to Figure 4.60, having the bottom chord extensions in place (Stages 1, 2, 4 and 5) again increases the third bending mode natural frequency of the footbridge.

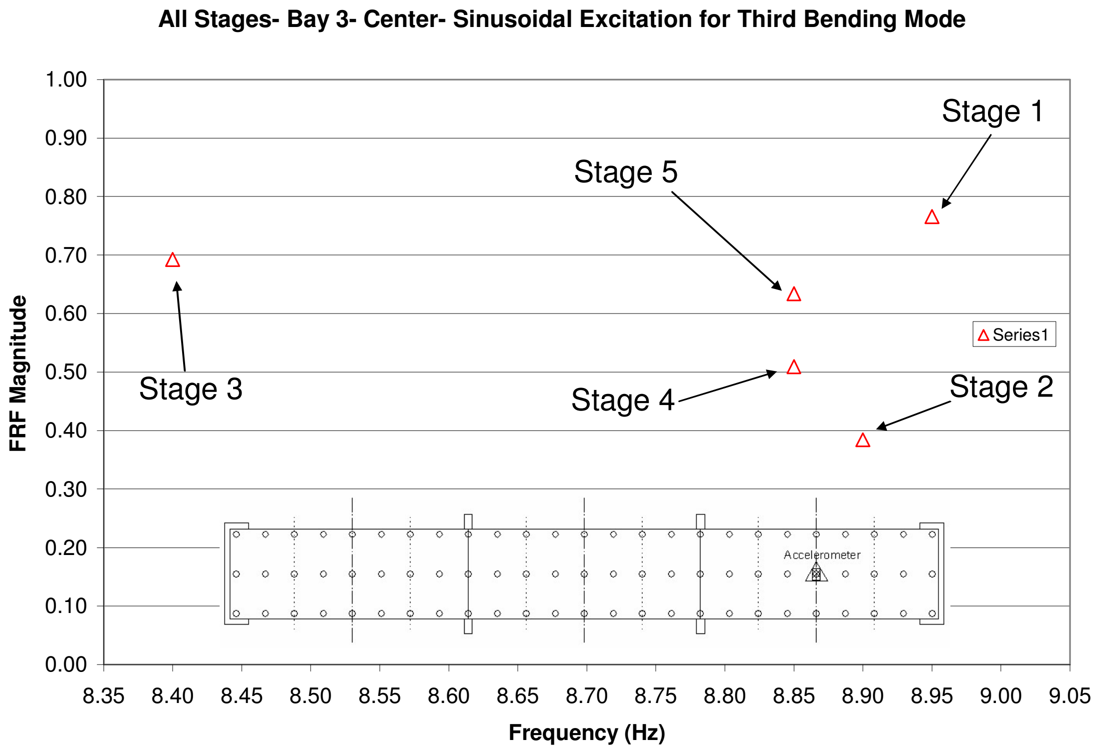

Figure 4.52 Frequency Response Function vs. Sinusoidal Excitation Frequency at Bay 3 Center- Third Bending Mode

For Stage 3- No bottom chord extensions in place, the measured first bending mode natural frequency is 7.49 Hz. The Design Guide 11 calculation yields a natural frequency of 7.33 Hz while the corresponding SAP model natural frequency is 7.49 Hz (Table 4.6). The DG-11 natural frequency value is 2% lower than the measured natural frequency while the SAP natural frequency is the same as the measured frequency. The DG-11 calculations were made as previously outlined except with a damping ratio of 0.00281 (β= 0.281%) from MEScope analysis.

The amplitudes of the excitations (input) for the three natural frequencies, the corresponding estimated peak accelerations (output) and frequency response function magnitudes (output/input) are shown in Table 4.6. The total weight of the three span footbridge is calculated as 40,824 lbs and for the DG-11 calculations W is taken as the weight of one bay only (W_{total} / 3 = 13,608 lbs). The weight of the bay is not multiplied by 1.5 since there is no continuity for Stage 3- No bottom chord extensions case.

Table 4.6 First Bending Mode Sinusoidal Excitations- Three Span Footbridge- Stage 3

Parameter	First Bending Mode		
f_n	7.49 Hz (measured)	7.334 Hz (DG11)	7.489 Hz (FE)
$P_0 e^{-0.35 f_n}$	6.688 lbs	7.063 lbs	6.690 lbs
$\frac{a_p}{g} = \frac{P_0 e^{-0.35 f_n}}{\beta W}$	17.5% g	18.5% g	17.5% g
FRF (Output / Input)	2.617	2.619	2.616

A sine excitation at Bay 2 center was simulated in the FE model with an excitation frequency of 7.489 Hz (first bending mode of the model), an excitation amplitude of $P_0 e^{-0.35.(7.489)}$=6.69 lbs. and a modal damping ratio of 0.281% (MEScope). The resulting peak acceleration and FRF magnitudes are 4.5%g and 0.673, respectively, which are significantly lower than the DG-11 predicted numbers of Table 4.6.

During the experimental phase, sine excitations with higher amplitudes were applied at the Bay 2 center. For example, a test with excitation amplitude of 42.7 lb and an excitation frequency of 7.50 Hz (first bending mode- Stage 3) resulted in a peak acceleration of 16.6% g at the Bay 2 center. However, when this test is simulated in the FE model, the peak acceleration is 28.7% g at the Bay 2 center (73% higher than the test result). This discrepancy is due to the very low damping ratios obtained from the MEScope analyses. When the damping ratios are also hand-calculated by the half-power method from the chirp frequency response functions, the numbers are always higher than the ones computed by MEScope. The average of the damping ratios from different chirp excitations for Stage-3 first bending mode is 0.70%. When this number is used in the FE model, the peak acceleration is 11.5% g at the Bay 2 center, which is a closer value to the test result.

Considering the fact that when the damping ratios are in very low levels, the difference between them can make a bigger difference in their ratios, which results in significant differences in measured, DG11 and FE acceleration response results. Both 0.281% and 0.70% are very low damping ratios, however their use in any model can vary in the range of their ratio (0.70/0.281= 2.49).

To further investigate the footbridge, heel drop excitations were performed on the force plate, which was placed at Bay 2 of the footbridge. Heel drop data was recorded for all three bottom chord extension configurations. The FRF comparisons between Stages 1, 3, 4 and 5 (Stage 2 missing) are shown in Figure 4.53.

It is shown in Figure 4.53 that the first bending mode natural frequency of Stage 1 is at 7.75 Hz and the corresponding FRF magnitude peak is 3.55. For Stage 3 the natural frequency is at 7.50-7.55 Hz range and the corresponding FRF magnitude peak is 1.50. For the third bending mode, the natural frequency of Stage 1 is 9.05 Hz and the corresponding FRF magnitude peak is 2.70. For Stage 3 the natural frequency is in the 8.50-8.55 Hz range and the corresponding FRF magnitude peak is 3.25. Re-installing the interior bottom chord extensions (Stage 4) increased the first bending mode natural frequency to 7.60 Hz and the third bending mode natural frequency to 8.85-8.90 Hz. The FRF magnitudes decreased about 50% for the first bending mode and 70% for the third bending mode when the interior bottom chord extensions were re-installed in the system (Stage 4). Re-installing the exterior bottom chord extensions (Stage 5) increased the first bending mode natural frequency to 7.80 Hz and kept the third bending mode natural frequency around 8.85 Hz. Also, the FRF magnitudes increased about 240% for the first bending mode and decreased about 100% for the third bending mode when the exterior bottom chord extensions were re-installed in the system (Stage 5).

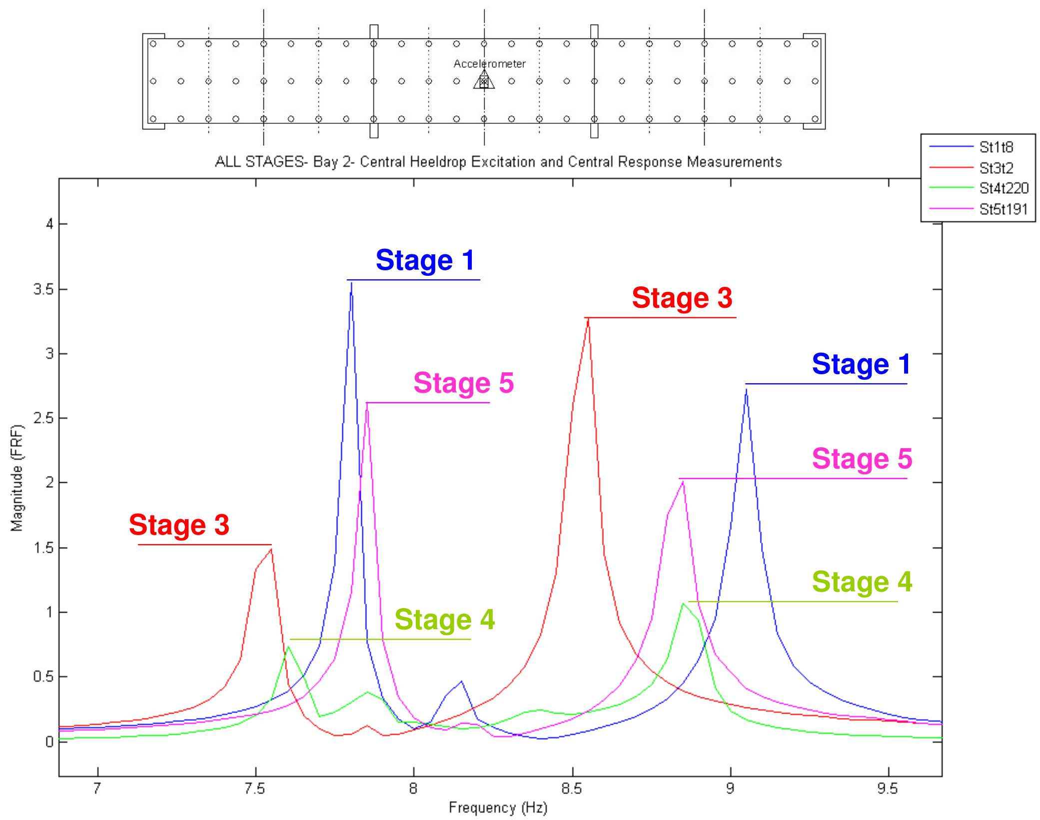

Figure 4.53 Heel drop FRF comparisons for Bay 2 Central Point Excitation- First and Third Bending Mode- Three Span Footbridge

After the heel drop tests, walking excitations were performed with different walking pace frequencies. Because the input excitation can not be measured for walking excitations, frequency response functions are, again, not available. Acceleration versus time traces of walking excitations, as well as RMS and $\sqrt{2}$ RMS values, were used for comparison of bottom chord extension effects. Acceleration time histories from two pedestrians (162 lbs and 240 lbs) walking side-by-side at 1/3rd of the measured first bending mode natural frequency of the three span footbridge are shown in Figure 4.54. The associated autospectra of the time history data with RMS and $\sqrt{2}$ RMS records are shown in Figure 4.55 (1 Volt = 1 g).

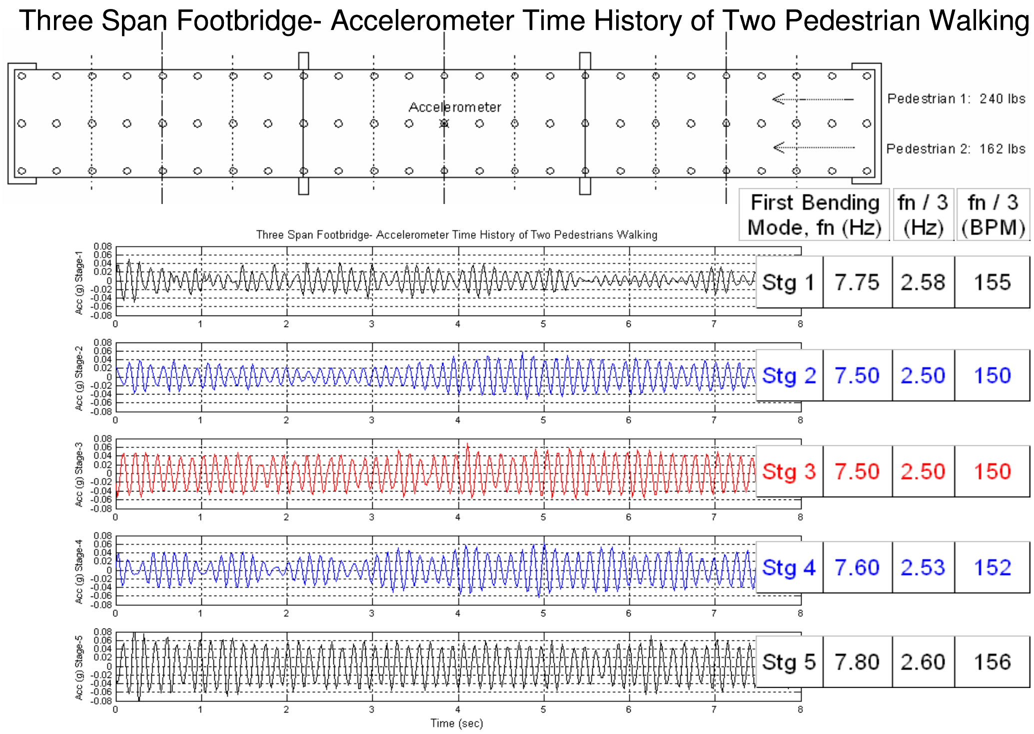

Figure 4.54 Accelerometer Time History of Two Pedestrians Walking on Three Span Footbridge

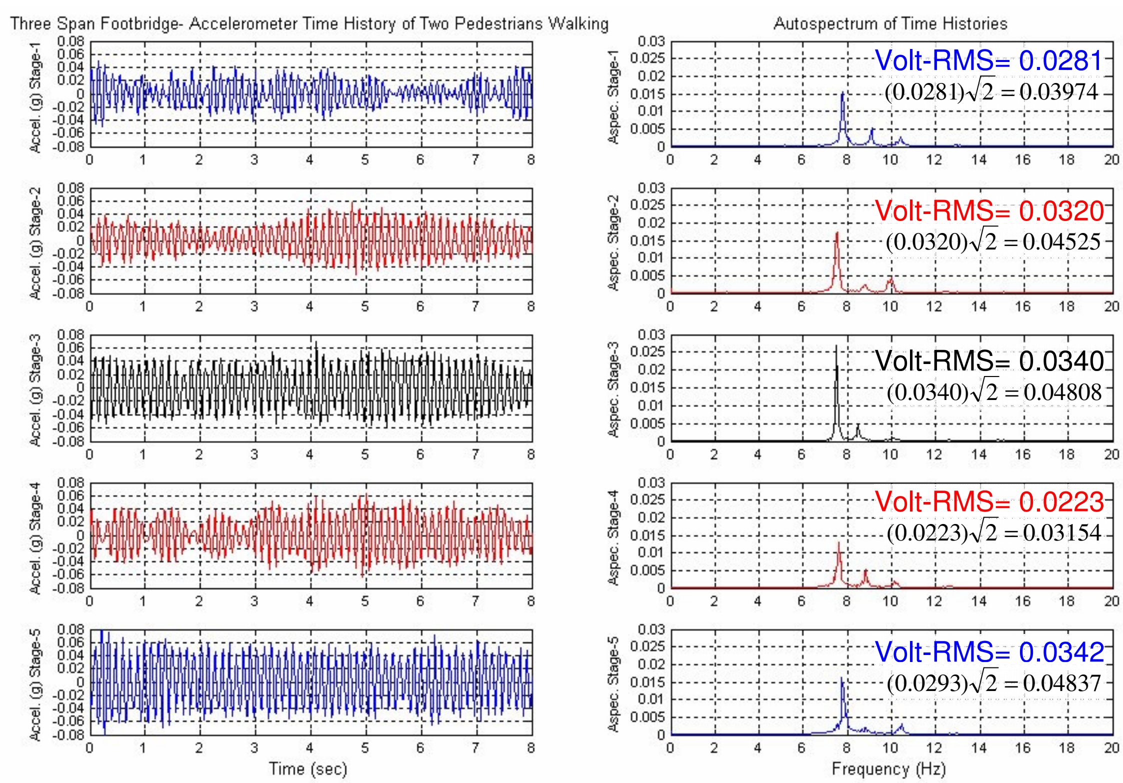

Figure 4.55 Accelerometer Time History of Two Pedestrians Walking on Three Span Footbridge and Associated Autospectra

Examining the responses of all five stages in Figure 4.55, it is realized that the responses for Stage 1 (RMS= 0.0281) and Stage 2 (RMS= 0.0320) are relatively lower than for the other stages. Removing the exterior bottom chord extensions for Stage 2 increased the RMS value of Stage 1 by 14%. Removing the interior bottom chord extensions for Stage 3 increased the RMS value of Stage 2 by 6%. Re-installing the interior bottom chord extensions for Stage 4 decreased the RMS value by 34%. Re-installing the exterior bottom chord extensions for Stage 5 resulted in a higher RMS value than Stage 4. The Stage 5 RMS value is almost the same as the one for Stage 3. It can be seen in the autospectra that the first bending mode of each stage was excited by the walking.

To see the effect of walking pace frequency on the footbridge response, the time history, associated autospectra and RMS values from walking excitations of Stage 5 (first bending mode natural frequency of 7.80 Hz) are shown in Figure 4.56. The footbridge was excited by two pedestrians walking side-by-side with walking frequencies of 128 BPM (Beats per Minute), 136 BPM, 144 BPM, 150 BPM, 154 BPM and 156 BPM. The effect of the resonance is clearly seen in the 154 BPM and 156 BPM results. A 3% increase (from 150 BPM to 154 BPM) in the walking pace frequency increased the RMS value 120% (from 0.0133 to 0.0293).

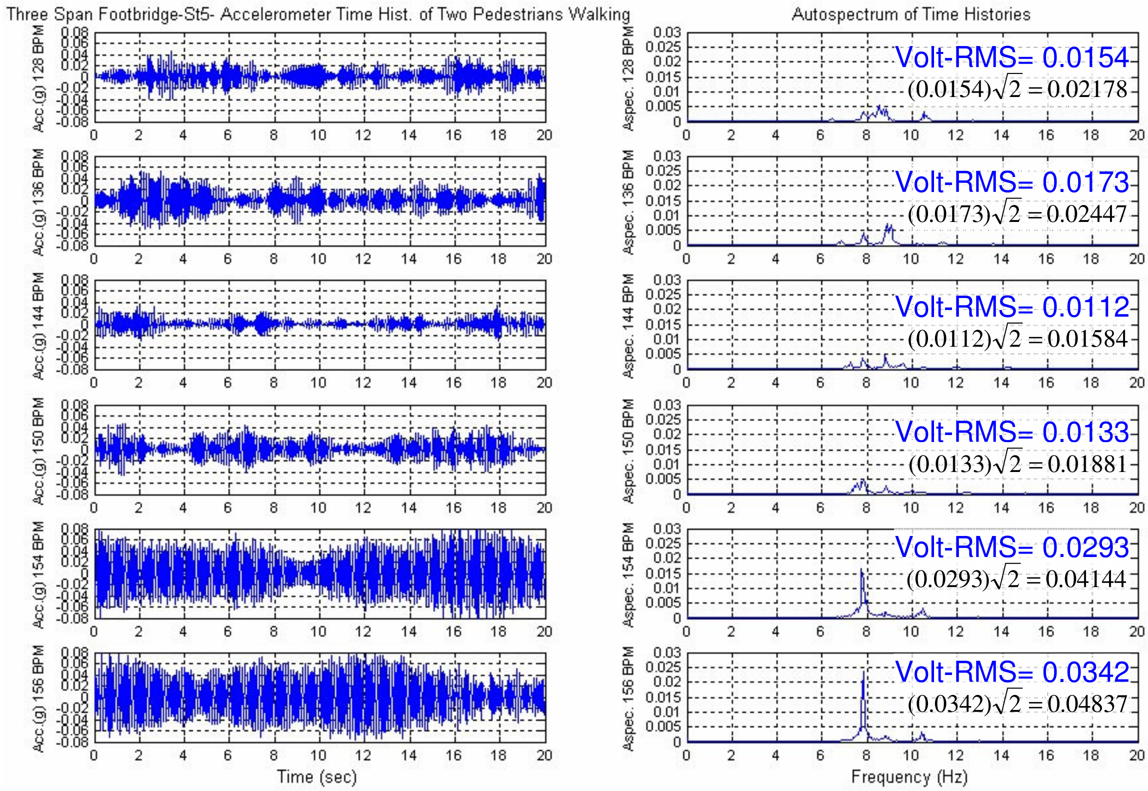

Figure 4.56 Accelerometer Time History of Two Pedestrians Walking with Different Pace Frequencies on Three Span Footbridge (Stage 5) and Associated Autospectra

4.3 Effective Mass Calculations

When a system is vibrating at a natural frequency, its deformation follows a specific pattern which is called a mode shape. For each mode shape the amount of mass contributing to the system response is different. Effective mass is an indication of mass sensitivity of each mode to an excitation.

Mode shapes can be calculated experimentally using modal testing data. Each accelerometer location is assigned a lumped mass of the tested structure (Figure 4.57) and collected chirp data for each lumped mass location can then be loaded into a commercial vibration analysis software package (for example MEScope) and the mode shapes can be determined (Figure 4.58).

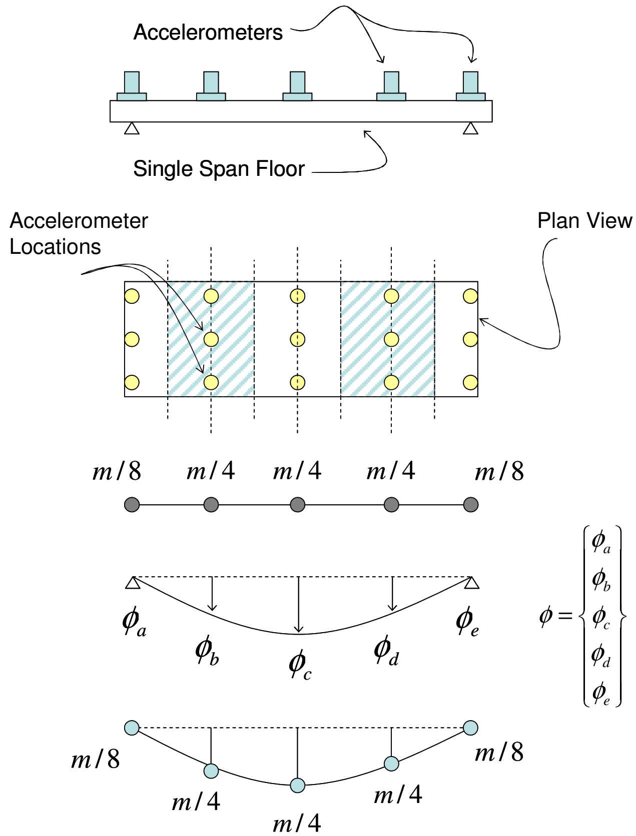

Figure 4.57 Mode Shape Determination

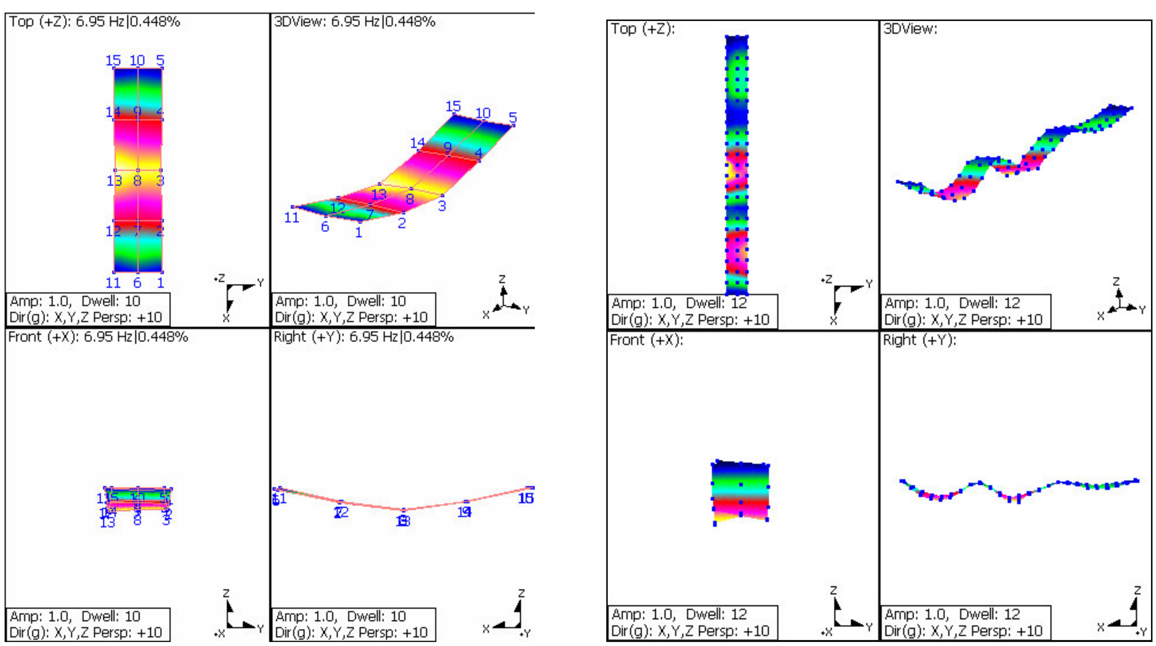

(a) Single Span Footbridge **(b) Three Span Footbridge**

Figure 4.58 MEScope Mode Shape Animation

When a mode shape of a structure is known, the effective mass corresponding to that mode can be calculated. Effective mass of a mode in a one way system is defined as (Perry 2003)

$$M_{eff} = \int_0^L M(x)(\phi(x))^2 dx \tag{4.11}$$

where

$M(x)$ = mass density of the system (a constant for floor systems)

$\phi(x)$ = mode shape normalized with respect to maximum midspan deflection

Equation 4.11 can also be written as

$$M_{eff} = \phi^T M \phi \tag{4.12}$$

where

M_{eff} = effective mass (modal mass),

M = lumped mass matrix due to the tributary area of each accelerometer point on the floor, and

ϕ = mode shape vector normalized with respect to maximum midspan deflection

For the single span footbridge, accelerometer locations and the first bending mode shape are shown in Figure 4.59. The corresponding mass matrix is

$$M = \begin{bmatrix} m/8 & 0 & 0 & 0 & 0 \\ 0 & m/4 & 0 & 0 & 0 \\ 0 & 0 & m/4 & 0 & 0 \\ 0 & 0 & 0 & m/4 & 0 \\ 0 & 0 & 0 & 0 & m/8 \end{bmatrix} \tag{4.13}$$

where m is the total mass of the single span footbridge.

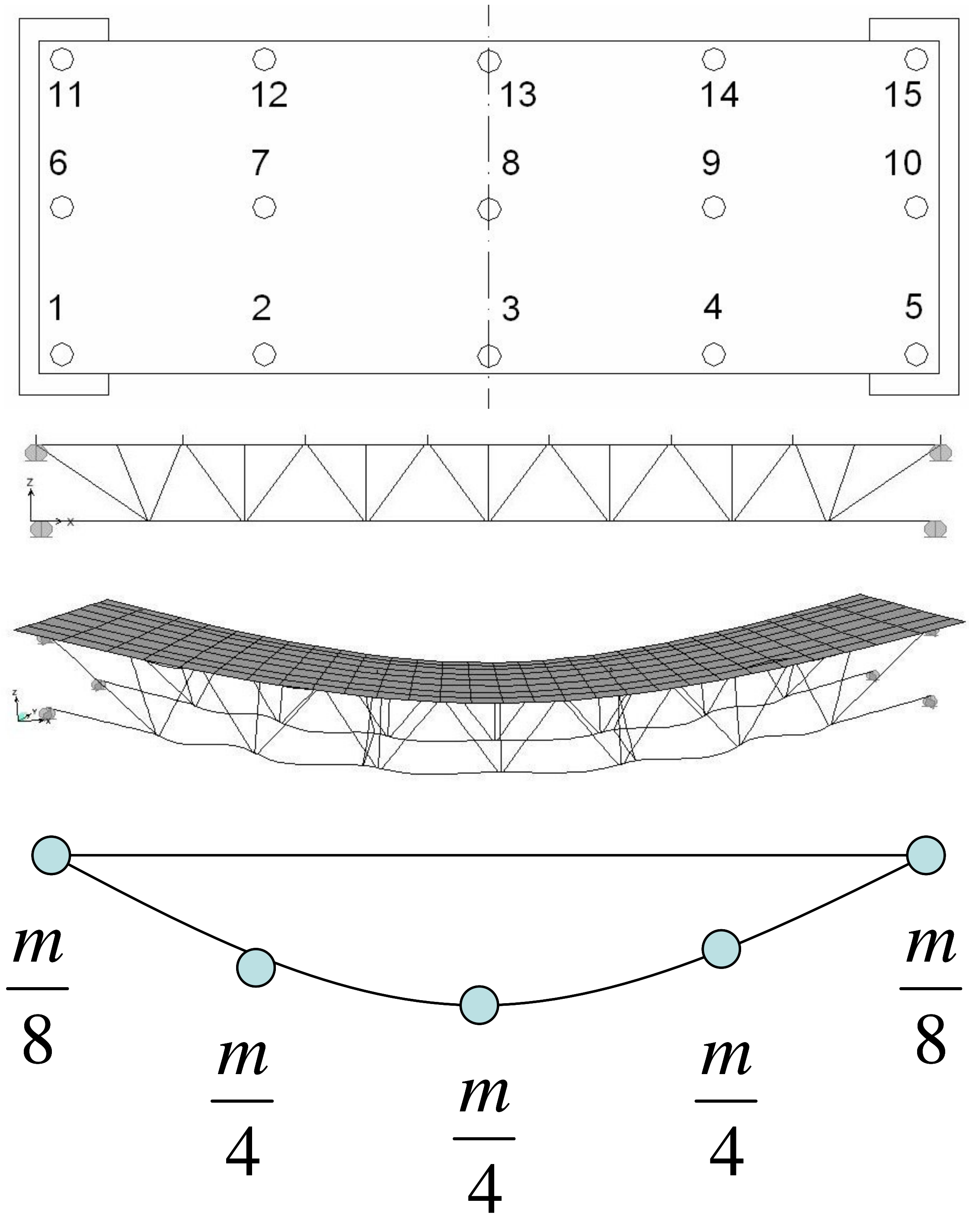

Figure 4.59 Accelerometer Locations and First Bending Mode Shape- Single Span Footbridge

For the three span footbridge, accelerometer locations and first three bending mode shapes are shown in Figure 4.60, and the corresponding mass matrix is

$$M = \begin{bmatrix}
\frac{m}{48} & 0 & 0 & 0 & 0 & 0 & 0 & 0 & 0 & 0 & 0 & 0 & 0 & 0 & 0 & 0 & 0 & 0 & 0 & 0 & 0 & 0 & 0 & 0 & 0 \\
0 & \frac{m}{24} & 0 & 0 & 0 & 0 & 0 & 0 & 0 & 0 & 0 & 0 & 0 & 0 & 0 & 0 & 0 & 0 & 0 & 0 & 0 & 0 & 0 & 0 & 0 \\
0 & 0 & \frac{m}{24} & 0 & 0 & 0 & 0 & 0 & 0 & 0 & 0 & 0 & 0 & 0 & 0 & 0 & 0 & 0 & 0 & 0 & 0 & 0 & 0 & 0 & 0 \\
0 & 0 & 0 & \frac{m}{24} & 0 & 0 & 0 & 0 & 0 & 0 & 0 & 0 & 0 & 0 & 0 & 0 & 0 & 0 & 0 & 0 & 0 & 0 & 0 & 0 & 0 \\
0 & 0 & 0 & 0 & \frac{m}{24} & 0 & 0 & 0 & 0 & 0 & 0 & 0 & 0 & 0 & 0 & 0 & 0 & 0 & 0 & 0 & 0 & 0 & 0 & 0 & 0 \\
0 & 0 & 0 & 0 & 0 & \frac{m}{24} & 0 & 0 & 0 & 0 & 0 & 0 & 0 & 0 & 0 & 0 & 0 & 0 & 0 & 0 & 0 & 0 & 0 & 0 & 0 \\
0 & 0 & 0 & 0 & 0 & 0 & \frac{m}{24} & 0 & 0 & 0 & 0 & 0 & 0 & 0 & 0 & 0 & 0 & 0 & 0 & 0 & 0 & 0 & 0 & 0 & 0 \\
0 & 0 & 0 & 0 & 0 & 0 & 0 & \frac{m}{24} & 0 & 0 & 0 & 0 & 0 & 0 & 0 & 0 & 0 & 0 & 0 & 0 & 0 & 0 & 0 & 0 & 0 \\
0 & 0 & 0 & 0 & 0 & 0 & 0 & 0 & \frac{m}{24} & 0 & 0 & 0 & 0 & 0 & 0 & 0 & 0 & 0 & 0 & 0 & 0 & 0 & 0 & 0 & 0 \\
0 & 0 & 0 & 0 & 0 & 0 & 0 & 0 & 0 & \frac{m}{24} & 0 & 0 & 0 & 0 & 0 & 0 & 0 & 0 & 0 & 0 & 0 & 0 & 0 & 0 & 0 \\
0 & 0 & 0 & 0 & 0 & 0 & 0 & 0 & 0 & 0 & \frac{m}{24} & 0 & 0 & 0 & 0 & 0 & 0 & 0 & 0 & 0 & 0 & 0 & 0 & 0 & 0 \\
0 & 0 & 0 & 0 & 0 & 0 & 0 & 0 & 0 & 0 & 0 & \frac{m}{24} & 0 & 0 & 0 & 0 & 0 & 0 & 0 & 0 & 0 & 0 & 0 & 0 & 0 \\
0 & 0 & 0 & 0 & 0 & 0 & 0 & 0 & 0 & 0 & 0 & 0 & \frac{m}{24} & 0 & 0 & 0 & 0 & 0 & 0 & 0 & 0 & 0 & 0 & 0 & 0 \\
0 & 0 & 0 & 0 & 0 & 0 & 0 & 0 & 0 & 0 & 0 & 0 & 0 & \frac{m}{24} & 0 & 0 & 0 & 0 & 0 & 0 & 0 & 0 & 0 & 0 & 0 \\
0 & 0 & 0 & 0 & 0 & 0 & 0 & 0 & 0 & 0 & 0 & 0 & 0 & 0 & \frac{m}{24} & 0 & 0 & 0 & 0 & 0 & 0 & 0 & 0 & 0 & 0 \\
0 & 0 & 0 & 0 & 0 & 0 & 0 & 0 & 0 & 0 & 0 & 0 & 0 & 0 & 0 & \frac{m}{24} & 0 & 0 & 0 & 0 & 0 & 0 & 0 & 0 & 0 \\
0 & 0 & 0 & 0 & 0 & 0 & 0 & 0 & 0 & 0 & 0 & 0 & 0 & 0 & 0 & 0 & \frac{m}{24} & 0 & 0 & 0 & 0 & 0 & 0 & 0 & 0 \\
0 & 0 & 0 & 0 & 0 & 0 & 0 & 0 & 0 & 0 & 0 & 0 & 0 & 0 & 0 & 0 & 0 & \frac{m}{24} & 0 & 0 & 0 & 0 & 0 & 0 & 0 \\
0 & 0 & 0 & 0 & 0 & 0 & 0 & 0 & 0 & 0 & 0 & 0 & 0 & 0 & 0 & 0 & 0 & 0 & \frac{m}{24} & 0 & 0 & 0 & 0 & 0 & 0 \\
0 & 0 & 0 & 0 & 0 & 0 & 0 & 0 & 0 & 0 & 0 & 0 & 0 & 0 & 0 & 0 & 0 & 0 & 0 & \frac{m}{24} & 0 & 0 & 0 & 0 & 0 \\
0 & 0 & 0 & 0 & 0 & 0 & 0 & 0 & 0 & 0 & 0 & 0 & 0 & 0 & 0 & 0 & 0 & 0 & 0 & 0 & \frac{m}{24} & 0 & 0 & 0 & 0 \\
0 & 0 & 0 & 0 & 0 & 0 & 0 & 0 & 0 & 0 & 0 & 0 & 0 & 0 & 0 & 0 & 0 & 0 & 0 & 0 & 0 & \frac{m}{24} & 0 & 0 & 0 \\
0 & 0 & 0 & 0 & 0 & 0 & 0 & 0 & 0 & 0 & 0 & 0 & 0 & 0 & 0 & 0 & 0 & 0 & 0 & 0 & 0 & 0 & \frac{m}{24} & 0 & 0 \\
0 & 0 & 0 & 0 & 0 & 0 & 0 & 0 & 0 & 0 & 0 & 0 & 0 & 0 & 0 & 0 & 0 & 0 & 0 & 0 & 0 & 0 & 0 & \frac{m}{24} & 0 \\
0 & 0 & 0 & 0 & 0 & 0 & 0 & 0 & 0 & 0 & 0 & 0 & 0 & 0 & 0 & 0 & 0 & 0 & 0 & 0 & 0 & 0 & 0 & 0 & \frac{m}{48}
\end{bmatrix} \tag{4.14}$$

where m is the total mass of the three span footbridge.

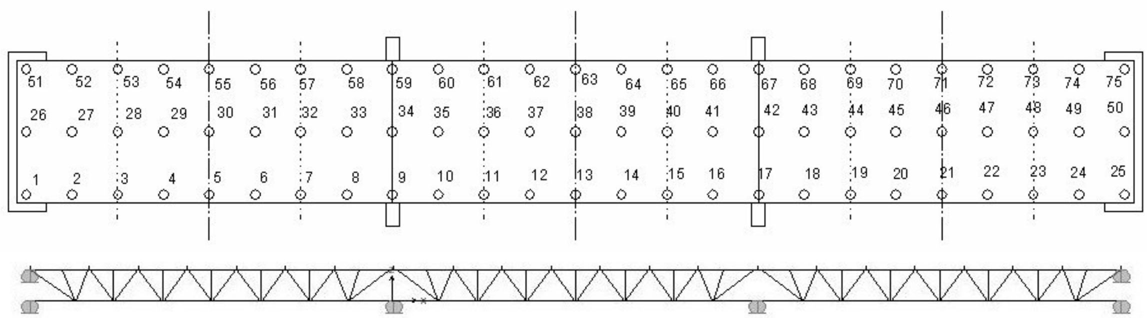

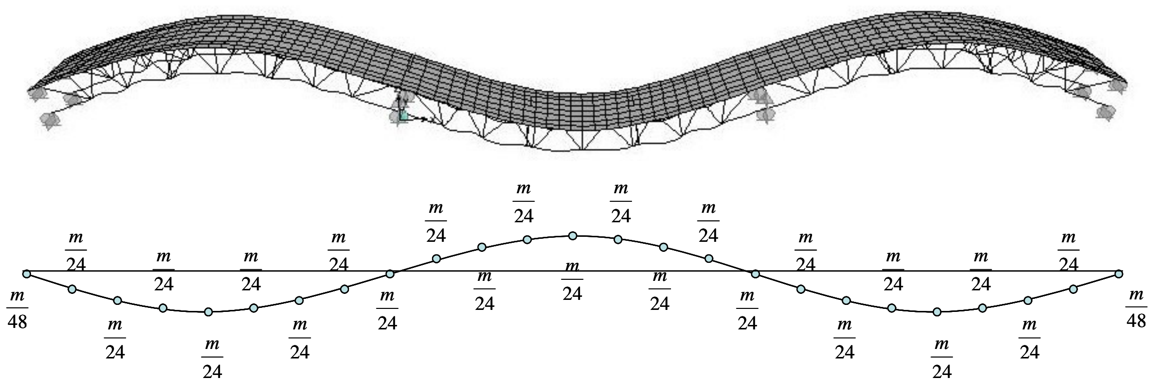

First Bending Mode

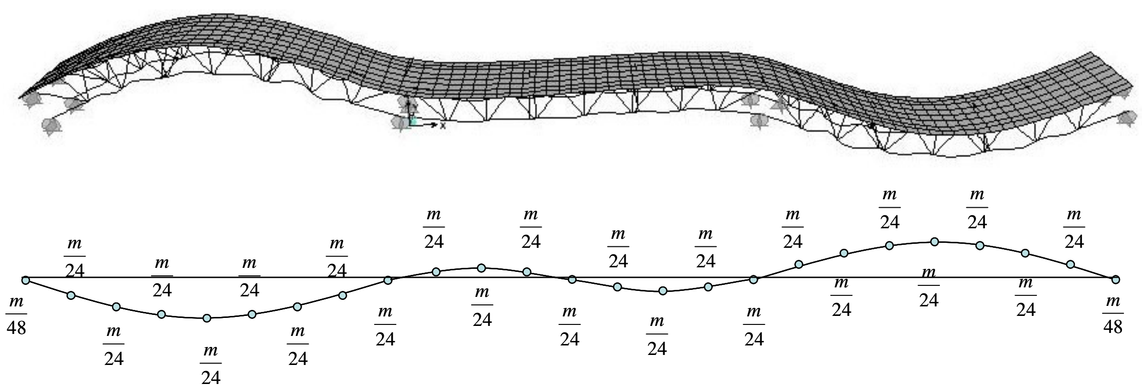

Second Bending Mode

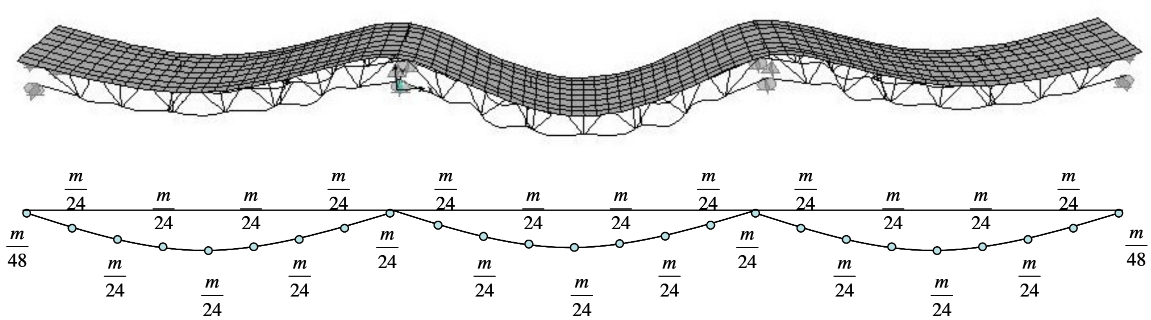

Third Bending Mode

Figure 4.60 Accelerometer Locations and First Three Bending Mode Shapes-Three Span Footbridge

For both the single span and three span footbridges, acceleration data was collected on three parallel lines in the longitudinal direction. For the effective mass calculations, the average mode shape of the three lines is used and the system is treated as a beam. The mode shape vectors for the first bending mode of the single span footbridge and the first three bending modes of the three span footbridge were determined for each bottom chord extension configuration. Each mode shape vector was normalized to establish the ϕ-matrix of Equation 4.12, and the effective mass of the entire footbridge for each mode was calculated. The single span footbridge results are shown in Table 4.7, while the three span footbridge results are shown in Table 4.8.

Table 4.7 First Three Bending Mode Natural Frequencies, Damping Ratios, and Effective Mass Results for the Single Span Footbridge

	First Bending Mode				
	f_{n1} (Hz)	ζ_1 (%)		Effective Mass From Mode Shapes	
	MEScope	MEScope	Half-Power Method	MEScope	FE Model
Stage 1	8.08	0.451	0.639	0.426m	0.517m
Stage 2	6.95	0.448	0.453	0.466m	0.524m
Stage 3	7.65	0.409	0.452	0.413m	0.517m

Table 4.8 First Three Bending Mode Natural Frequencies, Damping Ratios, and Effective Mass Results for the Three Span Footbridge

	First Bending Mode					Second Bending Mode					Third Bending Mode				
	f_{n1} (Hz)	ζ_1 (%)		Effective Mass		f_{n2} (Hz)	ζ_2 (%)		Effective Mass		f_{n3} (Hz)	ζ_3 (%)		Effective Mass	
	MEScope	MEScope	Half-Power Method	MEScope	FE Model	MEScope	MEScope	Half-Power Method	MEScope	FE Model	MEScope	MEScope	Half-Power Method	MEScope	FE Model
Stage 1	7.76	0.265	0.450	0.247m	0.419m	8.11	0.255	0.460	0.289m	0.307m	8.93	0.332	0.660	0.437m	0.225m
Stage 2	7.51	0.272	0.580	0.479m	0.438m	7.90	0.361	0.800	0.343m	0.307m	8.81	0.539	0.700	0.237m	0.201m
Stage 3	7.49	0.281	0.700	0.300m	0.416m	7.81	0.402	0.420	0.255m	0.307m	8.37	0.213	0.420	0.257m	0.193m
Stage 4	7.60	0.273	0.480	0.259m	0.438m	8.14	-	0.740	0.357m	0.307m	8.78	0.203	0.370	0.214m	0.201m
Stage 5	7.80	0.178	-	0.271m	0.419m	8.13	0.235	-	0.256m	0.307m	8.89	0.571	-	0.255m	0.225m

From the MEScope mode shapes for the single span footbridge, installing the bottom chord extensions before the concrete placement (Stage 1) resulted in an effective mass of 0.426m for the first bending mode of the single span footbridge. Removing the bottom chord extensions from the system (Stage 2) resulted in a 9% increase (from 0.426m to 0.466m) in the effective mass vibrating with the first bending mode. Re-installing the bottom chord extensions decreased the effective mass about 11% (from 0.466m to 0.413m) for the first bending mode. The trend is the same for the finite element mode shapes. The effective mass results are 0.517m, 0.524m and 0.517m for Stages 1, 2 and 3, respectively, as shown in Table 4.7.

It is shown in Table 4.8 from the MEScope mode shapes that placing all the bottom chord extensions in place before the concrete is placed (Stage 1) resulted in effective masses of 0.247m, 0.289m and 0.437m for the first, second and the third bending modes of the three span footbridge, respectively. Removing the exterior bottom chord extensions from the system (Stage 2) resulted in a 94% increase (from 0.247m to 0.479m) in the effective mass of the first bending mode, a 19% increase (from 0.289m to 0.343m) in the effective mass of the second bending mode and a 46% drop (from 0.437m to 0.237m) in the effective mass of the third bending mode of the three span footbridge. Removing the interior bottom chord extensions from the system (Stage 3) resulted in a 37% drop (from 0.479m to 0.300m) in the effective mass of the first bending mode, a 26% drop (from 0.343m to 0.255m) in the effective mass of the second bending mode and an 8% increase (from 0.237m to 0.257m) in the effective mass of the third bending mode. Re-installing the interior bottom chord extensions in the system (Stage 4) resulted in a 14% drop (from 0.300m to 0.259m) in the effective mass of the first bending mode, a 40% increase (from 0.255m to 0.357m) in the effective mass of the second bending mode and an 17% drop (from 0.257m to 0.214m) in the effective mass of the third bending mode. Finally, re-installing the exterior bottom chord extensions in the system (Stage 5) resulted in a 5% increase (from 0.259m to 0.271m) in the effective mass of the first bending mode, a 28% drop (from 0.357m to 0.256m) in the effective mass of the second bending mode and an 19% increase (from 0.214m to 0.255m) in the effective mass of the third bending mode of the three span footbridge.

For the three span footbridge, the highest effective mass for the first bending mode is 0.479m in Stage 2, which is lower than the theoretical effective mass for a corresponding three span continuous beam first bending mode (0.500m). The highest effective masses for the second bending mode are 0.343m (Stage 2) and 0.357m (Stage 4), which are also lower than the theoretical effective mass value for a corresponding three span continuous beam second bending mode (0.375m). The highest effective mass for the third bending mode is 0.437m, which is calculated for Stage 1, and again it is still lower than the theoretical effective mass value for the three span continuous beam third bending mode (0.500m). The trend is not the same for the finite element mode shapes. The effective mass results due to FE mode shapes are 0.419m, 0.438m, 0.416m, 0.438m and 0.419m for the first bending mode of the five stages, respectively. For the second bending mode, effective mass results from FE mode shapes are 0.307m for all stages. For the third bending mode, the effective mass results from FE mode shapes are 0.225m, 0.201m, 0.193m, 0.201m and 0.225m for the five stages, respectively, as shown in Table 4.8.

It is noticed that removal or re-installation of bottom chord extensions does not create the same effect on the effective masses of the three bending modes for a specific stage. For example, according to MEScope results, removing the exterior bottom chord extensions from the system (Stage 2) causes an increase in the first and second bending mode effective masses, with a large decrease in the third bending mode effective mass. In the same manner, removing the interior bottom chord extensions (Stage 3) causes a decrease in the first and second bending modes, with an increase in the third bending mode effective mass.

According to FE model results, removing the exterior bottom chord extensions from the system (Stage 2) causes an increase in the first bending mode effective mass, while the second mode effective mass remains the same. There is a relatively smaller drop in the third bending mode effective mass. Removing the interior bottom chord extensions (Stage 3) causes drops in the first and third bending mode effective masses; again the second bending mode effective mass remains the same.

From the MEScope mode shape calculations, the effective masses for the first three bending modes of Stage 1 are 0.247m, 0.289m and 0.437m, respectively. The corresponding numbers for Stage 5 are 0.271m, 0.256m and 0.255m, respectively. The bottom chord extension configurations of Stage 1 and Stage 5 are the same, but the bottom chord extensions of Stage 5 were re-installed in the system with a cured concrete slab, without jacking up. Although there is an increase in the first bending mode effective mass, there is a drop in the second bending mode, especially in the third bending mode. Using the FE model mode shapes, the effective masses for the first three bending modes of both Stage 1 and Stage 5 are 0.419m, 0.307m and 0.225m, respectively. The effective masses due to MEscope and FE model mode shapes are inconsistent.

It is known from the frequency response function results for the three span footbridge that re-installation of the bottom chord extensions for Stages 4 and 5 did not have the same effect as having the bottom chord extensions installed before the concrete placement (Stages 1 and 2). However this conclusion can not be made by looking at the effective mass results from the MEScope and FE model mode shapes.

As mentioned earlier, when a structure is excited with a harmonic driving force at its natural frequency, the response will be resonant. It is known that for a system excited with a harmonic force at its natural frequency, the resulting peak acceleration is given by (Perry 2003):

$$a_p = \frac{p_0}{2\beta M_{eff}} \tag{4.15}$$

where

a_p = peak acceleration

p_0 = force amplitude of the sinusoidal forcing function

β = modal damping ratio

M_{eff} = effective mass (modal mass)

The first bending mode effective mass of a simply supported beam, and the first and third bending mode effective masses of a three span continuous beam, are equal to 50% of the total mass of the structure; therefore

$$a_p = \frac{p_0}{2\beta M_{eff}} = \frac{p_0}{2\beta \frac{M_{total}}{2}} = \frac{p_0}{\beta M_{total}} \tag{4.16}$$

where M_{total} = the total mass of the beam.

Also,

$$\frac{a_p}{g} = \frac{p_0}{2\beta W_{eff}} \tag{4.17}$$

where W_{eff} = the effective weight.

When the sinusoidal excitation test results for Stage 2 (Figures 4.32 and 4.33) of the single span footbridge are input to Equation 4.17, that is, a_p =0.1196g, P_0 = 7.59 lbs and β = 0.00448 from the MEScope procedures, the effective weight is 7036 lbs. The total weight of the footbridge is approximately 13,986 lbs; therefore the effective weight is 50.6% of the total weight. This ratio is very close to the effective mass value calculated with measured mode shape vectors (Equation 4.12) and almost the same as the theoretical effective weight value of 50%. This means that the system was able to be put into resonance and the computed modal damping ratio should be very close to the actual value.

However when the same calculations are done for Stage 1 with a_p =0.14g, P_0 = 12.4 lbs and β = 0.00451, the effective weight is 9819 lbs which is 70.2% of the total weight of the single span footbridge. This ratio is about 40% higher than from the mode shape approach and the theoretical value. However, when the FRF half power method damping ratio of β = 0.00639 is used, the effective weight is 6930 lbs which is 49.6% of the total weight of the single span footbridge, almost equal to the theoretical value of 50%. (Stage 3 of the single span footbridge was not put into resonance as it was not sinusoidally excited at its first bending mode natural frequency.)

Since it is already known that the damping ratio in the denominator of Equation 4.17 is a very significant factor affecting the resonance situation, and the damping ratios from MEScope and the FRF half power method do not agree, first the damping ratios are back-calculated using the MEScope and FE model mode shape effective masses, for the three span footbridge. The back-calculated damping ratios of MEScope mode shapes are shown in Table 4.9, while the back-calculated damping ratios of FE model mode shapes are shown in Table 4.10.

Table 4.9 Damping Ratio, β, Back-calculated using MEScope Mode Shapes for the Three Span Footbridge

Sinusoidal Excitations for Resonance		P_0 (lbs) (Test)	a_p/g (Test)	Effective Weight / Total Weight (MEScope Mode Shapes)	Total Weight (lbs)	Back-calculated β
Stage 1	Mode1	38.2	0.177	0.247	40824	0.0107
	Mode2	36.7	0.185	0.289	40824	0.0084
	Mode3	39.2	0.154	0.437	40824	0.0071
Stage 2	Mode1	43.0	0.159	0.479	40824	0.0069
	Mode2	54.4	0.170	0.343	40824	0.0114
	Mode3	40.7	0.148	0.237	40824	0.0142
Stage 3	Mode1	42.5	0.147	0.300	40824	0.0118
	Mode2	28.6	0.218	0.255	40824	0.0063
	Mode3	32.3	0.210	0.257	40824	0.0073
Stage 4	Mode1	52.4	0.245	0.259	40824	0.0101
	Mode2	38.7	0.161	0.357	40824	0.0082
	Mode3	31.0	0.215	0.214	40824	0.0083

Table 4.10 Damping Ratio, β, Back-calculated using FE Model Mode Shapes for the Three Span Footbridge

Sinusoidal Excitations for Resonance		P_0 (lbs) (Test)	a_p/g (Test)	Effective Weight / Total Weight (FE Mode Shapes)	Total Weight (lbs)	Back-calculated β
Stage 1	Mode1	38.2	0.177	0.419	40824	0.0063
	Mode2	36.7	0.185	0.307	40824	0.0079
	Mode3	39.2	0.154	0.225	40824	0.0139
Stage 2	Mode1	43.0	0.159	0.438	40824	0.0076
	Mode2	54.4	0.170	0.307	40824	0.0128
	Mode3	40.7	0.148	0.201	40824	0.0168
Stage 3	Mode1	42.5	0.147	0.416	40824	0.0085
	Mode2	28.6	0.218	0.307	40824	0.0052
	Mode3	32.3	0.210	0.193	40824	0.0098
Stage 4	Mode1	52.4	0.245	0.438	40824	0.0060
	Mode2	38.7	0.161	0.307	40824	0.0096
	Mode3	31.0	0.215	0.201	40824	0.0088

According to the damping ratio values from Tables 4.9 and 4.10, both MEScope and FRF half power method damping ratios are underestimated; MEScope computed damping ratio values are very low. When the MEScope damping ratios are used in the resonance equation, the corresponding effective weights are back-calculated as shown in Table 4.11. Most of the effective weight-to-total weight ratios are above 80%, which are very much above the theoretical values.

Table 4.11 Effective Weight-to-Total Weight Ratio Back-calculated using MEScope Damping Ratios for the Three Span Footbridge

Sinusoidal Excitations for Resonance		P_0 (lbs) (Test)	a_p/g (Test)	MEScope calculated β	Total Weight (lbs)	Back-calc. Effective Weight / Total Weight
Stage 1	Mode1	38.2	0.177	0.0027	40824	0.997
	Mode2	36.7	0.185	0.0026	40824	0.953
	Mode3	39.2	0.154	0.0033	40824	0.939
Stage 2	Mode1	43.0	0.159	0.0027	40824	1.218
	Mode2	54.4	0.170	0.0036	40824	1.086
	Mode3	40.7	0.148	0.0054	40824	0.625
Stage 3	Mode1	42.5	0.147	0.0028	40824	1.260
	Mode2	28.6	0.218	0.0040	40824	0.400
	Mode3	32.3	0.210	0.0021	40824	0.884
Stage 4	Mode1	52.4	0.245	0.0027	40824	0.960
	Mode2	38.7	0.161	0.0144	40824	0.204
	Mode3	31.0	0.215	0.0020	40824	0.870

When the frequency response function half-power method damping ratios are used in the resonance equation, the corresponding effective weights are back-calculated as shown in Table 4.12. The effective weight-to-total weight ratios are more reasonable and closer to the theoretical numbers, which means the damping ratios computed from the frequency response functions by the half power method are closer to the actual damping ratios than the ones predicted by MEScope, for the three span footbridge.

Table 4.12 Effective Weight-to-Total Weight Ratio Back-calculated using FRF Half Power Method Damping Ratios for the Three Span Footbridge

Sinusoidal Excitations for Resonance		P_0 (lbs) (Test)	a_p /g (Test)	FRF Half-Power Method, β	Total Weight (lbs)	Back-calc. Effective Weight / Total Weight
Stage 1	Mode1	38.2	0.177	0.0045	40824	0.587
	Mode2	36.7	0.185	0.0046	40824	0.528
	Mode3	39.2	0.154	0.0066	40824	0.472
Stage 2	Mode1	43.0	0.159	0.0058	40824	0.571
	Mode2	54.4	0.170	0.0080	40824	0.490
	Mode3	40.7	0.148	0.0070	40824	0.481
Stage 3	Mode1	42.5	0.147	0.0070	40824	0.506
	Mode2	28.6	0.218	0.0042	40824	0.383
	Mode3	32.3	0.210	0.0042	40824	0.449
Stage 4	Mode1	52.4	0.245	0.0048	40824	0.546
	Mode2	38.7	0.161	0.0074	40824	0.398
	Mode3	31.0	0.215	0.0037	40824	0.477

The effective weight-to-total weight ratios are back-calculated using the FRF half power method damping ratios and finite element model acceleration predictions, Table 4.13. The effective weight-to-total weight ratios are reasonable and close to the theoretical numbers; however, there is no specific pattern regarding the effect of bottom chord extensions on the vibration response.

Table 4.13 Effective Weight to Total Weight Ratio Back-calculated using FRF Half Power Method Damping Ratios and FE Model Acceleration Predictions for the Three Span Footbridge

Sinusoidal Excitations for Resonance		P_0 (lbs) (FE)	FRF Half-Power Method, β	a_p /g (FE)	Total Weight (FE) (lbs)	Back-calc. Effective Weight / Total Weight
Stage 1	Mode1	38.2	0.0045	0.238	40888	0.436
	Mode2	36.7	0.0046	0.276	40888	0.353
	Mode3	39.2	0.0061	0.165	40888	0.476
Stage 2	Mode1	43.0	0.0058	0.162	40888	0.560
	Mode2	54.4	0.0080	0.263	40888	0.316
	Mode3	40.7	0.0070	0.341	40888	0.209
Stage 3	Mode1	42.5	0.0070	0.117	40888	0.635
	Mode2	28.6	0.0042	0.265	40888	0.314
	Mode3	32.3	0.0042	0.467	40888	0.201
Stage 4	Mode1	52.4	0.0048	0.237	40888	0.563
	Mode2	38.7	0.0074	0.202	40888	0.317
	Mode3	31.0	0.0037	0.491	40888	0.209

For the finite element model acceleration predictions, the time history function is created with an excitation frequency of the resonant frequency of the corresponding mode determined by the finite element program. In the finite element model, the amplitude of the excitation is set as the excitation amplitude used in the actual test. The time history analyses were run with different mode numbers for "modal analysis" in the software, for each run. The number of modes was gradually increased in each run for the time history analysis to determine the effect of different modes in the vibration response. For the three span footbridge, it was realized that the whole vertical system behavior is governed by the first three bending modes used in this study. For the single span footbridge, behavior is governed by the first bending mode.

Because all three bending modes are closely spaced for the three span footbridge, the sinusoidal excitations for a specific mode may also excite the other two bending modes. The three bending modes are within 1 Hz and the interaction of these modes in the response of the footbridge to any excitations is expected. The finite element model results showed that when the footbridge is excited at an exterior midspan location in the Stage 3 condition, for the first bending mode excitation the contributions to the acceleration response from the second bending mode are negligible while the contributions from the third bending mode are around 8% of the total response. For a second bending mode excitation, the contributions to the acceleration response from the first bending mode are around 10% on the total acceleration response, while the contributions from the third bending mode are negligible. For the third bending mode excitation, the contributions to the acceleration response from the first bending mode are around 17% of the total acceleration response, while the contributions from the second bending mode are around 32% of the total acceleration response. For all the sinusoidal excitations of the three bending modes, finite element model time history analyses showed that there was not any contribution to the total response from the local modes.

For the effective weight-to-total weight ratios in Tables 4.11, 4.12 and 4.13, it is obvious that there is no specific pattern regarding the effect of bottom chord extensions on the vibration response. As has already been shown, the effect of bottom chord extensions on the effective mass is also not specific. The three closely spaced modes of the three span footbridge may be the reason for these inconsistencies.

Another issue that needs to be considered is the difficulty of exciting the system to resonance. Throughout the experimental study, for some sinusoidal excitations the system was not able to be put into resonance. It is noted that in the derivation of Equation 4.17, it is assumed that the system is in full resonance.

To further investigate the resonance excitation, a detailed chirp signal study was conducted on the Stage 4 bottom chord extension configuration of the three span footbridge (Table 4.14). The shaker was placed in Bay 2, at the center of the footbridge, and different chirp excitations were run (Tests 140, 141, 142 and 143, Stage 4, Appendix E) to check whether or not the peak spectral line information belonged to the real natural frequency value. When 1024 spectral lines were used, chirp FRF's showed the first bending mode natural frequency to be 7.60 Hz. When 2048 spectral lines were used (Test 143), it was observed that the natural frequency was 7.575 Hz, although the peak of the FRF was not very sharp. For the same shaker location, sinusoidal excitations were run below and above the natural frequency determined by the chirp excitation. The frequency response functions for the corresponding sine excitation frequencies were compared and it was found that the 7.55 Hz sine excitation resulted in the highest FRF value (Table 4.14). As a result, for this set of measurements, the natural frequency value falls slightly to the left of the FRF peak spectral line from the chirp excitations. However, this is not the case for all of the single span and three span footbridge tests. It was observed that sometimes natural frequencies determined from chirp excitations vary +/- 0.05 Hz from measurement to measurement (depending on the excitation amplitude, time of the day, temperature, etc.). This shift in the natural frequency values usually has a very significant effect on the outcome of the sinusoidal excitation test results. There were some cases during the three span footbridge modal testing where it was observed that even a 0.05 Hz shift in sinusoidal excitation frequency can affect the acceleration responses up to 80%. If the amplitude dependent damping phenomenon is added to the above discussion (damping ratio is a very critical number in the denominator and half-power method damping ratios do not match with the MEScope curve fitted damping ratios), it is realized that using Equations 4.16 and 4.17 is not the best method for determining the effective mass of a specific mode experimentally. Importing the experimental modal analysis data to software such as MEScope and determining the effective mass through the computed mode shapes is definitely a more reliable approach.

Table 4.14 Investigation on Natural Frequency Determination with Chirp and Sinusoidal Excitations- Three Span Footbridge- Stage 4

			Frequency Response Function Coordinates					
Excitation	**Resolution**	**Test No.**	**7.55 Hz**	**(7.575 Hz)**	**7.60 Hz**	**(7.625 Hz)**	**7.65 Hz**	Modal Damping (Half Power Method)
Chirp (**4-16 Hz)**	1024 Spectral Lines	Test 140	0.8111	-	**1.379**	-	0.1488	0.349%
Chirp (**4-12 Hz)**	1024 Spectral Lines	Test 141	0.8348	-	**1.174**	-	0.09081	0.434%
Chirp (**4-10 Hz)**	1024 Spectral Lines	Test 142	0.8536	-	**1.013**	-	0.2611	0.599%
Chirp (**4-10 Hz)**	2048 Spectral Lines	Test 143	0.9187	**1.143**	0.9686	0.4238	0.1979	0.436%
		AVG	**0.8546**	**1.1430**	**1.1337**	**0.4238**	**0.1747**	**0.4545%**

			Frequency Response Function Coordinates				
Excitation	**Resolution**	**Test No.**	**7.55 Hz**	**(7.575 Hz)**	**7.60 Hz**	**(7.625 Hz)**	**7.65 Hz**
Sinusoidal	1024 Spectral Lines	Test 144	**0.8075**	-	-	-	-
Sinusoidal	1024 Spectral Lines	Test 145	-	-	**0.6118**	-	-
Sinusoidal	1024 Spectral Lines	Test 146	-	-	-	-	**0.3461**

It is strongly recommended that when modal testing of a structure is conducted, the natural frequencies determined from the chirp frequency response functions be checked with sinusoidal excitations at different resonant frequencies very slightly above and below the chirp natural frequency spectral line. Also, instead of accelerometer FTT RMS values, the FRF values corresponding to sinusoidal excitation frequencies have to be taken into consideration for comparison. When the true natural frequency of any mode is known, then the sinusoidal excitations can be applied and the results of Equations 4.16 and 4.17 are more reliable.

4.4 Conclusions from Vibration Testing

A summary of results for the single span footbridge is shown in Tables 4.15 (a) and (b) from which the following conclusions were made.

Table 4.15(a) Summary of Results- Single Span Footbridge

	Bending Natural Frequencies (Hz)	Bending Mode Damping Ratios (%)		20 psf deflection (in)	Chirp Excitaiton FRF Peak		Sinusoidal Excitation (Low Amplitude) FRF Peak	Heeldrop FRF Peak		One Pedestrian Walking w/ (1/3)f_{n1} (RMS)	Effective Mass From Mode Shapes	
	f_{n1}	ζ_1		Bay1	Quarter Point Excitation		Center Point Excitation	Center Point Excitation	Quarter Point Excitation		Bending Mode 1	Bending Mode 1
Stage	MEScope	MEScope	Half-Power Method	Test	Accel @ Center	Accel @ Quarter Point	Accel @ Center	Accel @ Center	Accel @ Quarter Point	Accel @ Center	MEScope	FE Model
1	8.08	0.451	0.639	0.054	1.8	1.2	2.5	5.6	2.3	0.00925	0.426m	0.517m
2	6.95	0.448	0.453	0.068	2.2	1.3	3.1	3.5	1.5	0.00820	0.466m	0.524m
3	7.65	0.409	0.452	0.058	2.3	1.4	1.2*	3.2	1.7	0.00905	0.413m	0.517m

*Not in Resonance

Table 4.15(b) Sinusoidal Excitations- Single Span Footbridge

	Excitation Level 1			Excitation Level 2			Excitation Level 3			Excitation Level 4		
	Sine Excitation Amplitude (lbs)	Acc. (g)	Ratio (g / lbs)	Sine Excitation Amplitude (lbs)	Acc. (g)	Ratio (g / lbs)	Sine Excitation Amplitude (lbs)	Acc. (g)	Ratio (g / lbs)	Sine Excitation Amplitude (lbs)	Acc. (g)	Ratio (g / lbs)
	Test	Test	Test	Test	Test	Test	Test	Test	Test	Test	Test	Test
Stage 1	-	-	-	12.4	0.14	0.0114	26.6	0.25	0.0096	44.1	0.36	0.0081
Stage 2	7.6	0.12	0.0158	12.4	0.17	0.0137	26.8	0.24	0.0091	43.8	0.32	0.0074
Stage 3*	-	-	-	15.7	0.08	0.0054	33.0	0.15	0.0045	50.8	0.21	0.0041

*Not in Resonance

The natural frequency for the first bending mode is the highest for Stage 1. Removing the bottom chord extensions for Stage 2 decreased the natural frequency value, and re-installing the bottom chord extensions for Stage 3 increased the natural frequency, as both expected. However, the Stage 3 natural frequency is lower than the Stage 1 natural frequency. Having, removing and re-installing the bottom chord extensions do not have any significant effect on the modal damping ratio of the first bending mode.

The 20 psf live load deflections are the lowest for Stage 1. Removing the bottom chord extensions for Stage 2 increased the deflections, and re-installing the bottom chord extensions for Stage 3 decreased the deflections, as both expected. However, the Stage 3 deflection is greater than the Stage 1 deflection.

The chirp excitation FRF peaks are the lowest for Stage 1, not as expected since it is the stiffest stage. The vibration response of a single span system is governed by the first bending mode. As the stiffness of a single span structure increases, the response of the system to an excitation is expected to increase as the effective mass vibrating for the first bending mode decreases. Removing the bottom chord extensions for Stage 2 increased the chirp excitation FRF peaks, again not as expected. Re-installing the bottom chord extensions for Stage 3 increased the chirp excitation FRF peaks. This result was expected, but it is inconsistent with the trend of Stages 1 and 2. Also, chirp excitation FRF peaks are inconsistent with the natural frequency and 20 psf deflection trend for Stages 1 and 2.

The sinusoidal excitation FRF peaks are lower for Stage 1 as compared to Stage 2 for low amplitude excitations (Excitation Level 2, 12 lbs), which was not expected. (Stage 3 data is omitted since the system was not in resonance). Sinusoidal excitation FRF peaks for low excitation amplitude (12 lbs) are inconsistent with the previous natural frequency and 20 psf deflections trend. Sinusoidal excitation FRF peaks for higher excitation amplitudes (Excitation Levels 3 and 4, 27 lbs and 44 lbs, respectively) are consistent with the previous natural frequency and 20 psf deflections trend. (Again, Stage 3 data is omitted since the system was not in resonance). The acceleration / input force ratio values increased when bottom chord extensions were removed.

The heel drop excitation FRF peaks are the highest for Stage 1, as expected. Removing the bottom chord extensions for Stage 2 decreased the heel drop excitation FRF peaks, and re-installing the bottom chord extensions for Stage 3 increased the heel drop excitation FRF peaks (for quarter point excitation), both as expected. Quarter point heel drop excitation FRF peaks are consistent with the natural frequency and 20 psf deflection trend.

Accelerations due to one pedestrian walking at $1/3^{rd}$ of the natural frequency are the highest for Stage 1, which was expected. Removing the bottom chord extensions for Stage 2 decreased the accelerations, and re-installing the bottom chord extensions for Stage 3 increased the accelerations again, both as expected.

Walking excitation acceleration results are consistent with the natural frequency, 20 psf deflection, and quarter point heel drop excitation trend. Effective mass values (calculated by MEScope mode shapes) for the first bending mode are the highest for Stage 2. Stage 1 and 3 are stiffer than Stage 2 and lower effective masses are expected for Stages 1 and 3. Removing the bottom chord extensions for Stage 2 increased the effective mass, and re-installing the bottom chord extensions for Stage 3 decreased the effective mass, both as expected. The effect of bottom chord extensions on measured effective mass results is consistent with the natural frequency results, 20 psf deflection results, quarter point heel drop FRF results and the walking acceleration trend. The finite element model effective masses also increase when the bottom chord extensions are removed from the system. This agrees with the test results. Measured effective mass and finite element model effective mass results are consistent.

In conclusion, the effect of bottom chord extensions on the single span footbridge is consistent for natural frequency, 20 psf live load deflections, sinusoidal excitations with high amplitudes, quarter point heel drop excitations, walking excitations, and effective mass values.

A summary of results for the three span footbridge is shown in Tables 4.16 (a) and (b). It must be noted that for all Stage 5 measurements, the power box was not functioning with proper calibration during the modal testing. Hence, Stage 5 data are shaded in Tables 4.16 (a) and (b) and the results are not considered in the following discussion.

Table 4.16(a) Summary of Results- Three Span Footbridge

Stage	Bending Natural Frequencies (Hz)			Bending Mode Damping Ratios (%)			20psf deflection (in.)			Chirp Excitation FRF Peak					Sinusoidal Excitation FRF Peak*					Heeldrop FRF Peak		Two Ped. Walking w/ (1/3)f_{n1} (RMS)
										Bay 2 Center Excitation		Bay 3 Center Excitation			Bay 2 Center Excitation		Bay 3 Center Excitation			Bay 2 Center Excitation		
										Accel @ Bay2 center	Accel @ Bay2 center	Accel @ Bay3 center	Accel @ Bay3 center	Accel @ Bay3 center	Accel @ Bay2 center	Accel @ Bay2 center	Accel @ Bay3 center	Accel @ Bay3 center	Accel @ Bay3 center	Accel @ Bay2 center	Accel @ Bay2 center	Accel @ Bay2 center
	f_{n1}	f_{n2}	f_{n3}	ζ_1	ζ_2	ζ_3	Bay1 Midspan	Bay2 Midspan	Bay3 Midspan	Bending Mode 1	Bending Mode 3	Bending Mode 1	Bending Mode 2	Bending Mode 3	Bending Mode 1	Bending Mode 3	Bending Mode 1	Bending Mode 2	Bending Mode 3	Bending Mode 1	Bending Mode 3	
1	7.76	8.11	8.93	0.265	0.255	0.332	0.051	0.047	0.045	2.0	1.3	0.7	2.2	1.0	1.0	0.7	0.5	1.0	0.8	3.5	2.7	0.0281
2	7.51	7.90	8.81	0.272	0.361	0.539	0.062	0.050	0.056	1.2	1.4	1.2	2.5	0.7	0.8	0.8	0.7	0.7	0.4	-	-	0.0320
3	7.49	7.81	8.37	0.281	0.402	0.213	0.069	0.053	0.065	2.5	3.9	5.3	3.5	1.4	0.7	1.3	0.4	1.7	0.7	1.5	3.3	0.0340
4	7.60	8.14	8.78	0.273	-	0.203	0.054	0.047	0.054	1.7	3.4	4.8	2.1	0.9	0.7	1.0	0.7	0.7	0.5	0.7	1.0	0.0223
5	7.80	8.13	8.89	0.178	0.235	0.571	0.048	0.048	0.051	4.2	2.3	1.3	3.3	0.8	0.8	1.2	0.4	0.7	0.6	2.6	2.0	0.0342

*Resonance Questionable

Table 4.16(b) Sinusoidal Excitations- Three Span Footbridge

	First Bending Mode					Second Bending Mode					Third Bending Mode				
	Effective Mass From Mode Shapes		Sinusoidal Excitations for Resonance			Effective Mass From Mode Shapes		Sinusoidal Excitations for Resonance			Effective Mass From Mode Shapes		Sinusoidal Excitations for Resonance		
			Amplitude (lbs)	Acceleration (g)	Ratio (g / lbs)			Amplitude (lbs)	Acceleration (g)	Ratio (g / lbs)			Amplitude (lbs)	Acceleration (g)	Ratio (g / lbs)
	MEScope	FE Model	Test	Test	Test	MEScope	FE Model	Test	Test	Test	MEScope	FE Model	Test	Test	Test
Stage 1	0.247m	0.419m	38.2	0.18	0.0047	0.289m	0.307m	36.7	0.19	0.0052	0.437m	0.225m	39.2	0.15	0.0038
Stage 2	0.479m	0.438m	43.0	0.16	0.0037	0.343m	0.307m	54.4	0.17	0.0031	0.237m	0.201m	40.7	0.15	0.0037
Stage 3	0.300m	0.416m	42.5	0.15	0.0035	0.255m	0.307m	28.6	0.22	0.0077	0.257m	0.193m	32.3	0.21	0.0065
Stage 4	0.259m	0.438m	52.4	0.25	0.0048	0.357m	0.307m	38.7	0.16	0.0041	0.214m	0.201m	31.0	0.22	0.0071
Stage 5	0.271m	0.419m	-	-	-	0.256m	0.307m	-	-	-	0.255m	0.225m	-	-	-

The natural frequency for the first bending mode is highest for Stages 1 and 5 for all three bending modes, which was expected. Removing the exterior bottom chord extensions for Stage 2 decreased the natural frequency values for all three bending modes and removing all of the bottom chord extensions for Stage 3 decreased the natural frequency values for all three bending modes, both as expected. Re-installing the interior bottom chord extensions for Stage 4 increased the natural frequency values for all three bending modes, as expected. Re-installing the exterior bottom chord extensions for Stage 5 further increased the natural frequency values for all three bending modes, as expected.

Removing and re-installing the bottom chord extensions did not have any significant effect on the modal damping ratios. The 20 psf live load deflections are the lowest for Stages 1 and 5, as expected. Removing the exterior bottom chord extensions for Stage 2 increased the deflections, as expected. Removing all of the bottom chord extensions for Stage 3 further increased the deflections, again as expected. Re-installing the interior bottom chord extensions for Stage 4 decreased the deflections, and re-installing the exterior bottom chord extensions for Stage 5 decreased the deflections, both as expected. The 20 psf deflection results are consistent with the natural frequency results.

The vibration response of a three span system is governed by the first three bending modes. As the stiffness of the structure increases, the response of the system to an excitation is not necessarily affected at the same level for the three modes. For example, the chirp excitation FRF peaks for the central Bay 2 excitation location are consistent with the natural frequency and 20 psf deflections trends for the first bending mode. The chirp excitation FRF peaks for the central Bay 2 excitation location are inconsistent for the third bending mode since the FRF peaks increased when the bottom chord extensions were removed from the system (Stages 2 and 3). However, both MEScope and FE effective masses increased for Stage 2 and then decreased for Stage 3. The chirp FRF peaks decreased as the bottom chord extensions were re-installed in the system (Stages 4 and 5).

The chirp excitation FRF peaks for the central Bay 3 excitation location are inconsistent for the first and second bending modes. The FRF peaks increased where the bottom chord extensions were removed from the system. Also, the FRF peaks decreased when the bottom chord extensions were re-installed into the system. The chirp excitation FRF peaks for the central Bay 3 excitation location are consistent for the third bending mode when MEScope effective mass results are considered. However, they are inconsistent with the FE model effective mass results.

The sinusoidal excitation FRF peaks for the central Bay 2 excitation location are consistent for the first bending mode. The sinusoidal excitation FRF peaks for the central Bay 2 excitation location are inconsistent for the third bending mode (for MEScope effective mass results). The FRF peaks increased when the bottom chord extensions were removed from the system (Stages 2 and 3), and the FRF peaks decreased when the bottom chord extensions were re-installed in the system (Stages 4 and 5). The sinusoidal excitation FRF peaks for the central Bay 3 excitation location are consistent for all of the three bending modes.

The heel drop excitation FRF peaks for the central Bay 2 excitation location are consistent for the first bending mode since the highest FRF peak is for Stage 1. The heel drop excitation FRF peaks for the central Bay 2 excitation location are inconsistent for the third bending mode (for MEScope effective mass results) since the highest FRF peak is for Stage 1 (Stage 2 data is missing and it is assumed that the FRF peak for that stage is between the peaks of Stages 1 and 3).

Accelerations due to two pedestrians walking side-by-side at 1/3rd of the first bending mode natural frequency increased when the exterior bottom chord extensions were removed (Stage 2). Removing all of the bottom chord extensions (Stage 3) increased the accelerations due to two pedestrians walking side-by-side at 1/3rd of the first bending mode natural frequency. Re-installing the interior bottom chord extensions for Stage 4 decreased the accelerations, and re-installing the exterior bottom chord extensions for Stage 5 increased the accelerations. No conclusions can be made for the walking data, since the 20 psf deflections data, walking acceleration values, MEScope effective mass results and FE model effective mass results are all inconsistent with each other.

Effective mass results for all three bending modes do not follow a specific pattern. For the effective masses calculated from MEScope mode shapes, removing the exterior bottom chord extensions for Stage 2 increased the first bending mode effective mass, and likewise in the FE model. Removing the interior bottom chord extensions for Stage 3 decreased the first bending mode effective mass, as in the FE model. Re-installing the interior bottom chord extensions for Stage 4 decreased the first bending mode effective mass, again as in the FE model. Re-installing the exterior bottom chord extensions for Stage 5 increased the first bending mode MEScope effective mass, however the FE model effective mass decreased. For the second bending mode, MEscope and FE model effective mass results are inconsistent for all stages. This inconsistency is also present for Stages 2, 3 and 4 for the third bending mode effective mass results.

In conclusion, the effect of bottom chord extensions on the three span footbridge is consistent for the natural frequency and 20 psf deflections. The FRF peaks of chirp, heel drop, sinusoidal excitations, accelerations from walking data, and the MEScope and FE model effective mass results do not follow a common trend.

It can be concluded that even though the footbridge was stiffened by the bottom chord extensions, that does not necessarily mean that the acceleration levels, and hence the frequency response function peaks, decrease. However, bottom chord extensions do increase the natural frequencies for all three governing bending modes.

CHAPTER 5
SUMMARY OF RESULTS AND CONCLUSIONS

5.1 Summary of Results

The purpose of this study was to examine the effect of bottom chord extensions on deflections and vibration characteristics of joist supported floor systems when joist bottom chord extensions are installed. To understand the effect of bottom chord extensions on deflections, natural frequency, damping, mode shape and effective mass, extensive analytical and experimental studies were conducted on single span and three span joist supported laboratory footbridges with different bottom chord extension configurations. Finite element computer models were created to simulate and compare the results of stiffness and vibration tests. Testing was done with a) the bottom chord extensions in-place before the concrete was placed, b) with all or part of the bottom chord extensions removed, and c) after the bottom chord extensions had been reinstalled with jacking for the single span footbridge and without jacking for the three-span footbridge.

5.1.1 Static Test Results

The objective of stiffness testing was to determine the effect of bottom chord extensions on deflections. For that purpose, the footbridges were loaded with point and 20 psf uniformly distributed loads.

Single Span Footbridge Results. Midspan point loading tests showed that the deflections at maximum loading increased from 0.025 in. to 0.037 in. (48% increase) when the bottom chord extensions were removed and decreased to 0.029 in. when they were re-installed (with the center of the footbridge were raised approximately 0.5 in. The deflection numbers for all three stages are closer to the simply supported beam case than the fixed-fixed beam case. For reference, the corresponding mechanics simple span and fixed end deflections are 0.008 in. and 0.033 in., respectively.

The 20 psf uniform loading tests showed that the deflections at maximum loading increased from 0.0545 in. to 0.0675 in. (24% increase) when the bottom chord extensions were removed and decreased to 0.057 in. when they were re-installed. Again, the deflection numbers for all three stages are closer to the simply supported beam case than the fixed-fixed beam case. For reference, the corresponding mechanics simple span and fixed end deflections are 0.014 in. and 0.071 in., respectively.

In summary, re-installing the bottom chord extensions in the joists of the single span footbridge with cured concrete and with the center of the span raised helps to reduce the uniform load deflections to some extent, but not as much as placing the bottom chord extensions before the concrete pour.

The instrumented bottom chord extension results show that for midspan point loading, the measured data is linear and the force in the bottom chord extensions before the members are removed is close to the force after re-installing the members. However, for 20 psf uniform loading tests, the force in the bottom chord extensions before the members were removed is greater than the force after re-installing the members.

Three Span Footbridge Results. Stiffness test results for the three span footbridge showed that the deflections due the midspan point loading are reduced around 20% when both exterior and interior bottom chord extensions are in place. The deflections due to the 20 psf uniform loading are reduced around 30% on the outside bays and about 10% on the interior bay when both exterior and interior bottom chord extensions are in place.

In summary, re-installing the bottom chord extensions to the joists of the three span footbridge helps to reduce the deflections, since the force monitored on the bottom chord extensions after the re-installation has almost the same stiffness slope as the ones in the stages where the chord extensions were in place before the concrete placement. However, placing the bottom chord extensions before the concrete placement gives better results.

5.1.2 Dynamic Test Results

The objective of vibration testing conducted in this study was to experimentally determine the natural frequency, damping, mode shape, and effective mass properties of the laboratory footbridges and to determine the effect of bottom chord extensions on these items for each configuration.

Single Span Footbridge Results. Removing the bottom chord extensions for Stage 2 decreased the natural frequency and re-installing the bottom chord extensions for Stage 3 increased the natural frequency, both as expected.

Removing the bottom chord extensions for Stage 2 increased the chirp excitation FRF peaks, not as expected. Re-installing the bottom chord extensions for Stage 3 increased the chirp excitation FRF peaks, which was expected, but is inconsistent with the trend of Stages 1 and 2.

Sinusoidal excitation FRF peaks for low excitation amplitude (12 lbs) are inconsistent with the previous natural frequency and 20 psf deflections trend. Sinusoidal excitation FRF peaks for higher excitation amplitudes (27 lbs and 44 lbs, respectively) are consistent with the previous natural frequency and 20 psf deflections trends; the acceleration/input force ratio values increased when bottom chord extensions were removed.

Removing the bottom chord extensions for Stage 2 decreased the heel drop excitation FRF peaks, and re-installing the bottom chord extensions for Stage 3 increased the heel drop excitation FRF peaks (for quarter point excitation), both as expected.

Removing the bottom chord extensions for Stage 2 decreased the accelerations due to one pedestrian walking at 1/3rd of the natural frequency, and re-installing the bottom chord extensions for Stage 3 increased the accelerations again, both as expected.

Removing the bottom chord extensions for Stage 2 increased the effective mass, and re-installing the bottom chord extensions for Stage 3 decreased the effective mass, both as expected. The effect of bottom chord extensions on measured effective mass results is consistent with the natural frequency results, 20 psf deflection results, quarter point heel drop FRF results and the walking acceleration trend. Measured effective mass and finite element model effective mass results are consistent.

In summary, the effect of bottom chord extensions on the single span footbridge is consistent for natural frequency, 20 psf live load deflections, sinusoidal excitations with high amplitudes, quarter point heel drop excitations, walking excitations, and for effective mass values.

Three Span Footbridge Results. Removing the exterior bottom chord extensions for Stage 2 decreased the natural frequency values for all three bending modes, and removing all of the bottom chord extensions for Stage 3 decreased the natural frequency values for all three bending modes, both as expected. Re-installing the interior bottom chord extensions for Stage 4 increased the natural frequency values for all three bending modes, as expected. Re-installing the exterior bottom chord extensions for Stage 5 further increased the natural frequency values for all three bending modes, as expected.

For the central Bay 3 excitation location, the chirp excitation FRF peaks are inconsistent for the first and second bending modes. The FRF peaks increased where the bottom chord extensions were removed from the system. Also, the FRF peaks decreased when the bottom chord extensions were re-installed into the system. The chirp excitation FRF peaks for the central Bay 3 excitation location are consistent for the third bending mode when MEScope effective mass results are considered. However, they are inconsistent with the FE model effective mass results.

The sinusoidal excitation FRF peaks for the central Bay 2 excitation location are consistent for the first bending mode. The sinusoidal excitation FRF peaks for the central Bay 2 excitation location are inconsistent for the third bending mode (for MEScope effective mass results). The FRF peaks increased when the bottom chord extensions were removed from the system (Stages 2 and 3), and the FRF peaks decreased when the bottom chord extensions were re-installed in the system (Stages 4 and 5). The sinusoidal excitation FRF peaks for the central Bay 3 excitation location are consistent for all three bending modes.

The heel drop excitation FRF peaks for the central Bay 2 excitation location are consistent for the first bending mode, as the highest FRF peak is for Stage 1. The heel drop excitation FRF peaks for the central Bay 2 excitation location are inconsistent for the third bending mode (for MEScope effective mass results), as the highest FRF peak is for Stage 1.

For the two pedestrians walking side-by-side at 1/3rd of the first bending mode natural frequency, the accelerations increased when the exterior bottom chord extensions were removed (Stage 2). Removing all of the bottom chord extensions (Stage 3) increased the accelerations. Re-installing the interior bottom chord extensions for Stage 4 decreased the accelerations, and re-installing the exterior bottom chord extensions for Stage 5 increased the accelerations. No conclusions can be made for the walking data, since the 20 psf deflections data, walking acceleration values, MEScope effective mass results and FE model effective mass results are all inconsistent with each other.

Effective mass results for all three bending modes do not follow a specific pattern. For the effective masses calculated from MEScope mode shapes, removing the exterior bottom chord extensions for Stage 2 increased the first bending mode effective mass, and likewise in the FE model. Removing the interior bottom chord extensions for Stage 3 decreased the first bending mode effective mass, as in the FE model. Re-installing the interior bottom chord extensions for Stage 4 decreased the first bending mode effective mass, again as in the FE model. Re-installing the exterior bottom chord extensions for Stage 5 increased the first bending mode MEScope effective mass, however the FE model effective mass decreased. For the second bending mode, MEscope and FE model effective mass results are inconsistent for all stages. This inconsistency is also present for Stages 2, 3 and 4 for the third bending mode effective mass results.

In summary, the effect of bottom chord extensions on the three span footbridge is consistent for the natural frequency and 20 psf deflections. The FRF peaks of chirp, heel drop, sinusoidal excitations, accelerations from walking data, and the MEScope and FE model effective mass results do not follow a common trend.

5.2 Conclusions

Effect of Bottom Chord Extensions. For static loading, having bottom chord extensions in place before the concrete placement or re-installing the bottom chord extensions to the joists of both the single span and three span footbridges with cured concrete helps to reduce the midspan point and 20 psf uniform load deflections to some extent, but placing the bottom chord extensions before the concrete pour gave better results.

For dynamic loading it is concluded that bottom chord extensions do increase the natural frequencies for all three governing bending modes. However, although the footbridges were stiffened by the bottom chord extensions, that does not necessarily mean that the acceleration levels, and hence the frequency response function peaks, decrease.

Damping Ratios. The damping ratio values play an important role in floor vibration calculations. However, it is difficult to find the correct damping ratio for a specific mode. A modal damping ratio calculated from a specific FRF curve by the half power method will not be the same as the damping ratio computed by curve fitting, as done for example in MEScope, for a set of data. In fact, the MEScope damping ratios were observed to be very low. Because the damping ratios are at very low levels for both of the footbridges, the difference between the real and predicted damping ratio values can even make a bigger difference in the vibration calculations. This results in significant differences in measured, manually predicted (e.g. Design Guide 11 procedures) and finite element model acceleration values. "Burst chirp" excitations will have cleaner and more reliable FRF curves since damping ratios as the one chirp average will not contain any response from a previous average as in “continuous” chirp. “Slow sine sweep” is another option to have a more reliable approximated FRF curve, hence damping ratio, than continuous chirp.

Amplitude dependent damping is another phenomenon that needs to be considered. It is realized that with increasing vibration amplitude, the damping ratio also increases. So, attention must be paid to keep a record of excitation amplitudes in modal testing. Chirp signals with very different excitation amplitudes should not be used in the same set of data.

Resonance. The resonance equation (Equation 4.17) is not recommended for effective mass calculations since in its derivation it is assumed that the system is in full resonance. Testing showed that the natural frequency values are not necessarily at the FRF peaks; generally they are slightly to the left of the FRF peak spectral line from the chirp excitations, and using the peak spectral line natural frequency for sinusoidal excitations does not put the system in resonance.

It was also observed that natural frequencies determined from chirp excitations may vary +/-0.05 Hz from measurement to measurement (depending on the excitation amplitude, time of the day, temperature, etc.). In addition to amplitude dependent damping, the natural frequencies may also be amplitude dependent due to change of stiffness and coupling with other eigenmodes.

These kinds of shifts in the natural frequency values usually have a very significant effect on the outcome of the sinusoidal excitation test results. Thus, Equations 4.16 and 4.17 do not apply to these cases. It is strongly recommended that for modal testing of any structure, the natural frequencies determined from the chirp frequency response functions be checked with sinusoidal excitations with different resonant frequencies slightly above and below the chirp natural frequency spectral line. Also, instead of accelerometer FFT RMS values, the FRF values corresponding to sinusoidal excitation frequencies have to be taken into consideration for sinusoidal excitation comparisons. When the actual natural frequency of any mode is known, then the sinusoidal excitations can be applied where the results of Equations 4.16 and 4.17 are more reliable.

LIST OF REFERENCES

Allen, D.E. and Murray, T.M. (1993). "Design Criterion for Vibrations Due to Walking." *Engineering Journal*, AISC, Chicago, Illinois, pp. 117-129.

Alvis, S. R. (2001). "An Experimental and Analytical Investigation of Floor Vibrations." M.S. Thesis, Virginia Polytechnic Institute and State University, Blacksburg, Virginia.

Bachmann, H. et al. (1995). Vibration Problems in Structures. Birkhauser, Basel, Switzerland.

Band, B.S. Jr. (1996). "Several Vibration Performance Aspects of Joist and Joist-Girder Supported Floors." M.S. Thesis, Virginia Polytechnic Institute and State University, Blacksburg, Virginia.

Band, B.S. and Murray, T. M. (1996). "Vibration Characteristics of Joist and Joist-Girder Supported Members." Research Report CE/VPI-ST-96/07, Virginia Polytechnic Institute and State University, Blacksburg, Virginia.

Beavers, T.A. (1998). "Fundamental Natural Frequency of Steel-Joist Supported Floors." M.S. Thesis, Virginia Polytechnic Institute and State University, Blacksburg, Virginia.

Boice, M.D. (2003). "Study to Improve the Predicted Response of Floor Systems Due To Walking." M.S. Thesis, Virginia Polytechnic Institute and State University, Blacksburg, Virginia.

Boice, M.D. and Murray, T.M. (2003). "Study to Improve the Predicted Response of Floor Systems Due to Walking Case Studies Data." Research Report CE/VPI-ST-03/05, Virginia Polytechnic Institute and State University, Blacksburg, Virginia.

Bracewell, R.N. (2000). The Fourier Transform and Its Applications (Third Edition). McGraw-Hill, New York.

Clough, R.W. and Penzien, J. (1993). Dynamics of Structures (Second Edition). McGraw-Hill, New York.

Computers and Structures, Inc. (2002). <u>SAP2000 Linear and Nonlinear Static and Dynamic Analysis and Design of Three-Dimensional Structures - GETTING STARTED</u>. Berkeley, California.

Ewins, D.J. (2000). Modal Testing: Theory, Practice and Application (Second Edition). Research Studies Press, Hertfordshire, England.

Falati, S. (1999). "The Contribution of Non-Structural Components to the Overall Dynamic Behavior of Concrete Floor Slabs." Ph.D. Dissertation, University of Oxford, United Kingdom.

Fisher, J.M., West, M.A. and Van De Pas, J. (1991). Designing with Steel Joists, Joist Girders and Steel Deck. Vulcraft, Nucor Corporation.

Gibbings, D.R. (1990). "Evaluation of Long Span Composite Joists" M.S. Thesis, Virginia Polytechnic Institute and State University, Blacksburg, Virginia.

Hanagan, L.M. (1994). "Active Control of Floor Vibrations." Ph.D. Dissertation, Virginia Polytechnic Institute and State University, Blacksburg, Virginia.

He, J. and Fu, Z.F. (2001). Modal Analysis. Butterworth-Heinemann, Woburn, MA.

Ifeachor, E.C. and Jervis, B.W. (2002). Digital Signal Processing (Second Edition). Prentice-Hall, Essex, England.

Inman, D.J. (2000). Engineering Vibration (Second Edition). Prentice-Hall, Upper Saddle River, New Jersey.

International Standards Organization (ISO) (1989). “Evaluation of Human Exposure to Whole-Body Vibrations – Part 2: Human Exposure to Continuous and Shock-Induced Vibrations in Buildings (1 to 80Hz).” *International Standard ISO 2631-2*.

Jackson, R.L. (2002). “Vibration and Flexural Strength Characteristics of Composite Castellated Beams.” M.S. Thesis, Virginia Polytechnic Institute and State University, Blacksburg, Virginia.

Kittermann, S.S. (1994). “Investigation of Several Aspects of the Vibration Characteristics of Steel Member-Supported Floors.” M.S. Thesis, Virginia Polytechnic Institute and State University, Blacksburg, Virginia.

Leonard, D.R. and Eyre, R. (1975). “ Damping and Frequency Masurements on Eight Box Girders”, Report No. LR682, Transport and Road Research Laboratory (TRRL), Department of the Environment, Crowthorne, UK

Murray, T.M., Allen, D.E. and Ungar, E.E. (1997). “Steel Design Guide Series 11: Floor Vibrations Due to Human Activity.” American Institute of Steel Construction, Inc. (AISC). Chicago, Illinios.

Ohmart, R. D. and Lenzen, K.H. (1968). “An Approximate Method for the Response of Stiffened Plates to Aperiodic Motion.” Studies in Engineering Mechanics, Report No. 30, The University of Kansas Center for Research in Engineering Science, Lawrence, Kansas.

Perry, J. D. (2003). “A Study of Computer Modeling Techniques to Predict the Response of Floor Systems Due to Walking.” M.S. Thesis, Virginia Polytechnic Institute and State University, Blacksburg, Virginia.

Ritchey, J. (2003). "Application of Magneto-Rheological Dampers in Tuned Mass Dampers for Floor Vibration Control." M.S. Thesis, Virginia Polytechnic Institute and State University, Blacksburg, Virginia.

Rottmann, C. (1996). "The Use of Tuned Mass Dampers to Control Floor Vibrations." M.S. Thesis, Virginia Polytechnic Institute and State University, Blacksburg, Virginia.

Shamblin, C.L. (1989). "Floor System Response to Heel-Drop Impact." M.S. Thesis, Virginia Polytechnic Institute and State University, Blacksburg, Virginia.

Sladki, M.J. (1999). "Prediction of Floor Vibration Response Using the Finite Element Method." M.S. Thesis, Virginia Polytechnic Institute and State University, Blacksburg, Virginia.

Warmoth, F.J. Jr. (2002). "Floor Vibrations: Girder Effective Moment of Inertia and Cost Study." M.S. Thesis, Virginia Polytechnic Institute and State University, Blacksburg, Virginia.